THE UNIVERSITY OF CHICAGO

LOCALIZED MULTIREFERENCE METHODS FOR STRONGLY CORRELATED SYSTEMS

A DISSERTATION SUBMITTED TO
THE FACULTY OF THE DIVISION OF THE PHYSICAL SCIENCES
IN CANDIDACY FOR THE DEGREE OF
DOCTOR OF PHILOSOPHY

DEPARTMENT OF CHEMISTRY

BY
RIDDHISH UMESH PANDHARKAR

CHICAGO, ILLINOIS
AUGUST 2022

TABLE OF CONTENTS

LIST OF FIGURES

LIST OF TABLES

ACKNOWLEDGMENTS

I'd like to thank my advisor Prof. Laura Gagliardi for her mentorship and support throughout my graduate studies. Her constant encouragement to pursue tough problems and explore new ideas has greatly helped me mature as a researcher. I would also like to thank my co-advisors at the University of Minnesota, Prof. Christopher J. Cramer, and at Argonne National Lab, Dr. Stephen Gray, for their motivation and guidance in my explorations in various diverse research topics.

It has been a great pleasure to collaborate with fantastic researchers in the Gagliardi group: Matt, Hung, Abhishek, and Debmalya. Many other group members - Carlo, Prachi, Mukunda, Aleks, Meagan, Thais, Paul and Ruhee - were kind and patient enough to teach various concepts, techniques and skills. In addition, the entire Gagliardi and Cramer research groups have been phenomenal and made my journey so much more valuable.

I'd like to thank my committee members, Prof. David Mazziotti and Prof. Giulia Galli for valuable feedback on my research. I have had the privilege to collaborate with Prof. Don Truhlar, Prof. Omar Farha, Prof. Joachim Sauer, Dr. Yuri Alexeev, Dr. Alex Martinson, Dr. Massimiliano Delferro, Prof. Joseph Hupp, Prof. Justin Notestein on various projects. These collaborations have helped me understand a broad range of research fields.

I am grateful for the many supportive and efficient people in the chemistry departments and the supercomputing centers at University of Chicago and University of Minnesota, who supported my work me through out the program, including Vera, Melinda, Nsa Melanie, Nancy, and Ben.

And finally I am immensely grateful for the many friends I have made through out grad school, who have made my time hear so much more special, and to my family whose constant support and encouragement made this degree possible.

ABSTRACT

Computational modelling of molecules and materials with strongly correlated electrons has been a long-standing challenge in the field of theoretical chemistry. While, conventional multireference wave function methods provide a robust way to account of strong electron correlation, the high cost associated with them prohibits their application even for moderately sized systems.

This dissertation focuses on development and application of low-cost, chemically-guided multireference methods. The primary emphasis is on the localized active space self-consistent field (LASSCF) method. This method is designed for systems with strongly correlated orbitals that are localized in different regions of the system. LASSCF scales better than the conventional complete active space (CAS) method and gives qualitatively accurate results for various classes of compounds. To extend the applications of LASSCF beyond capturing qualitative behavior, we developed methods that account for further electron correlation. The LAS-PDFT (pair density functional theory) method is less susceptible to approximations of the wave function and shows better agreement to the corresponding CAS results even for systems for which LASSCF fails to do so. The LAS-State interaction method systematically restores entanglement between the fragments and provides better insights for practical applications. The LAS-Unitary coupled cluster (UCC) method (chapter 5) is designed for fault-tolerant quantum computers in order to leverage their power to do unitary operations in order to rebuild correlation between LAS fragments. Lastly, we discuss the hybrid multiconfiguration pair-density functional theory (HMC-PDFT) that provides a significant improvement over the conventional PDFT in calculating excitation energies for a wide range of systems.

These methods greatly extend our reach to get qualitatively accurate wave functions and quantitatively accurate energies for a wide range of challenging systems at a significantly lower computational cost.

CHAPTER 1

INTRODUCTION

1.1 Motivation

Computational chemistry aims at developing simple and ingenious mathematical models of the chemically interesting systems and phenomena present around us. Today these models are used in most fields of experimental chemistry to not only gain fundamental understanding of the chemistry but also to provide significant advantage and acceleration in the large-scale processes like material design and drug discovery.[3–7] The rapid advancement in computing technology has allowed us to formulate more rigorous models as well as extend our reach to more complex systems.[8–14] One significant barrier in modeling the electronic structure of increasingly larger systems is the exponentially increasing cost of computing all electron interaction energies. Even though quantum mechanics provides the fundamental laws to model these interactions, the difficulty, as Dirac points out in his famous quote, "lies only in the fact that application of these laws leads to equations that are too complex to be solved." The pursuit to overcome these limitations has spawned many approaches that introduce various approximations to make the equations easier to solve. These approximations are often based on the observations and assumptions about the specific domains of systems to which the method is to be used for. The severity of these approximations determines the accuracy of the method. Numerous efforts have been made in the past few decades to effectively capture this electron correlation[15–17]. Wave function based methods like multiconfiguration self-consistent field (MC-SCF)[18], coupled cluster (CC)[19–21] and perturbation theory[20,22] have been shown to be successful in approximating this interaction. Kohn-Sham DFT[23,24] introduces many simple and versatile ways to model the exchange and correlation interactions of electrons[25–28].

MC-SCF methods uses chemical knowledge of the systems being studied to simplify the

computation- the most common of which is the complete active space self-consistent field (CASSCF).[18] This method captures a significant part of the static correlation and the resulting wave function provides a good qualitative description of the system. The wave function also serves as a reference for many post-SCF methods that attempt to account for the correlation energy of the electrons outside the active space - like the second-order perturbation theory[22,29] and multiconfiguration pair-density functional theory (MC-PDFT).[30,31] A common approach, generally, is to obtain a qualitatively accurate wave function using these MC-SCF methods and use the post-SCF methods for further quantitative accuracy. This approach has proven to be highly useful in modeling various systems and phenomena - like charge transfer in conjugated organic molecules[32–35], electronic excitations in DNA[36–38], spin interactions in single molecular magnets[39–41] and mechanisms of biochemical reactions.[42–45]

The exponentially scaling cost of methods like CASSCF with the active space of the molecule restrict their applicability to relatively small systems. To bypass this high cost without compromising on the multireference character of the wave function, we developed the localized active space self-consistent field (LASSCF) method.[1,46] The LAS wave function is obtained by decomposing the active space into multiple subspaces that are localized in different parts of the molecule and solving for the exact wave function in each of the smaller subspaces separately. This method is designed for systems with strongly correlated orbitals that are localized in different regions of the system. In Chapter 2 lays the foundation of LASSCF and studies its performance for modeling bond dissociation in organic compounds and spin state ordering in bimetallic complexes. The LAS wave function proves to be a good approximation to the CAS wave function in many cases without incurring the high cost associated with the CASSCF. In other cases, however, the variational penalty of fragmenting the active space compromises the LAS energies significantly. In order to ameliorate this problem we study three post-LASSCF methods that aim to capture further

electron correlation. We do this in the following three chapters. Chapter 3 discusses the LAS-PDFT (pair density functional theory) that attempts to account for electron correlation beyond the LASSCF method. It computes the energy of the system based on the density and pair-density of electrons obtained from the reference LAS wave function. We demonstrate that LAS-PDFT energies are less susceptible to approximations of the LAS wave function and gives more accurate results even for systems for which LASSCF fails. Chapter 4 uses a systematic approach to introduce inter-fragment correlation through a state-interaction (SI) formalism of LASSCF that selectively restores some entanglement between the fragments. This method allows us to calculate excitation energies in highly conjugated organic compounds and magnetic coupling constants in multi-metallic systems with lower costs - extending the range of application for LAS based methods to systems that are not usually thought of as fragmentable. Moreover, we were able to demonstrate the use of these methods for insights in practical applications in spin coupling in magnets and charge transfer in organic molecules. In Chapter 5, we propose the "local active space unitary coupled cluster" (LAS-UCC) ansatz. This is a hybrid classical-quantum algorithm that leverages the power of quantum computers to do unitary operations in order to improve upon the LAS wave function. This scales linearly with system size for certain geometries, providing a polynomial reduction in the total number of gates compared to the quantum phase estimation (QPE), while providing accuracy above that of the variational quantum eigensolver (VQE) using the UCCSD ansatz as well as the classical LASSCF. To complement the efforts to lower the cost of obtaining multireference wave functions, accurate and efficient post-SCF methods need to be developed as well. Chapter 6 focuses on the development of hybrid multiconfiguration pair-density functional theory (HMC-PDFT) that provides a significant improvement over the conventional PDFT in calculating excitation energies for a wide range of systems. The methods can be used with any multireference wave function including but not limited to LASSCF. The remaining portion of the chapter establishes a background of

the fundamental concepts of electronic structure theory this work is based on.

1.2 Theoretical Background

The quantum mechanical Hamiltonian that is most commonly used for electronic structure calculations includes energy contributions of the inter-nuclear repulsion, the kinetic energy of the electrons, their interaction with the nuclei, the inter-electronic interaction. This excludes the effects like the coupling between the nuclear degrees of freedom from the electronic ones (Born-Oppenheimer approximation), spin-orbit coupling and scalar relativistic contributions.[47,48]. The inter-electronic interaction term in the Hamiltonian couples the degrees of freedom of all N electrons. This makes an analytical solution impossible for all but hydrogen atom like systems[49]. The problem is not that we lack the mathematical adroitness to figure out a clever analytical solution but that the inherent structure of the model is such that the terms in the operator are defined in terms of the solution of that operator - i.e. we need one to get the other. A conventional approach used to solve such problems is through self-consistent iterations starting from a good initial guess[50]. In this case, the exact wave function is expressed as an optimal linear combination of all possible electronic configurations that span the same Hilbert space as the wave function. These configurations can be represented by occupation number vectors (ONVs) in the second quantization formalism.[51,52] For a system with M electrons and N spin orbitals an example of a single ONV would be

$$|\mathbf{k}\rangle = |\underbrace{1,1,...,1}_{1,2,...,M}\underbrace{,0,0,0,...0}_{M+1,...,M}\rangle \tag{1.1}$$

where the 1s indicate that orbitals 1 through M are occupied and the 0s indicate that orbitals M+1 through N are unoccupied.[48]. Figure 1.1 shows all singlet configurations of two electrons occupying four spin orbitals. With each spin orbital having two possible occupation numbers, a space having N spin orbitals has 2^N possible basis vectors. Out of

which only $\binom{N}{M}$ have a total of M electrons. The exact wave function, $|\psi\rangle$, can then be

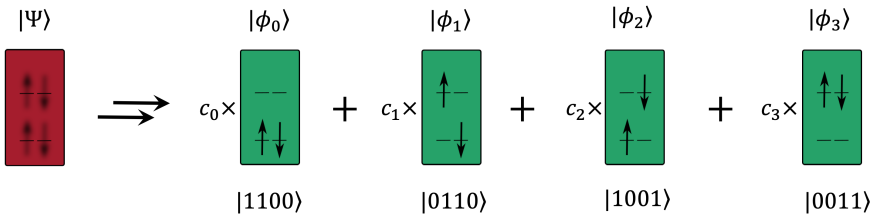

Figure 1.1: The exact wave function (in brown) of 2 electrons in 4 spin orbitals is a linear combination (with coefficients c_i of all the configurations (in green). The ONVs of each configuration are printed below.

written as a linear combination of these ONVs.

$$|\psi\rangle = \sum_{\mathbf{k}} c_k |\mathbf{k}\rangle \tag{1.2}$$

where c_k is the contribution of each configuration. The expression in equation 1.2 indicates that exact wave functions can be obtained by calculating the coefficients c_k for all possible configurations. We can obtain these 'best' set of coefficients using the variational principle [48] which states that the exact solution will be a stationary point (unchanged by first order perturbations) of the expectation value of the energy. In other words, the coefficients should be optimized to get lowest possible value for the energy E.

$$E = min_{\{c_k\}} \frac{\langle\psi|\hat{H}|\psi\rangle}{\langle\psi|\psi\rangle} \tag{1.3}$$

Generally, more the configurations, more is the variational freedom enjoyed by the system resulting in a better solution. If all possible configurations in a given set of orbitals are considered, the solution is called a full configuration interaction (FCI) wave function [48]. In order to systematically enumerate all these configurations, they are categorized based on how different they are compared to a reference. The reference configuration is typically

chosen to be the one that has the N lowest energy spin orbitals occupied by the N electrons. The configurations that can be obtained by moving one electron from an occupied to an unoccupied orbital are classified as singly excited. The ones that have two electrons moved into unoccupied orbitals are called doubly excited and so on. It is to be noted that the term 'excited' is not used in a strict spectroscopic sense but only because it appears like the electron has 'excited' from a lower orbit to a higher one. It is generally true that the lower order excitations have higher contributions compared to the higher order ones[53].

The formal and conceptual simplicity of this approach, however, belies the difficulty in its application even to moderately large systems[54]. The number of configurations to be considered for a FCI solution increases factorially with the size of the system. In most cases the vast majority of the configurations contribute very little to the wave function. This allows us to come up with more affordable and yet reliable approaches if we identify the important configurations over the 'deadwood'.[55]

One of the first and the simplest approaches - the Hartree-Fock method - expresses the wave function only as a single configuration and accounts for the electronic interaction by approximating it as an effective mean field. While this model does a reasonable job in some cases, it fails to account for some key aspects of the electron interactions. These effects that it fails to capture are generally defined as electron correlation[56]. It is useful to quantify the severity of the HF approximation using the correlation energy E_{corr} which is formally defined as the difference between the exact energy and the HF energy[56]

$$E_{\text{corr}} = E_{\text{exact}} - E_{\text{HF}} \tag{1.4}$$

All the various post-HF methods try to approximate this E_{corr} in various ways. The correlation energy recovered by any other method is similarly defined as the difference between its energy and E_{HF}. This will be smaller in magnitude than the total E_{corr} for all post-HF variational wave function methods. The correlation energy is further classified in two concep-

tual types, dynamic and static correlation, based on two reasons why the HF energy is higher than the exact one. The first reason is the treatment of inter-electronic interactions using a mean field and the lack of explicit interaction between all electron pairs. This effect is called the dynamic correlation. The second reason is the description of the wave function using only a single configuration rather than as a linear combination of multiple configurations. The effect of this often termed as static correlation. There exists, however, no clear way to isolate the effects of either of these types of correlations - i.e. we cannot rigorously quantify the energy contribution of each type of correlation separately. Any conceptual distinction between the two is made even more ambiguous by noting that the recipe to account for more static and dynamic correlation is to express the wave function in terms of more electronic configurations. This distinction, however, useful to understand the performance of some methods and to improve them in systematic ways. Often some methods are referred to as capturing static correlation or others include more dynamic correlation. This description, though not formal, is useful in deciding which methods should be uses in which case and what can be done to improve it.

CASSCF, a method which aims at capturing significant static correlation, is a middle ground between expressing the wave function using all the configurations (like FCI) and expressing it with only one of them. In CASSCF specific orbitals selected by the user are allowed to have variable occupancies (different than those in the HF wave function) and all possible excitations within those orbitals are allowed. An active space of N_e electrons in N_o orbitals is commonly reported using the compact notation (N_e, N_o). Figure 1.2 shows a schematic of the differences in the HF, CASSCF and FCI methods.

The wave function is expressed as

$$|\psi_{CASSCF}\rangle = \exp(-\hat{\kappa}) \sum_i C_i \, |\mathbf{k}_i\rangle \tag{1.5}$$

The operator $\exp(-\hat{\kappa})$ performs a unitary transformation among the spin orbitals to obtain

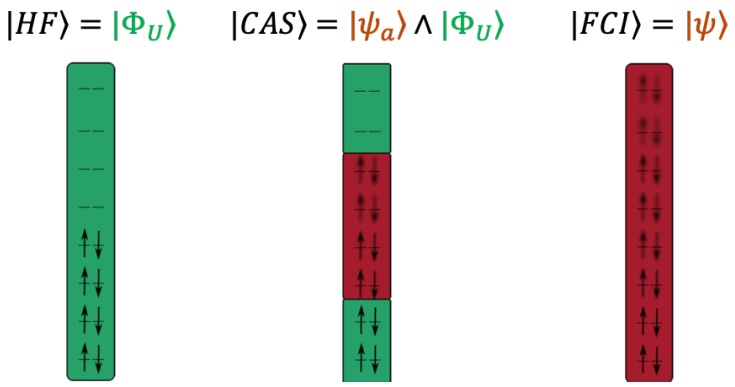

Figure 1.2: Schemes of wave function methods: The HF method (left) has only one electronic configurations with orbitals having fixed integer occupancy (shown in green and with clear arrows). The FCI (right) is a weighted average over all possible configurations with none of the orbitals having fixed integer occupanices (shown in brown and with blurred arrows). The CASSCF in the middle has a subspace with FCI within it (blurred arrows) with the rest similar to HF with clear arrows.

the optimal set of orbitals and expansion coefficients, C_i, are normalized to unity. The wave function is optimized variationally by self-consistently improving the orbital rotation operator $\exp(-\hat{\kappa})$ and the contributions $\{C_i\}$ of the configurations.

CASSCF calculations are well suited to obtain a good multiconfiguration wave functions and thus capture a significant amount of static correlation. This is necessary to describe systems where there is degeneracy or low-lying unoccupied orbitals like in case of a homolytically cleaved bond or a transition metal with a partially filled d-shell etc. In its extreme limit where all orbitals are active and all electrons are included, we reach the FCI limit. The objective, then, is to use the smallest possible number of active orbitals that capture as much static correlation as possible. Since the results depend significantly on the choice of the active orbitals, which is a choice made by the user, this method demands a certain level of expertise from the user. Efforts to establish a standard programmable protocol for choosing these active spaces, not only for CASSCF but for other such methods too, is an active field of research [57–59]. Various techniques have been used to overcome or avoid this

exponential scaling of the computational cost with respect to the active space. The restricted and generalized active space (RAS[60,61] and GAS[62]) approaches consider only a subset of the configurations from CASSCF by classifying the active orbitals in subspaces based on chemical information. In RAS, orbitals that are expected to be 'mostly' occupied or 'mostly' unoccupied are categorized in spaces from which the user control the maximum number of holes and electrons respectively. In the GAS method multiple sub-spaces are defined by the user such that all possible excitations are considered within the subspaces and only a few (if any) excitations across the subspaces are considered. Methods like occupation-restricted multiple active space (ORMAS)[63], generalized valence bond (GVB)[64,65], separated pair (SP) approximation[66] also reduce the number of configurations using chemical knowledge of the orbitals. These approaches, while more affordable than CASSCF, still do not overcome the exponential scaling completely and cannot be applied to cases where the user defined chemical intuition is unreliable. Methods like the density matrix renormalization group (DMRG)[67], doubly occupied configuration interaction[68,69], and active-space two-electron reduced-density-matrix[70] methods scale polynomially.

Even for the multireference calculations performed with these methods, where the number active orbitals and electrons are significantly smaller than those required to reach a FCI limit, dynamic correlation is still, for the most part, unaccounted for. Multireference many-body perturbation theory has been a popular technique to compute the additional (dynamic) correlation energy beyond that of the multireference wave functions - particularly the complete active space second-order perturbation theory (CASPT2) and n–electron valence state second-order perturbation theory (NEVPT2). These methods, however, scale poorly with the size of the system and thus are too expensive for large systems. A recent alternative to these methods is the multiconfiguration pair-density functional theory.[30,31]. This method blends multiconfiguration wave function theory and density functional theory in order to quantitatively model the static and dynamic correlation. The Kohn–Sham density func-

tional theory[23,24] that uses a single Slater determinant to represent the electron density is not appropriate for inherently multireference systems. While the use of broken symmetry Slater determinants with approximate density functionals can sometimes predict reasonable energies, the solutions are unphysical and cannot be interpreted easily. This motivates the need for MC-PDFT that uses the physically sound multireference wave functions. This methods takes the kinetic energy, total electron density (the probability density of finding an electron at a point in space) and the on-top pair density (the probability density of finding two electrons at a point in space) from the reference wave function. These serve as inputs to an 'on-top' functional that gives the total energy of the system. It is worth noting that unlike perturbation theory that calculates a correction to the total energy, MC-PDFT recomputes the total energy based on the density and pair density. PDFT has been shown to be applicable and effective in many applications for calculating both ground- and excited-state properties including potential energy curves[30], main-group bond energies,[66,71] chemical reaction barrier heights,[72] charge-transfer complexes[32], atomic and molecular excitation energies[30,73,74]

CHAPTER 2

THE VARIATIONAL LOCALIZED ACTIVE SPACE SELF-CONSISTENT FIELD METHOD

2.1 Introduction

Current targets of quantum chemical simulation such as lanthanide/actinide-ligand complexes[75–77] and metal-organic frameworks,[78–83] frequently contain a large number of strongly-correlated electronic degrees of freedom in their wave functions, which renders traditional multiconfiguration self-consistent field (MC-SCF) approaches like the complete active space self-consistent field (CASSCF) method[18] problematic due to the factorial explosion of the computational cost of the latter with respect to the size of the active space. However, in many of these systems, the strongly-correlated electronic degrees of freedom are centered around separable units, for example distant transition metal nuclei[2] or weakly-entangled monomers,[84] and a low-scaling local correlation[85] or fragmentation[86] approach to the MC-SCF framework may generate realistic chemical models.

Along these lines, we recently introduced the localized active space self-consistent field (LASSCF) method[1] for strongly-correlated systems characterized by weakly-entangled subunits. LASSCF was originally conceived as a generalization of density matrix embedding theory (DMET),[87–90] but unlike the latter, LASSCF generates a true wave function for the whole molecule and provides an upper bound to CASSCF and full configuration interaction (FCI) energies. LASSCF produces a localized active space (LAS) wave function, which is an approximation to a CASSCF wave function in which the active space is split into one or more non-overlapping, unentangled subspaces. This approximation to CASSCF eliminates the inherent factorial operation and storage cost explosion with increasing system size that is associated with handling a single configuration interaction (CI) vector spanning a direct-product basis of orbitals. Initial tests of LASSCF showed that it reproduces the

results of comparable CASSCF calculations, as long as the strong electron correlation of the test system was localized and short-range; whereas the more general DMET method using a CASSCF solver fails dramatically.[1] Further tests showed that LASSCF is an attractive alternative to CASSCF in determining spin-state energy ladders for organometallic compounds, especially multinuclear compounds.[2]

Equivalents to the LAS ansatz have been explored before in the literature. For example, the LAS wave function can be understood as a form of the cluster mean-field wave function explored by Jiménez-Hoyos and Scuseria in the context of 1D or 2D Hubbard model systems,[91] or as a "rank-one basis state" defined by Nishio and Kurashige in their studies of molecular aggregates,[84] or as the bond dimension = 1 case of an active-space decomposition (ASD) wave function[92–95] obtained using the density matrix renormalization group (DMRG) extension.[96] Among these works, the cluster mean-field method described in Ref. 91 and the *ad hoc* protocol employed for one particular test system in Ref. 84 are variational. All others leave the orbitals, CI vectors, or both constrained indirectly by orbital localization schemes in one way or another. When the orbitals are variationally optimized,[84,95] the authors tend to utilize a standard CASSCF orbital-optimization algorithm, which is mature[18,97] with many acceleration schemes and approximations to the general second-order approach having been explored.[98–104]

LASSCF as explored in Refs. 1 and 2 is not truly variational in the sense that not all of its wave function parameters minimize the energy. One consequence of this is that analytical molecular gradients are less straightforward to implement. Although analytical gradients are usually still possible, by using, for instance, Lagrange's method of undetermined multipliers,[105] this requires that the method be represented as a constrained energy minimization. In the case of LASSCF, the constraints on the orbital optimization are provided indirectly by the initial guesses for the active orbitals as well as the orbital-localization scheme used to split the atomic orbital (AO) space of the molecule into non-overlapping fragments. Strong

dependence of total energies and other observables on these initialization parameters is observed even for systems with only one physically reasonable state. Not only does this make the implementation of analytical molecular gradients more problematic, it impairs the reproducibility of total energies and density matrices calculated with the LASSCF method. Initial guess states are manifold, especially in the field of MC-SCF calculation, where workers are accustomed to exploring a wide variety of *ad hoc* protocols for generating initial guesses in the pursuit of elusive states;[101,106–109] a useful MC-SCF method should depend on the initial guess only inasmuch as the choice of the guess should allow the user to select a desired state from among a finite number of energy minima in the wave function parameter space.

Further steps in reference 46 developed an algorithm of LASSCF which fully minimizes the energy with respect to all possible transformations of the orbitals and CI vectors of a LAS wave function. This extension improves the robustness and reproducibility of the LAS wave function and energy, makes the method energetically equivalent to CASSCF and Hartree–Fock (HF) in the limits respectively of one active subspace and one determinant in the active superspace, and does not incur substantial additional computational cost. In this chapter, we compare the the performance of these algorithms with respect to the CASSCF reference. When comparing the two versions of the LASSCF, the one that fully minimizes the energy is referred to as "variational LASSCF" or vLASSCF in order to distinguish it from the method described in Ref. 1. In subsequent chapters, however, vLASSCF replaces LASSCF entirely- i.e. only the algorithm that minimize the total energy is used and thus the preceding 'v' is dropped.

2.2 Theory

The formulation of LASSCF is motivated by the observation that static correlation is often localized on different parts of the molecule. The corresponding wave function and energy

are defined as

$$|\mathrm{LAS}\rangle = \left(\bigwedge_K |\Psi_K\rangle\right) \wedge |\Phi_D\rangle\,, \tag{2.1}$$

$$E_{\mathrm{LAS}} = \langle \mathrm{LAS}|\hat{H}|\mathrm{LAS}\rangle\,, \tag{2.2}$$

where $\hat{H}$ is the standard molecular Hamiltonian, $|\Psi_{A_K}\rangle$ is a general correlated state describing N_{A_K} electrons occupying the M_{A_K} active orbitals ($|a_{Kn}\rangle$) of the Kth fragment, and $|\Phi_D\rangle$ is a single determinant of doubly-occupied inactive orbitals ($|d_n\rangle$).

2.2.1 Obtaining the LAS wave function

A LASSCF calculation requires the user to categorize the atoms of the molecule into fragments and provide an initial guess for the active orbitals and size of each subspace. The active orbitals of each subspace are expected to be localized on these fragment atoms in the converged LAS wave function. In order to obtain the many-body wave functions of the subspaces using existing electronic structure codes, we need to construct an effective Hamiltonian for each fragment. The "fragment orbitals" (indicated by f) are obtained by orthogonalizing the atomic orbital basis (using the meta-Löwdin method[110,111]) and then grouping the orthogonalized AOs of the atoms assigned to each fragment. These orbitals by themselves, however, are not sufficient to define a physical wave function since they are entangled to other orbitals in the system - as underscored by the observation that the fragment orbital space does not even have an integer number of electrons. This space needs to be augmented by including all the entangled orbitals in order to have a well-defined wave function of its own. This collective space is called the impurity space (indicated by i). The impurity orbitals are obtained by combining M_{F_K} "fragment" orbitals with up to M_{F_K} entangled partner orbitals *via* the Schmidt decomposition [i.e., singular value decomposition

(SVD) of the density matrix]:[112,113]

$$\left(1 - c^{p_1}_{f_{K1}} c^{f_{K1}}_{p_2}\right) D^{p_2}_{f_{K2}} = \sum_{p_3}^{M_{F_K}} u^{p_1}_{p_3} \sigma_{p_3} v^{f_{K2}}_{p_3}, \tag{2.3}$$

$$\{|f_{Kn}\rangle\} \cup \left\{|p_1\rangle\, u^{p_1}_{p_3}\right\} \rightarrow \{|i_{Kn}\rangle\}, \tag{2.4}$$

where p belongs to a general molecular orbital space, $c^{p_1}_{f_{K1}}$ is an element of a unitary transformation matrix between fragment orbitals and some general set of molecular orbitals, and only the left-singular vectors ($u^{p_1}_{p_3}$) corresponding to nonzero singular values (σ_{p_3}) are retained. The role of the Schmidt decomposition is to augment the fragment orbitals, which are entangled to the rest of the molecule and cannot be assigned a wave function on their own, with additional degrees of freedom that account for all entanglement and therefore ensure that the impurity space is occupied by an integer number of electrons;[87,88] this allows Eq. (2.6) to be solved with standard implementations of CASSCF.[1] The fragment orbitals themselves are non-overlapping sets of localized orbitals which collectively span the whole AO space and which each must enclose at most exactly one set of active subspace orbitals:

$$\sum_{f_{L1}} |\langle a_{K1}|f_{L1}\rangle|^2 = \delta_{KL}, \tag{2.5}$$

The fragment orbitals are chosen to resemble a set of orthogonalized AOs as closely as possible while satisfying Eq. (2.5). The LASSCF method obtains |LAS⟩ (as defined in eq. 2.1) in several overlapping sets of impurity orbitals ($|i_{Kn}\rangle$):

$$|\Psi_{A_K}\rangle = \underset{|\Psi_{A_K}\rangle}{\operatorname{argmin}} \left(\min_{|\Phi_{I_K}\rangle} \langle\Phi_{I_K}| \wedge \langle\Psi_{A_K}|\hat{H}_{I_K}|\Psi_{A_K}\rangle \wedge |\Phi_{I_K}\rangle \right). \tag{2.6}$$

where $|\Phi_{I_K}\rangle$ is a single determinant of doubly-occupied linear combinations of impurity orbitals, and the impurity Hamiltonian ($\hat{H}_{I_K}$) is

$$\begin{aligned}\hat{H}_{I_K} &= \left(h^{i_{K1}}_{i_{K2}} + \{v^{(jk)}_\sigma\}^{i_{K1}}_{i_{K2}} - \{v^{(\mathrm{self})}_\sigma\}^{i_{K1}}_{i_{K2}}\right) \hat{a}^\dagger_{i_{K1}\sigma}\hat{a}_{i_{K2}\sigma} \\ &\quad + \frac{1}{2} g^{i_{K1}i_{K3}}_{i_{K2}i_{K4}} \hat{a}^\dagger_{i_{K1}\sigma}\hat{a}^\dagger_{i_{K3}\tau}\hat{a}_{i_{K4}\tau}\hat{a}_{i_{K2}\sigma}, \end{aligned} \tag{2.7}$$

omitting an irrelevant constant, where

$$\{v^{(jk)}_\sigma\}^{\mu_1}_{\mu_2} = g^{\mu_1\mu_3}_{\mu_2\mu_4} D^{\mu_3}_{\mu_4} - g^{\mu_1\mu_3}_{\mu_4\mu_2}\{\gamma_\sigma\}^{\mu_3}_{\mu_4}, \tag{2.8}$$

$$\{v^{(\mathrm{self})}_\sigma\}^{i_{K1}}_{i_{K2}} = g^{i_{K1}i_{K3}}_{i_{K2}i_{K4}} D^{i_{K3}}_{i_{K4}} - g^{i_{K1}i_{K3}}_{i_{K4}i_{K2}}\{\gamma_\sigma\}^{i_{K3}}_{i_{K4}}, \tag{2.9}$$

and where $\hat{a}^\dagger_{i_{Kn}\sigma}$ ($\hat{a}_{i_{Kn}\sigma}$) creates (annihilates) an electron at the i_{Kn}th orbital with spin σ, h and g are respectively the one- and two-electron molecular Hamiltonian matrix elements, D and γ_σ are respectively the spin-summed and spin-separated one-body reduced density matrices (1-RDMs; $D = \gamma_\uparrow + \gamma_\downarrow$), and we again sum over repeated internal indices including the spin indices σ and τ (which take the values $\uparrow$ and $\downarrow$), but not the fragment subindices K [e.g., i_{K3} in Eq. (2.9) ranges over the impurity orbitals of the Kth subspace only]. Since the active orbitals in each impurity interact with all other active subspaces through this mean field, the LAS wave function is simultaneously equivalent to the wave function in the impurity space at convergence. In a single cycle of the LASSCF iteration, Eqs. (2.3)–(2.9) are used for each fragment to obtain an updated guess for the active orbitals and CI vectors. The active orbitals will tend to develop nonzero overlaps across fragments from being optimized asynchronously and must be explicitly orthogonalized once per cycle. They are then frozen along with the CI vectors while the whole-molecule inactive orbitals ($|d_n\rangle$) are optimized. The cycle repeats until fragment orbitals, density matrices, and energies stop changing.

2.2.2 LASSCF and spin

The standard (nonrelativistic) molecular Hamiltonian commutes with both $\hat{S}^2$ and $\hat{S}_z$, and so the corresponding exact wave functions can always be represented as eigenstates of these two operators,

$$\hat{S}^2 |\Psi\rangle = s(s+1) |\Psi\rangle , \tag{2.10}$$

$$\hat{S}_z |\Psi\rangle = m_s |\Psi\rangle , \tag{2.11}$$

with half-integer quantum numbers s denoting the magnitude and $-s \leq m_s \leq s$ the projection onto the z-axis of the total spin angular momentum.

The many-electron spin operators are

$$\begin{aligned} \hat{S}^2 &= \hat{S}_x^2 + \hat{S}_y^2 + \hat{S}_z^2 \\ &= \hat{S}_z^2 + \frac{1}{2}\left(\hat{S}_+\hat{S}_- + \hat{S}_-\hat{S}_+\right), \end{aligned} \tag{2.12}$$

$$\hat{S}_x = \frac{1}{2}\left(\hat{S}_+ + \hat{S}_-\right), \tag{2.13}$$

$$\hat{S}_y = \frac{1}{2i}\left(\hat{S}_+ - \hat{S}_-\right), \tag{2.14}$$

where, in second quantization,

$$\hat{S}_z = \frac{1}{2}\sum_p \left(\hat{a}_{p\uparrow}^\dagger \hat{a}_{p\uparrow} - \hat{a}_{p\downarrow}^\dagger \hat{a}_{p\downarrow}\right), \tag{2.15}$$

$$\hat{S}_+ = \sum_p \hat{a}_{p\uparrow}^\dagger \hat{a}_{p\downarrow}, \tag{2.16}$$

$$\hat{S}_- = \sum_p \hat{a}_{p\downarrow}^\dagger \hat{a}_{p\uparrow} = \left(\hat{S}_+\right)^\dagger, \tag{2.17}$$

The LAS wave function is obtained by constrained energy minimization [i.e., constrained to the functional form of Eq. (2.1)], which inherently introduces the possibility of unphysical

symmetry breaking.[114] The individual factors of $|\mathrm{LAS}\rangle$ all satisfy both Eqs. (2.10) and (2.11) so long as spin-restricted, RHF-type orbitals and a spin-symmetry-observing FCI solver are used:

$$\hat{S}^2 |\Psi_{A_K}\rangle = s_K(s_K+1) |\Psi_{A_K}\rangle , \tag{2.18}$$

$$\hat{S}_z |\Psi_{A_K}\rangle = m_{s_K} |\Psi_{A_K}\rangle , \tag{2.19}$$

$$\hat{S}^2 |\Phi_D\rangle = \hat{S}_z |\Phi_D\rangle = \hat{S}_+ |\Phi_D\rangle = \hat{S}_- |\Phi_D\rangle = 0. \tag{2.20}$$

Since $\hat{S}_z$ is a one-electron operator which is diagonal in any orbital basis [Eq. (2.15)], $|\mathrm{LAS}\rangle$ itself also satisfies Eq. (2.11):

$$\hat{S}_z |\mathrm{LAS}\rangle = \left(\sum_K m_{s_K} \right) |\mathrm{LAS}\rangle = m_s |\mathrm{LAS}\rangle , \tag{2.21}$$

but since $\hat{S}^2$ is a non-local two-electron operator, which contains linked excitations across active subspace parts which describe coupled spin-flips [compare the second line of Eq. (2.12) to Eqs. (2.16) and (2.17)], $|\mathrm{LAS}\rangle$ itself does not generally satisfy Eq. (2.10).

To evaluate the amount of spin contamination in a LAS wave function (using RHF-type orbitals), let us separate the generators $\hat{S}_z$, $\hat{S}_+$, and $\hat{S}_-$ into terms addressing each active subspace as

$$\hat{S}_z^{(K)} = \frac{1}{2} \sum_{a_{K1}} \left(\hat{a}^\dagger_{a_{K1}\uparrow} \hat{a}_{a_{K1}\uparrow} - \hat{a}^\dagger_{a_{K1}\downarrow} \hat{a}_{a_{K1}\downarrow} \right) , \tag{2.22}$$

$$\hat{S}_+^{(K)} = \sum_{a_{K1}} \hat{a}^\dagger_{a_{K1}\uparrow} \hat{a}_{a_{K1}\downarrow}, \tag{2.23}$$

$$\hat{S}_-^{(K)} = \sum_{a_{K1}} \hat{a}^\dagger_{a_{K1}\downarrow} \hat{a}_{a_{K1}\uparrow}, \tag{2.24}$$

with $\hat{S}_z = \sum_K \hat{S}_z^{(K)}$, etc., and the inactive electrons can be ignored because of Eq. (2.20).

Then, for the expectation value of the total spin magnitude, we have

$$\langle \hat{S}^2 \rangle \;=\; \sum_{K,L} \left(\langle \hat{S}_z^{(K)} \hat{S}_z^{(L)} \rangle + \frac{1}{2} \langle \hat{S}_+^{(K)} \hat{S}_-^{(L)} \rangle + \frac{1}{2} \langle \hat{S}_-^{(K)} \hat{S}_+^{(L)} \rangle \right), \tag{2.25}$$

where $\langle \hat{O} \rangle \equiv \langle \mathrm{LAS} | \hat{O} | \mathrm{LAS} \rangle$. The diagonal case of the sum in Eq. (2.25), $K = L$, clearly corresponds to the total spin eigenvalue for the Kth active subspace, $s_K(s_K+1)$. For the off-diagonal case, the second and third terms in the summand vanish because they correspond to the above-mentioned linked double excitations which are excluded by construction from $|\mathrm{LAS}\rangle$, but the first term survives because each active subspace part is individually an eigenstate of $\hat{S}_z$. Therefore Eq. (2.25) simplifies to

$$\langle \hat{S}^2 \rangle \;=\; \sum_K s_K(s_K+1) + \sum_{K \neq L} m_{s_K} m_{s_L}, \tag{2.26}$$

which should be compared to $m_s(m_s+1)$ to evaluate the amount of spin contamination.

There are a number of ways in which the limitations of the LAS wave function in the context of spin symmetry might be addressed. Just as a small number of ROHF-type single determinants with the same electron configuration and same total m_s can be combined with Clebsch-Gordan coefficients to construct CSFs with good spin magnitude quantum numbers, $s \geq |m_s|$,[97] so too can LAS states with the same set of s_K and same total m_s but different individual m_{s_K} be combined to construct post-LAS states with good s. This is what is done in, for instance, Nishio and Kurashige's study[84] of "rank-one basis states" (= $|\mathrm{LAS}\rangle$ states). It preserves the total spin quantum numbers of the individual subspaces, s_K, although the corresponding spin orientations, m_{s_K}, are no longer good quantum numbers. It is also possible to generalize in the other direction, deliberately lifting spin symmetries by utilizing spin orbitals of the generalized-Hartree–Fock (GHF)[115] or unrestricted-Hartree–Fock (UHF) type in vLASSCF calculations. The advantage of this is that, in principle, local spin orientations (m_{s_K}) and/or spin magnitudes (s_K) no longer need to be specified by the user

but can be directly explored by the variational protocol itself. However, this sacrifices the corresponding whole-molecule quantum numbers, m_s and/or s, and the processes of evaluating spin contamination and restoring spin symmetry are more computationally involved.[116] A third approach is to use the LAS states themselves as a diabatic basis[93,94] in which to directly evaluate Hamiltonian matrix elements for characterizing charge transfer or spin-spin interactions. This last approach, which is specially facilitated by the LAS form of the wave function, is attractive from the point of view of chemical interpretation and intuition.

2.3 Results and Discussion

All electronic structure calculations, including the impurity model CASSCF steps [Eq. (2.6)] carried out within LASSCF and vLASSCF, were performed using PySCF version 1.7.0a.[111] We implemented LASSCF and vLASSCF in the *mrh* software package.[117] The testbed systems we use to explore vLASSCF are depicted in Fig. 2.1. The equilibrium geometries of test systems labeled a), b), c) were obtained respectively from Refs. 1, 2, and 118. In the case of system c), we replaced each amino ligand of the structure in Ref. 118 with ammonia and optimized the geometry of the ammonia hydrogens (with all other atoms frozen) with spin-unrestricted Kohn-Sham density functional theory in the septet spin state using the M06-L exchange-correlation functional[28], the Def2-TZVP basis set[119,120] and SDD[121] pseudopotential for the transition metal atoms, and the Def2-SVP basis set for all other atoms. For the LASSCF and vLASSCF calculations of system a), we used 6-31G; for system b), 6-31G(d), and for system c), cc-pVDZ.[122,123] The purpose to study systems a) was to explore how well the vLASSCF wave function can reproduce the CASSCF wave function.

2.3.1 Bisdiazene double-double bond dissociation potential energy curve

The bisdiazene [system a) in Fig. 2.1] was partitioned into fragments and assigned active subspaces as in Ref. 1: two fragments consisting of the pairs of nitrogen bonds and their

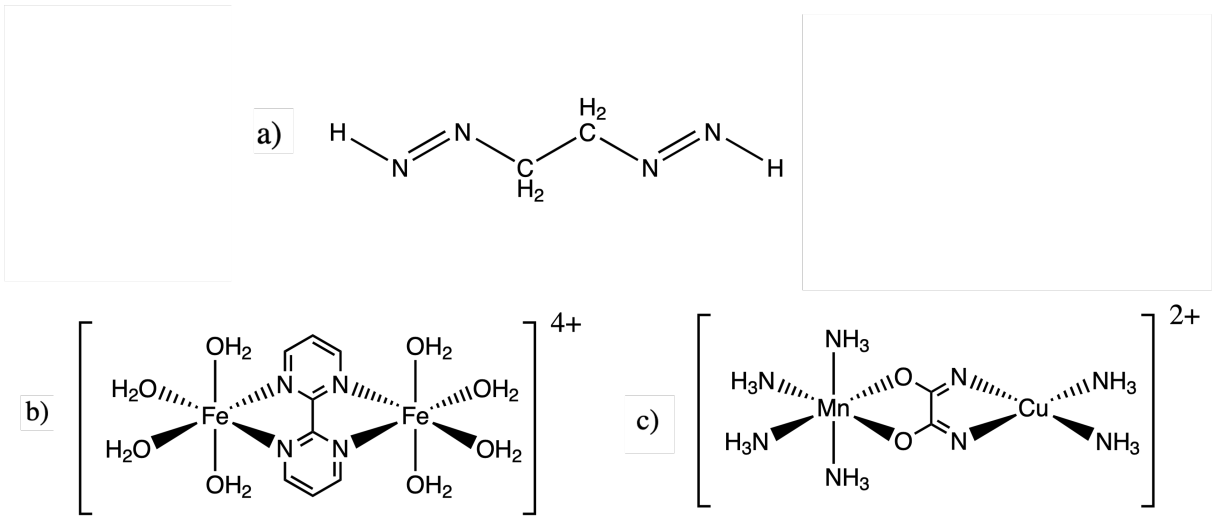

Figure 2.1: Test systems: a) 2-diazenylethyldiazene ("bisdiazene"), model bimetallic compounds b) $[Fe(H_2O)_4]_2$bpym^{4+}, and c) $[Mn(NH_3)_4]$oxamide$[Cu(NH_3)_2]^{2+}$.

terminal hydrogens, and one fragment consisting of the central C_2H_4 unit. Active spaces of (4,4) were assigned to the terminal diazene fragments and no active space was assigned to the central unit, for an overall CAS of (8,8). The potential energy surface was scanned along the simultaneous stretching coordinate of the two N=N double bonds from the reference equilibrium geometry, which is reported in Ref. 1.

Figure 2.2 shows the difference between the LASSCF and vLASSCF energies and the CASSCF reference along this potential energy curve. Because there are two active subspaces with non-trivial wave functions, LAS and CAS wave functions are not formally equivalent. Nevertheless, because the two active subspaces are physically separated and not entangled (e.g., *via* a connecting π-orbital system), the LAS wave function is only a mild approximation to the CAS wave function. For this reason, both LASSCF and vLASSCF predict total electronic energies within a few mE_h throughout most of the potential energy surface. However, the LASSCF potential energy curve is significantly less smooth (as well as everywhere higher) than the vLASSCF potential energy curve. Near the equilibrium geometry, the curve is reasonably smooth, but past $R_{\mathrm{N=N}} = 3.0$ Å, it becomes highly erratic and discontinuous, despite the fact that orbitals from converged LASSCF calculations at one point were used

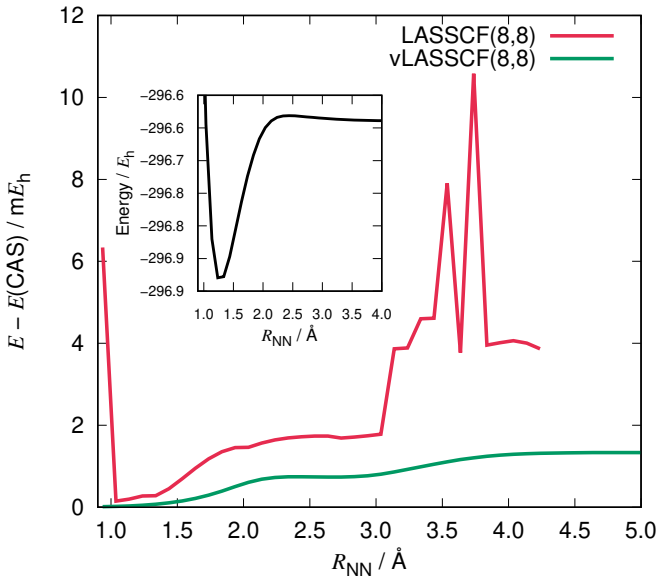

Figure 2.2: Energy difference between LASSCF(8,8), vLASSCF(8,8), CASSCF(8,8) models of bisdiazene in the 6-31G basis across the simultaneous nitrogen-nitrogen double-bond dissociation coordinate. The LASSCF data is taken from Ref. 1. Inset: the CASSCF(8,8)/6-31G potential energy curve.

to initialize calculations at another point only 0.1 Å further out or in. The discontinuities in the LASSCF curve demonstrate the consequences of the use of ill-defined, self-referential constraints in variational optimizations.

The vLASSCF extension entirely cures these defects of the LASSCF potential energy curve. Three regions are visible, corresponding to 1) the neighborhood of the equilibrium geometry, where the molecule is weakly correlated and vLASSCF and CASSCF are nearly indistinguishable, 2) a plateau at about $E_\mathrm{LAS} - E_\mathrm{CAS} = 0.7$ mE_h near the potential energy maximum along the dissociation coordinate, and 3) a second plateau of about 1.3 mE_h in the dissociation limit (confirmed out to $R_\mathrm{N{=}N} \approx 100$ Å). The transition between the first plateau and the second corresponds to the transition in the character of the CASSCF natural orbitals between pairs of bonding and anti-bonding σ and π orbitals at shorter distances, and isolated nitrogen p orbitals with more entanglement across the central fragment at longer distances, as depicted in Fig. 2.3. In the first plateau, around $R_\mathrm{N{=}N} = 2.5$ Å, the natural

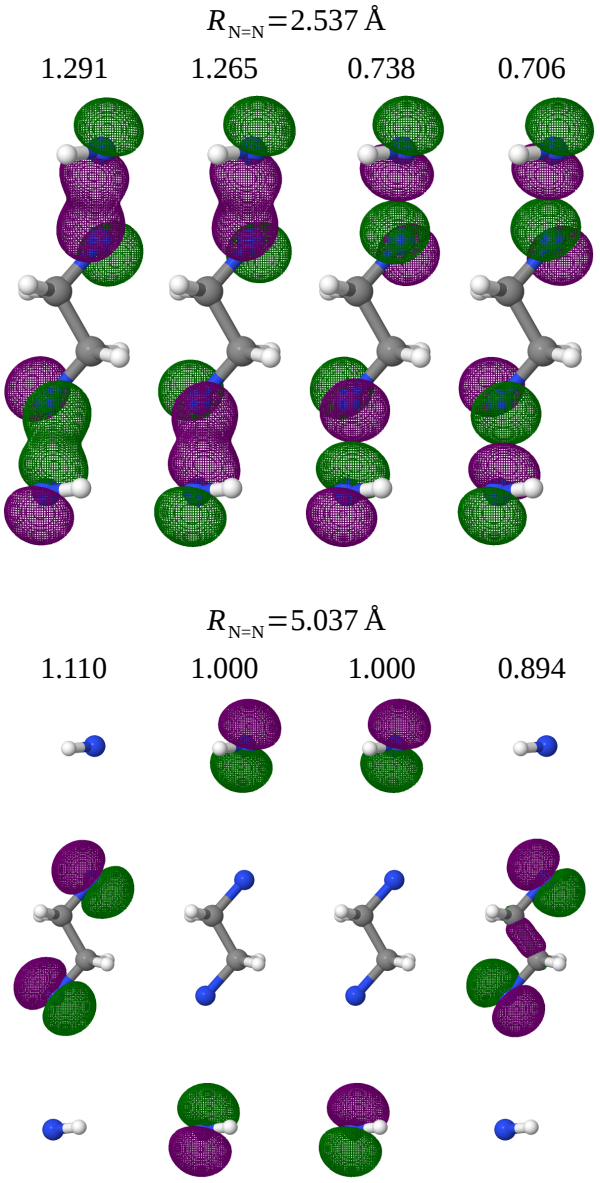

Figure 2.3: Selected CASSCF(8,8)/6-31G natural orbitals and their occupancies for bisdiazene at two geometries along the simultaneous nitrogen-nitrogen double-bond dissociation coordinate.

orbitals consist of four pairs of bonding and anti-bonding orbitals with NO occupancies differing by 0.03 to 0.04 between the in-phase combination (first and third orbitals in the top row of Fig. 2.3) and the out-of-phase combination (second and fourth). On the other hand, in the dissociation limit, one pair of CASSCF natural orbitals consist of the in-phase and out-of phase combinations of two nitrogen atom p orbitals in the two different fragments, with a difference in natural occupancies of more than 0.2. This greater difference in natural-orbital occupancies implies greater entanglement, and consequently that localization and approximation as unentangled fragments is a slightly more severe approximation in the latter case than in the former, corresponding to an additional variational penalty of about 0.6 mE_h.

2.3.2 Spin-state energy gaps of bimetallic compounds

Systems b) and c) of Fig. 2.1 are bimetallic complexes in which the electrons occupying the 3d-orbitals of the iron atoms can be characterized by their local spin. However, the CASSCF wave function obscures this information, whereas the LAS formalism makes it straightforward to explore, albeit by requiring the user to manually explore different local-spin states. The LASSCF and vLASSCF calculations reported in this section assigned each metal atom an active subspace consisting of the 3d orbitals and their corresponding electrons. The electron configurations of the iron, manganese, and copper atoms are respectively [Ar]3d^6, [Ar]3d^5, and [Ar]3d^9, corresponding to (6,5), (5,5), and (1,1) active subspaces respectively (the last is energetically equivalent to, and more computationally efficient than, specifying (9,5) because the wave function in a (9,5) active space will always be single-determinantal in the natural-orbital basis due to particle-hole symmetry). The corresponding CASs for these two molecules are respectively (12,10) and (6,6). The vLASSCF energies of the high-spin nonet and several quasi-singlet states for system b) are reported in Table 2.1 and compared to CASSCF and LASSCF energies previously reported in Ref. 2. Here those energies are

Table 2.1: Spin states energies (eV) of system b) ($[Fe(H_2O)_4]_2bpym^{4+}$) at the CASSCF, LASSCF, and vLASSCF levels relative to the CASSCF singlet energy, as well as the spin contaminations ($\langle\hat{S}^2\rangle_{\rm LAS} - \langle\hat{S}^2\rangle_{\rm CAS}$) of the LASSCF and vLASSCF wave functions. The CASSCF and LASSCF results are from Ref. 2.

s	m_{s_1}	m_{s_2}	$E_{\rm CAS}$	$E_{\rm LAS}$	$E_{\rm vLAS}$	$\langle\hat{S}^2\rangle_{\rm LAS} - \langle\hat{S}^2\rangle_{\rm CAS}$
4	2	2	0.00040	0.06443	0.00040	0
0	2	-2		0.06431	0.00058	4
0	1	-1	ref	4.30955	4.30953	2
0	0	0		5.61790	5.60176	0

reported to a precision of 10^{-5} eV in order to confirm the variational-principle energy ordering of $E_{\rm CAS} \leq E_{\rm vLAS} \leq E_{\rm LAS}$ (the total energy in all calculations was converged to at least 10^{-6} ev). The most dramatic improvement (in the variational sense) of vLASSCF over LASSCF is seen in the energies of the quintet and antiferromagnetic singlet states. Both vLASSCF and LASSCF reproduce the CASSCF degeneracy between the overall singlet and overall quintet states to a high precision, but LASSCF overestimated the total energy thus calculated by more than 60 meV, whereas vLASSCF agrees with CASSCF to within 1 meV. This reinforces the conclusion of Ref. 2 that the spin singlet of this molecule is antiferromagnetic in character, an observation that is straightforward to make in LASSCF and vLASSCF but somewhat obscured in the details of the CASSCF wave function. Furthermore, if one had only calculated the energy of the antiferromagnetic singlet and not the energy of the nonet, one might have mistakenly analyzed the 60 meV difference between the LASSCF antiferromagnetic singlet energy and the CASSCF singlet energy as a measurement of the non-antiferromagnetic character of the CASSCF singlet. But in fact, this energy difference was due to the poorly-defined constraints on optimization of the active orbitals under the old LASSCF algorithm, and the vLASSCF results show that the energetic effect of whatever small amount of non-antiferromagnetic character the CASSCF singlet has is orders of magnitude lower.

One price of this kind of chemical intuition is that total spin symmetry is broken in the LAS wave function. The amount of spin contamination in any given LAS state can

Table 2.2: Spin states energies (eV) of system c ([$Mn(NH_3)_4$]oxamide[$Cu(NH_3)_2$]$^{2+}$) at the CASSCF and vLASSCF levels relative to the CASSCF singlet energy, as well as the spin contaminations ($\langle\hat{S}^2\rangle_{\mathrm{LAS}} - \langle\hat{S}^2\rangle_{\mathrm{CAS}}$) of the vLASSCF wave functions.

s	$m_{s_{\mathrm{Mn}}}$	$m_{s_{\mathrm{Cu}}}$	E_{CAS}	E_{vLAS}	$\langle\hat{S}^2\rangle_{\mathrm{LAS}} - \langle\hat{S}^2\rangle_{\mathrm{CAS}}$
3	2.5	0.5	-4.18901	-4.18901	0
2	2.5	-0.5	-4.19066	-4.18850	1
2	1.5	0.5		-1.08835	0
1	1.5	-0.5	-1.12813	-1.08792	1
1	0.5	0.5		-0.00004	0
0	0.5	-0.5	ref	0.00008	1

be computed by hand, as explained in section 2.2.2, and is also tabulated for the di-iron complex in Table 2.1. Here, we see that the total energy for the three models of an overall singlet is inversely correlated to the magnitude of spin contamination; the pure diamagnetic singlet is more than 5 eV higher-energy than the CASSCF singlet.

The issue of spin contamination in the LAS context is also seen in the results for system c), the heterobimetallic complex, whose spin-state energies at the CASSCF and vLASSCF levels are reported in Table 2.2. A total spin of $s = 1$ or 2 for system c) can be modeled by either a ferromagnetic state, which has no spin contamination, or an antiferromagnetic LAS state, which has $\langle\hat{S}^2\rangle$ 1 greater than it should be. In every case, the spin-contaminated antiferromagnetic LAS state is nearly degenerate with the ferromagnetic model of the next-highest spin state, which in CASSCF are separated by at least 1 eV. On the other hand, the antiferromagnetic LAS energies differ from the CASSCF energies by no more than a few hundredths of an eV. This negative correlation of spin contamination and total energy in both systems is a demonstration of the symmetry dilemma,[114] whereby variational energy minimizations within the constraint of some definite form of the wave function [i.e., Eq. (2.1)] can often only reach good total energies only by breaking some symmetry of the true Hamiltonian and thereby sacrificing good quantum numbers.

The CASSCF spin-state energy ordering for system c) is not entirely reproduced by vLASSCF, as the nearly-degenerate quintets and septets are in opposite orders. However, the

energy differences in question are less than 2 meV, and this is a very unbalanced active space: the CAS has only one determinant in the septet case and 36 determinants in the quintet case. The LAS, on the other hand, has 1 determinant per subspace in both the septet and antiferromagnetic quintet cases. Whether this "balance" corresponds to improved predictive power awaits more comprehensive explorations of the accuracy of vLASSCF calculations with respect to the size of the active space and AO basis and is a matter for future investigation.

2.4 Conclusions

Our recently-developed LASSCF method defeats the exponential cost scaling of CASSCF with respect to the size of the active space by splitting the active space into unentangled fragments and uses a DMET-inspired algorithm to additionally break the orbital optimization process into many short steps. However, in the original theory and implementation, an ill-defined system of constraints on the optimization of the active orbitals limits its robustness and reproducibility. The variational version of the method, which is referred to as vLASSCF in this chapter, cures these deficiencies and is truly variational in the Hellmann-Feynman sense, which improves upon the consistency and transferability of the method and allows for more trustworthy analysis of small energy differences. We have therefore jettisoned some of the baggage of DMET (i.e., dependence on user choice of orbital localization protocol) while retaining the attractive feature of splitting an MC-SCF orbital optimization problem into several small coupled optimization problems. The superior smoothness of the bisdiazene potential energy curve, the confirmation of energetic equivalence between CASSCF and vLASSCF in the appropriate limit, and our formal and analytical operation cost analyses collectively demonstrate that we have succeeded in having our cake and eating it too.

In addition to the improved quality of the vLASSCF results compared to LASSCF, vLASSCF is amenable to the straightforward calculation of molecular gradients using the

Hellmann-Feynman theorem. We have already shown that LASSCF is an attractive alternative to CASSCF in the calculation of spin-state energetics,[2] in which the separable form of LASSCF facilitates chemical interpretation of the wave function in a manner that is often obscured by the CAS formalism. The variational formalism and forthcoming gradient implementation will allow LASSCF to explore the relationship between spin state energetics and molecular geometries as well. Finally, LAS wave functions of more robust accuracy offered by vLASSCF are expected to be critically important in the context of post-SCF methods such as MC-PDFT[30,31,71,124,125] as well as post-LAS wave function formalisms such as ASD.[92–96] It will be interesting in the future to test the method on systems containing multiple metal and/or lanthanide/actinide centers.

CHAPTER 3

LOCALIZED ACTIVE SPACE PAIR-DENSITY FUNCTIONAL THEORY

3.1 Introduction

Quantum mechanical electronic structure methods for making quantitative predictions of the properties of molecules and materials often present a tradeoff between accuracy and cost in computing electron correlation. Many approaches have been developed to account for static and dynamic correlation at a reasonable computational cost.[56,126–129] There is not a unique way to decompose the electron correlation energy into these two contributions,[130] but the distinction is useful for understanding the performance of various methods and improving them in systematic ways. A useful key to distinguishing different kinds of correlation effects is provided by the concept of entanglement.[131] Multiconfiguration self-consistent field (MCSCF) methods are often used as a first step when dealing with systems that have significant static correlation. The complete active space SCF (CASSCF) method expresses the wave function as a linear combination of all electronic configuration state functions that can be generated by allowing a set of active electrons to occupy a set of active orbitals in all possible ways that are consistent with selected space and spin symmetry choices.[18] With practically affordable active space sizes, CASSCF recovers only a relatively small portion of the dynamic correlation energy, and post-CASSCF methods are needed to make quantitative predictions. CASPT2 is a popular post-CASSCF method used to add dynamic correlation energy to the CASSCF energy,[22] but accurate CASPT2 calculations are prohibitively expensive except for small molecules.[132,133] One post-SCF treatment that is more affordable than CASPT2 and that has proven to be useful is multiconfiguration pair-density functional theory (MC-PDFT).[30] Instead of computing perturbation-theory corrections to the wave function, the MC-PDFT method involves an expression for the total energy as a functional of

the kinetic energy, electron density, and on-top pair density of an unmodified multiconfiguration wave function.[124,134] MC-PDFT has been shown to give CASPT2-quality results for many quantities like spin-state gaps, excitation energies, and binding energies for a variety of systems.[30,31,44,124]

Although CAS-PDFT allows us to tackle larger systems that are not affordable with CASPT2, obtaining the reference CASSCF wave function remains computationally challenging for large systems. Various methods have been proposed to address the difficulties related to the exponential cost scaling of CASSCF with respect to the size of the active space. The restricted active space (RAS)[60,61] and generalized active space (GAS)[62] approximations allow the user to reduce the number of configurations by defining subspaces based on chemical intuition. The density matrix renormalization group (DMRG),[67] doubly occupied configuration interaction,[68,69] and active-space two-electron reduced-density-matrix methods[70] can be implemented with polynomial, rather than exponential, cost scaling. The MC-PDFT has also been successfully employed with other reference wave functions, such as RASSCF,[135] GASSCF,[136–138] DMRG-SCF,[139,140] and RASCI[34] (where RASCI denotes RAS configuration interaction).

Although approximating the wave function using the above methods allows us to study increasingly large molecules and active spaces, they still suffer from the computational effort scaling exponentially with system size, and this limits their application. We recently proposed a method to obtain a new kind of multiconfiguration wave function called LASSCF.[1,46] To understand the motivation for this method, we may categorize the types of interaction between subsystems by using the concept of entanglement. In many cases, a system may be theoretically decomposed into fragments with little entanglement between the fragments, but high static correlation within one or more of the fragments. LASSCF is designed for this kind of system, and with LASSCF, the entire active space is decomposed in multiple unentangled active subspaces that are localized on user-defined fragments.

Since these subspaces are unentangled, the wave function for each of them can be well approximated by treating the interaction with other subspaces as a mean field. This means that the method scales exponentially only with the size of each individual active subspace, while it scales linearly with the number of subspaces. The LASSCF energy is a variational upper bound to the corresponding CASSCF energy.[46] In this work, we introduce a new method called localized-active-space pair-density functional theory (LAS-PDFT), which uses LASSCF wave functions as reference wave functions for PDFT calculations. We investigate if the modest sensitivity of the MC-PDFT energies to the 'quality' of the reference MCSCF wave function applies also to fragmented, unentangled active spaces. The new LAS-PDFT method is tested for calculating the spin-state energetics of conjugated organic molecules and bimetallic complexes. We investigate the differences in LASSCF and LAS-PDFT energies as compared to the corresponding CASSCF and CAS-PDFT energies, respectively. We also explore the effects of varying the sizes of the active spaces and basis sets.

3.2 Methods

In this section we briefly review LASSCF and MC-PDFT. More detailed treatments of both these methods are already in the literature.[1,30,31,46] We consider the case of multiple active subspaces and one inactive subspace. The inactive subspace is described by a closed-shell-singlet determinant. The LASSCF wave function is formulated as an antisymmetrized product (a.k.a. a generalized product function[141,142]) of wave functions, ψ, of the various active subspaces, $\mathrm{A_k}$, and the single-determinant wave function ϕ_U of the inactive electrons (the inactive subspace) as

$$|\mathrm{LAS}\rangle = \bigwedge_{\mathrm{K}} |\psi_{\mathrm{K}}\rangle \wedge |\phi_{\mathrm{U}}\rangle \tag{3.1}$$

where $\wedge$ denotes the antisymmetrized tensor product given mathematically by the Grassman wedge product.[143] The wave function is optimized variationally to minimize the energy

given by

$$E_{\mathrm{LAS}} = \langle \mathrm{LAS}|\hat{H}|\mathrm{LAS}\rangle \tag{3.2}$$

In practice, a LASSCF calculation is initialized by orthogonalizing the atomic orbital basis using the meta-Löwdin method[110,111] and selecting the orthogonalized AOs of various collections of atoms as "fragment orbitals" of the groups on which the user chooses to localize the active subspaces. Then, either an initial guess of the active orbitals (which typically are delocalized over the entire molecule) is projected on to these fragment orbitals, or the fragment orbitals are projected onto the initial guess. (The latter projection leads to faster SCF convergence if the initial guess is very near to the converged result; otherwise, the former is preferred.) In subsequent iterations, the energy is minimized with respect to orbitals and configuration interaction vectors without any constraint or any further orbital projection. The locality of the converged active orbitals is therefore due entirely to the initial guess. While this means there is no absolute guarantee that a physically meaningful LAS wave function can be obtained for any arbitrary combination of subspaces, we have observed that the orbitals deviate minimally from the initial guess provided the initial assignment to the fragments has been done reasonably well. This might not be the case when the subspaces are unphysical or when modeling some high-energy LAS state (e.g., a charge transfer from one subspace to another). We note that a LAS calculation requires the user not only to decide the active space, which is not always an intuitive task, but also to divide it in subspaces and assign properties (such as total charge, total spin, and spin-component quantum number) to each subspace. However, making these decisions can reduce the cost of the computation immensely, and it is fairly straightforward in most cases for which LASSCF is designed. In cases where chemical intuition is unable to provide clear enough guidance, for instance when exploring high-spin states that may be characterized by spin density localized in more than one possible way, one may choose among these possibilities by comparing the converged

LASSCF energies; the state with the lowest energy is likely to be the most reasonable, although this depends on the nature of the states the user is interested in exploring. The choices made for each system studied in this work are further elaborated in the discussion. The total LAS wave function, however, is not a spin eigenstate when multiple subspaces have non-singlet spins that are not mutually collinear (i.e., not all M_S = +S or all M_S = -S, where S and M_S refer here to the spin and spin component quantum numbers of a subspace), no matter what selection the user makes when distributing spins among fragments.

MC-PDFT calculates the total energy as[30]

$$E_{\mathrm{MC-PDFT}} = V_{\mathrm{nuc}} + \sum_{pq} \left[h_{pq} D_{pq} + \frac{1}{2}(pq|rs) D_{pq} D_{rs} \right] + E_{\mathrm{OT}} \left[\rho, \Pi\right] \tag{3.3}$$

where V_{nuc} is the nuclear repulsion, $p, q, ...$ are indices of general orbitals, $D_{pq} = \langle \psi | a_p^\dagger a_q | \psi \rangle$ (where $a^\dagger$ and a are creation and annihilation operators) is an element of the one-electron reduced density matrix (1-RDM), h_{pq} a matrix element of the electronic kinetic energy plus the electron–nuclear attraction, $(pq|rs)$ is a two-electron integral in the Mulliken notation, and Π is the on-top pair density (probability density of finding two electrons at a point in space). The functional E_{OT} is called the on-top functional which is a functional of ρ and the and on-top pair density π of ψ_{MC}. PDFT differs from methods that compute a correction to the CASSCF energy, which already includes some electron correlation effects (a prospect can possibly lead to electron-correlation double-counting when one adds a correction to the CASSCF energy), in that PDFT replaces the energy calculation of CASSCF entirely. As in Kohn-Sham theory, we do not know an exact functional form for the density functional, but various approximate functionals are available; the translated PBE (tPBE) functional is used in the present study. In this work, we use LASSCF wave functions for ψ_{MC}. We also compare the spin density[144] and unpaired density[145–147] of the underlying LASSCF wave function to those of the CASSCF wave function to get insight into the electronic structure

on individual subspaces. For each atom we report the Mulliken spin density, obtained from the difference between the α and β densities localized on each atom. The unpaired density on atom A, is

$$u_A = \sum_{\mu \in A} \sum_{\nu} \left(D_{\mu\nu} - \sum_{\kappa\lambda} D_{\mu\kappa} S_{\kappa\lambda} D_{\lambda\nu} \right) \tag{3.4}$$

where S is the overlap matrix, D is the spin-summed one-body reduced density matrix, and μ, ν, κ and λ are indices of basis functions, where μ spans only basis functions centered on atom A. This quantity gives the number of unpaired electrons of either spin, which is different from the spin density, and can be used to detect unpaired spins in hyper open shells, such as open-shell singlets, doublets with three unpaired electrons, triplets with four unpaired electrons, etc. Unlike the spin density, the unpaired density of the entire system does not integrate to any specific number, it is bounded from below by the net spin density and from above by the total number of electrons. All calculations reported in this work have been performed on a locally modified version of the mrh code.[117] The 6-31G basis set[123] was used for systems 1–3, and the cc-pVDZ basis set[122] was used for system 4. The geometries for systems 1 and 2 were optimized for each dihedral angle in Gaussian 09[148] by freezing the dihedral angle and relaxing the rest of the degrees of freedom with a singlet spin at M06-L[28]/Def2TZVP[119,120] level. The geometries for systems 3 and 4 were obtained from reference 46. Details about the active space and their partitioning into subspaces for each system are reported in their respective section.

3.3 Results and Discussion

The performance of LAS-PDFT was tested by computing absolute energies and spin-state energy gaps for four molecules and comparing them to the corresponding CAS-PDFT results.

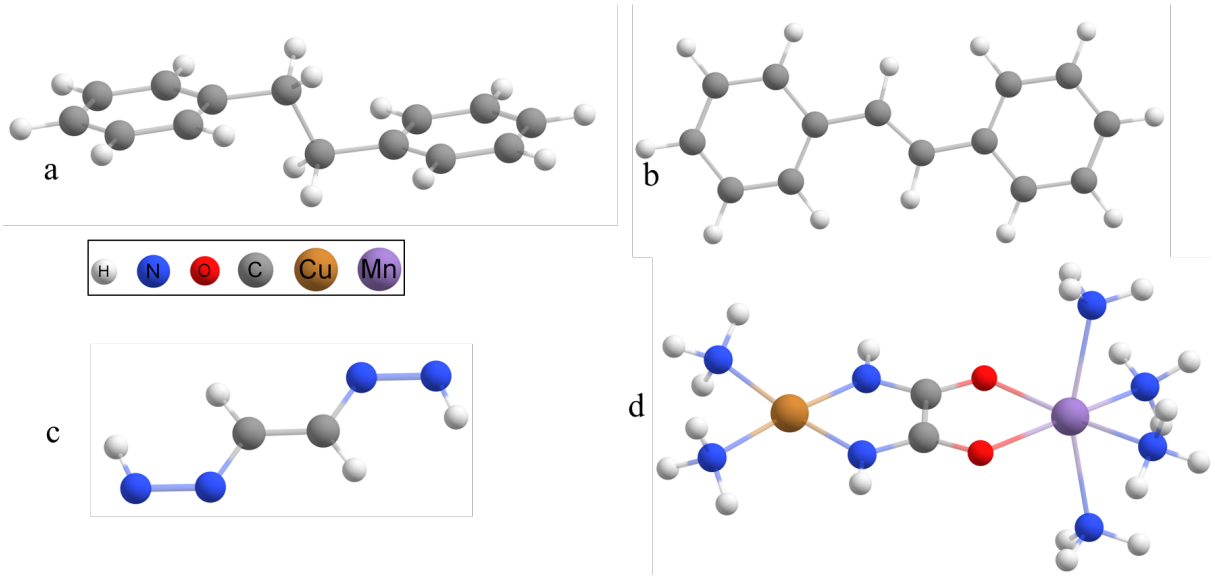

Figure 3.1: The systems studied in this work: (a) bibenzyl, (b) stilbene, (c) 1,2-bis (diazenyl) ethene, (d) ([$Mn(NH_3)_4$]oxamide[$Cu(NH_3)_2$]$^{2+}$).

The molecules are 1,2-bibenzyl (i.e., 1,2-diphenylethane), stilbene (i.e., 1,2-diphenylethene), 1,2-bis(diazenyl)ethene, and the bimetallic complex [$Mn(NH_3)_4$]oxamide[$Cu(NH_3)_2$]$^{2+}$), and they are shown in Fig. 3.1

3.3.1 Bibenzyl

The active space considered for the CASSCF calculation of bibenzyl has 12 active electrons in the 12 π and π^* orbitals (12,12). The two phenyl rings in this molecule are connected by a C–C single bond. An intuitive LASSCF scheme to decompose this active space is to localize an active subspace of 6 electrons in 6 orbitals on each phenyl ring (6,6). Thus, there are two active subspaces and one inactive subspace; note that, as usual in LASSCF calculations, the inactive subspace is delocalized over the whole system. With this scheme, we calculated the lowest singlet and triplet energies as a function of the internal rotation of the central C–C bond by changing the dihedral angle from 55° to 180°). The triplet configuration in the LASSCF wave function was obtained by imposing a triplet spin in one of the (6,6) subspaces while the other was kept as a singlet.

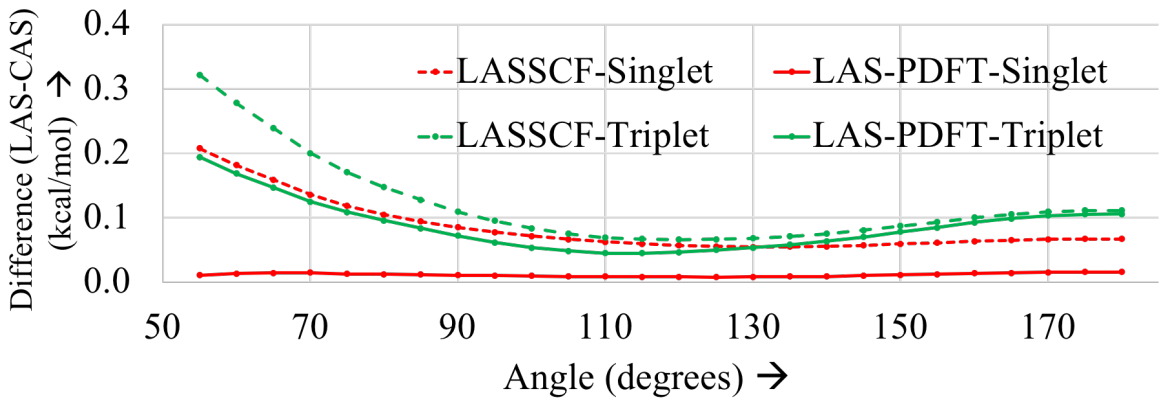

Figure 3.2: Difference in singlet (in red) and triplet (in green) LASSCF (dotted lines) and LAS-PDFT (solid lines) absolute energies for bibenzyl, computed as the difference with the corresponding CASSCF and CAS-PDFT energies, respectively.

Fig. 3.2 shows that the difference in LASSCF and LAS-PDFT energies with respect to their CAS equivalents is less than 0.5 kcal/mol for both the singlet and the triplet states along the entire curve. This confirms that the scheme of unentangling the active space into two subspaces is a reasonable approximation in this case. It is also to be noted that the difference for LAS-PDFT is always smaller than for LASSCF. The strong agreement in the triplet energies in spite of the fragmentation is due to the fact that even in the CASSCF wave function, the two unpaired electrons are localized on only one of the two chemically equivalent phenyl rings. Thus, the unentanglement of the subspaces in LASSCF does not cause a heavy energy penalty as it would if the unpaired electrons were delocalized. This result is particularly appealing because of the significant reduction in the cost of the computation in LASSCF. The number of configuration state functions (CSFs) is 226512 for the singlet and 382239 for the triplet CASSCF wave function, whereas it is 350 and 364 for the singlet and the triplet LASSCF wave functions, respectively. We note that bibenzyl is a case where one probably would have anticipated that separating the whole-molecule active space into subspaces would not be harmful and that, although the difference reduces with PDFT, the agreement between CAS-PDFT and LAS-PDFT is largely due to the agreement

between the starting wave functions.

3.3.2 Stilbene

A more difficult test for the theory is a case where unentangling of the active subspaces imposes a high variational penalty on the energies calculated – for example when active orbitals are highly delocalized. An example of such a case is stilbene. In stilbene the two phenyl rings are connected through a C–C double bond and thus the π and π^* orbitals in this molecule are not as localized as in bibenzyl. We study the relative energies (potential energy curves relative to the respective trans singlet) and spin gaps along a *cis* to *trans* dihedral scan using two active spaces (see Fig. 3.3) - an active space containing all π and π^* orbitals (of 14 electrons in 14 orbitals) and a smaller one of 10 electrons in 10 orbitals because this has been shown to be a useful active space for this molecule.[149] In addition to the MCSCF and MC-PDFT calculations we also perform second order n-electron valence state perturbation theory (NEVPT2)[29] calculations at both these active space. These methods have different sensitivities to active space and basis set sizes. The potential energy curves from CAS-PDFT (14,14) and NEVPT2 (14,14) have a mean absolute deviation (MAD) of 1.1 kcal/mol with respect to each other. The CAS-PDFT (10,10) curve has a MAD of 0.23 kcal/mol with respect to the (14,14) curve, while that of NEVPT2 is 1.25 kcal/mol. We compare the LASSCF energies to the CASSCF energies and LAS-PDFT energies to the CAS-PDFT and NEVPT2 at a given active space.

Since the molecule is conjugated, the scheme to decompose the active space into subspaces is not as obvious as for bibenzyl. We decomposed the (10,10) active space into three active subspaces where a (4,4) subspace is localized on each phenyl ring and a (2,2) subspace on the central CH–CH unit. We compare the singlet and triplet energies as the dihedral angle changes from 0 ° to 180 °, going from *cis* to *trans* stilbene. The LASSCF triplet is an example of the aforementioned case where chemical intuition does not decisively inform us

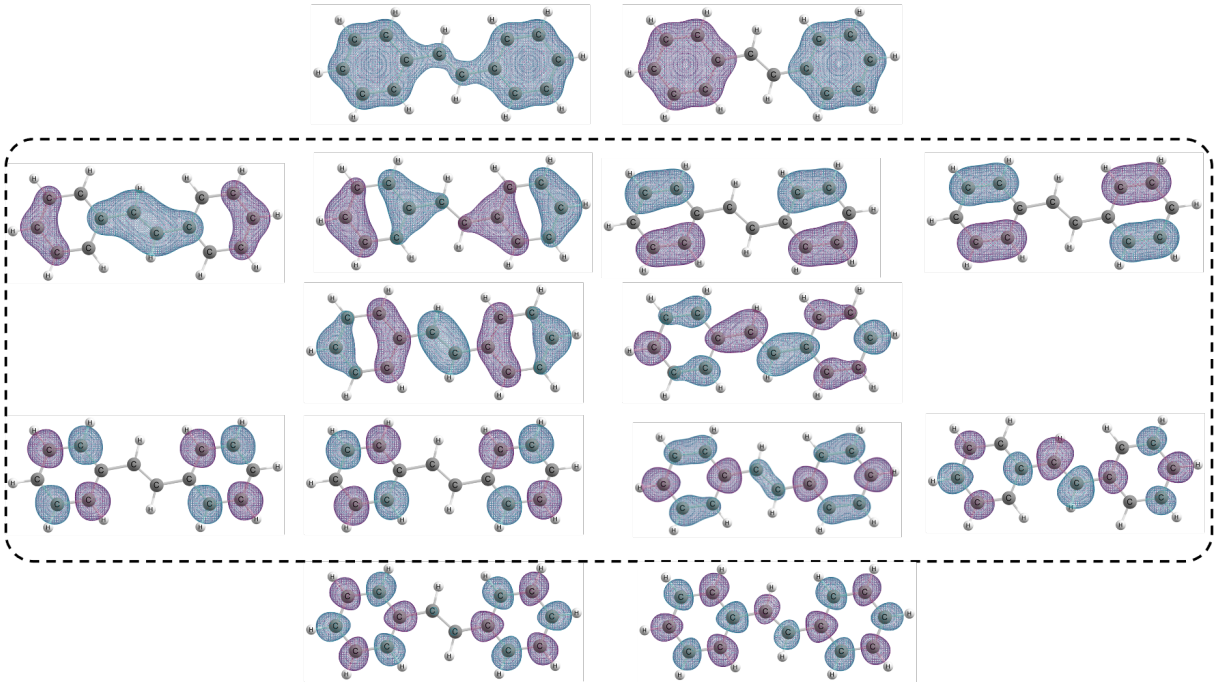

Figure 3.3: The (14, 14) active space for stilbene of which the (10,10) active space (shown inside the dotted box) is a subset. Shown here are the natural orbitals for a singlet CASSCF calculation at the trans geometry.

of the most appropriate subspace in which to impose a triplet. The lower-energy state is obtained by imposing a triplet spin on the (2,2) subspace. The other possible configuration – obtained by imposing a triplet on one of the (4,4) subspaces – was found to be higher in energy by 4–10 kcal/mol. This choice is also supported by the spin densities seen in the CASSCF wave function in fig.3.7. Fig. 3.4 shows the CAS and LAS energies with the (10,10) active space along the dihedral scan relative to the singlet CAS energy at the global minimum trans geometry. The triplet CAS energy is also reported relative to the same reference. This shows that LASSCF, in spite of the drastic unentanglement of subspaces, gives a reasonably accurate description for both spin states. The CASSCF vs. LASSCF energy difference for the triplet is higher than that for the singlet for most geometries. This is can be attributed to the energy penalty imposed by the unentanglement of the active unpaired electrons that would otherwise be more delocalized.

The (14,14) active space, which includes all the π and π^* orbitals of stilbene, is also

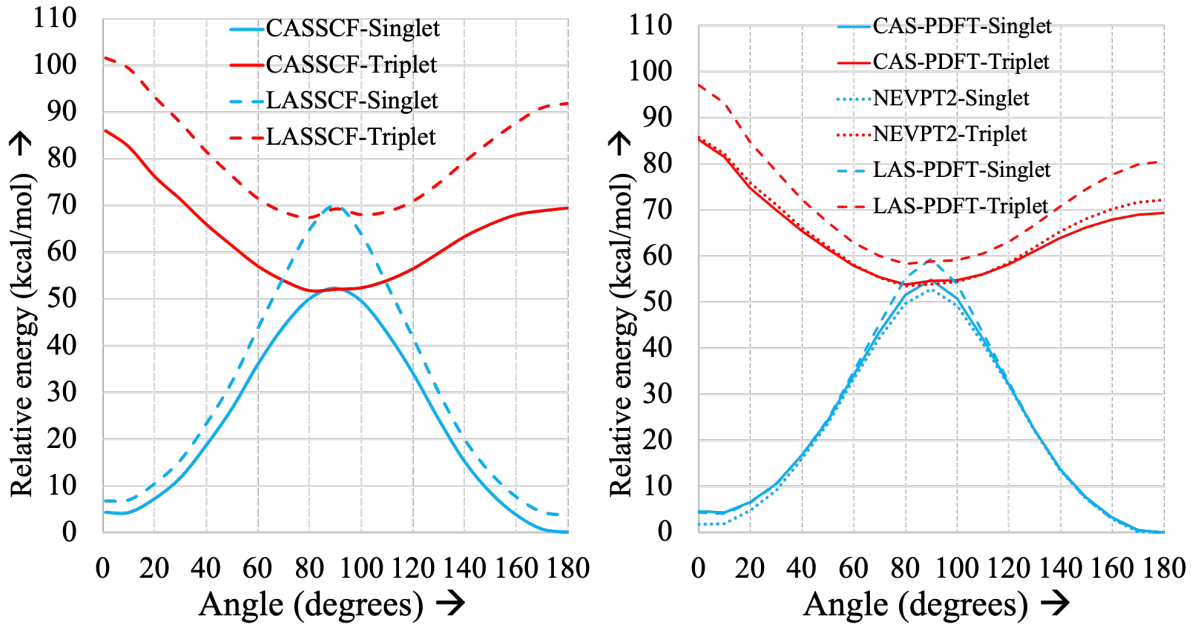

Figure 3.4: The singlet (blue) and triplet (red) energies (kcal/mol) with a (10,10) active space relative to the CASSCF (left) and CAS-PDFT (right) singlet for global minimum trans-stilbene calculated using LAS (dashed lines) and CAS (solid lines) wave functions.

decomposed in three active subspaces with a (6,6) subspace on each phenyl ring and a (2,2) subspace on the CH–CH unit. This leads to an even more drastic reduction in the cost. While the (14,14) CASSCF singlet and triplet have 2760615 and 5010005 CSFs respectively, the corresponding LASSCF wavefunctions have only 353 and 351 CSFs. The LASSCF and LAS-PDFT curves with a (14,14) active space show trends similar to the (10,10) case, but with larger errors as shown in Fig. 3.5.

In all cases the disagreements between CAS and LAS are greater for the (14,14) active space than for the (10,10) active space. However, for both active spaces, the LAS-PDFT approximates the corresponding CAS-PDFT much better than LASSCF agrees with CASSCF. We note that unlike CASSCF and NEVPT2, MC-PDFT does not reproduce FCI in the limit of a large active space; disagreement between LAS-PDFT and CAS-PDFT in the case of a large active space does not always imply inaccuracy in the former. For the remainder

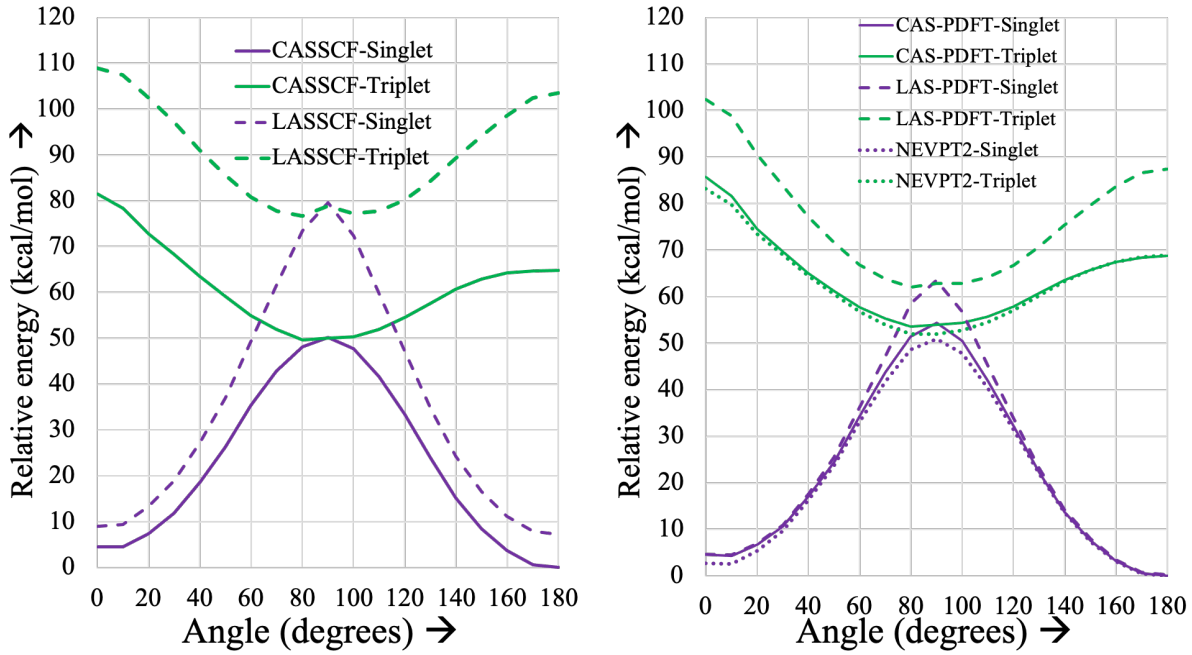

Figure 3.5: The singlet (blue) and triplet (red) energies (kcal/mol) with a (14,14) active space relative to the CASSCF (left) and CAS-PDFT (right) singlet for global minimum trans-stilbene calculated using LAS (dashed lines) and CAS (solid lines) wave functions.

of this section, we will analyze the results for the (10,10) active space. The difference in the LASSCF singlet peaks at around 90° because the wave function becomes more multireference near that geometry as compared to the *cis* or *trans* geometries. This is evident from the weight of the dominant (closed-shell singlet) configuration in the CASSCF wave function. It is nearly 91% at *cis* and *trans* geometries, while only 66% at 90°, where the wave function is more poorly described as a product of active subspaces. This is reflected in a higher variational penalty on the LASSCF energy at the 90° geometry compared to the *cis* or *trans* geometries. The agreement between the LAS-PDFT and CAS-PDFT energies is better than the one between the LASSCF and CASSCF energies for both spin states. Similarly, a faster convergence – with the size of the active space and bond dimension – was detected in previous work for the DMRG-PDFT energy and the CAS-PDFT energy as compared to the DMRG energy and the CASSCF energy.[139]

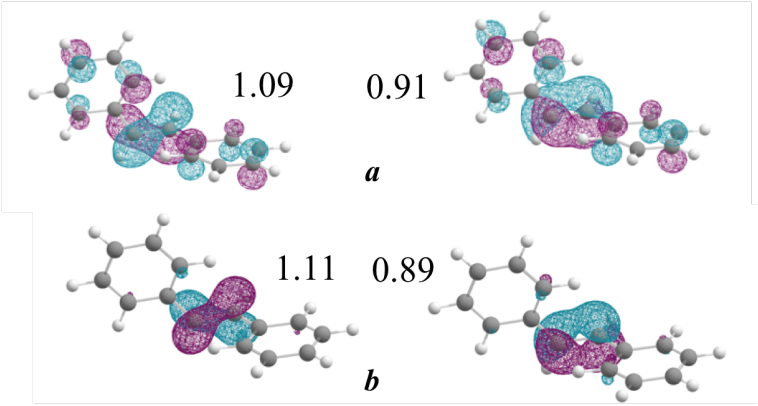

Figure 3.6: The two natural orbitals from the CASSCF (10,10) calculation at the 90° dihedral angle that are mostly singly occupied (top panel a); the natural orbitals from the (2,2) subspace in the singlet LASSCF(10,10) calculation (bottom panel b).

While the difference between LAS-PDFT and CAS-PDFT is nearly zero for the singlet state at most geometries, some difference still persists at around 90°. To further investigate this difference (and the parent wave functions), we inspected the natural orbitals and their occupancies. At the 90° geometry there is a near degeneracy in the π and π^* orbitals of the central C–C bond, and the singlet wave function has an open-shell character. This can be seen in Fig. 3.6 where the occupancy of both these natural orbitals is close to 1. The LASSCF wave function, which includes the singlet (2,2) localized subspace, shows an open-shell character as well. The natural occupation numbers of these orbitals are reasonably close to those in the CASSCF wave function. The orbitals, however, are significantly more localized.

We also observe that the difference between LAS-PDFT and CAS-PDFT energies for the triplet is higher than that for the singlet. This trend occurs also in the LASSCF versus CASSCF energies. More interesting, however, is the observation that the difference in the triplet curve of LAS-PDFT is lowest at around 90°. To further investigate this, we explored the unpaired density (for the singlet) and the spin density (for the triplet) localized over the three units (two phenyl rings and the C2H2 group) as seen in fig. 3.7.

We notice that the LAS unpaired density for the singlet is quantitatively similar to the

CAS unpaired density at the equilibrium geometries, and the difference is greatest around the 90° angle. This also demonstrates that the LAS wave function does capture the open-shell character at the 90° angle, but it has the unpaired electrons localized on the C–C bond. In the triplet case, however, since we impose a triplet on (2,2) subspace that is localized on the CH–CH unit for all the geometries, nearly the entire spin density of 1.8 electrons is localized in the CH–CH unit at all the angles in LASSCF. The "correct" CASSCF densities over each unit are not the same for all the angles. The *cis* and *trans* geometries have only about 1 electron worth of spin localized over the CH–CH unit while the other two phenyl rings have about 0.5 electrons each.

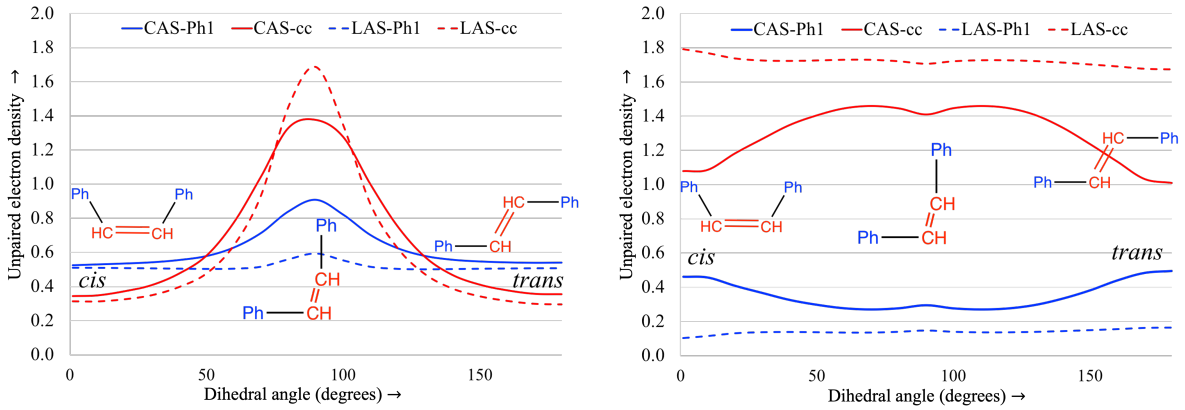

Figure 3.7: Unpaired density of the singlet (left) and the spin density of the triplet (right) wave functions localized on the phenyl (red) and CH–CH (blue) units in CASSCF (solid lines) and LASSCF (dotted lines) calculations

We can correlate the disagreement between the LASSCF and CASSCF energies at specific geometries for both spin states to the disagreement in the corresponding spin (for triplet) and unpaired (for singlet) densities that are delocalized in the entire molecule in CASSCF, while are restricted on the central CH–CH unit in LASSCF. When the LASSCF spin/unpaired densities are closer to the CASSCF ones, LAS-PDFT agrees with CAS-PDFT even more strikingly than LASSCF with CASSCF, perhaps indicating that LAS-PDFT energies are more immune to the changes in density as compared to the LASSCF energies.

3.3.3 Concerted dissociation of the N-N bonds in 1,2-bis(diazenyl)ethene

We explored the performance of LAS-PDFT for the concerted dissociation of 1,2-*bis* (diazenyl) ethene, previously studied using LASSCF.[46] This is an example where LASSCF fails to quantitatively predict the dissociation energy because there are two N–N double bonds connected by a central C–C double bond, so overall the π system is highly delocalized. Following our previous work, the (10,10) active space of this molecule is decomposed in three localized active subspaces with a (4,4) subspace on each N_2H unit and a (2,2) subspace on the C_2H_2 unit. Fig. 3.8 shows the energy difference along the dissociation reaction coordinate between LASSCF and CASSCF ($E_{LASSCF} - E_{CASSCF}$) and between LAS-PDFT and CAS-PDFT ($E_{LAS-PDFT} - E_{CAS-PDFT}$).

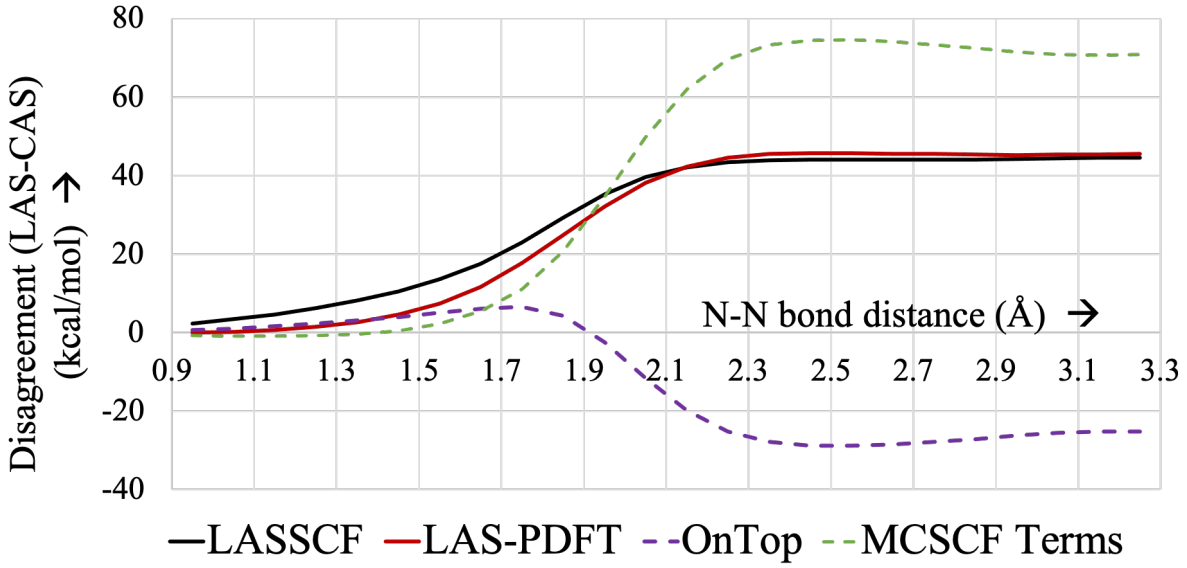

Figure 3.8: Difference (kcal/mol) between the LASSCF and CASSCF absolute energies (red) and LAS-PDFT and CAS-PDFT absolute energies (black) along the dissociation curves and break down of the LAS-PDFT difference in its components.

As the multireference character of the wave function increases with the N-N bond distance, ($E_{LASSCF} - E_{CASSCF}$) and ($E_{LAS-PDFT} - E_{CAS-PDFT}$) are about 45 kcal/mol. This was further investigated by plotting the differences in the components of the PDFT energies – namely the on-top energy and the MCSCF terms (sum of kinetic energy, nuclear electron

attraction, and classical Coulomb repulsion). The 45 kcal/mol difference at dissociation can be decomposed into the difference in the on-top energy (-25 kcal/mol) and in the MCSCF wave function part (70 kcal/mol). This shows that both components of energy have a significant difference. The LAS wave function itself is highly approximate at the dissociation limit, and thus it does not serve as a good reference for PDFT.

3.3.4 Spin state ordering in bimetallic compounds

Predicting the spin-state energy gaps of metal complexes with several metal centers is a challenge for electronic structure theories. In many complexes the metal centers have a high degree of intraatomic electron correlation due to the low-lying virtual d-orbitals being localized around them, but the correlation between two metal centers is not always high. In such cases partitioning the active space results in a substantial reduction of the computational cost without affecting the quality of the results, and, when several metals are present, only partitioning methods may be affordable. We studied the spin state ordering of a bimetallic complex containing a Cu and Mn atom, and we showed that LASSCF is able to qualitatively predict the spin ladder in agreement with CASSCF.[46]

The minimal active space (see Fig. 3.9) of the six electrons in the five 3d Mn orbitals and one electron in the Cu 3d orbitals is considered. The LAS wave function has two active subspaces – one with 5 electrons in 5 orbitals localized on the Mn and the other with 1 electron in 1 orbital localized on the Cu. (This is not intended to be an ideal active space for capturing the majority of electron correlation). The energies for all possible spin states are reported relative to the CASSCF septet state. Since the LAS wave function is not necessarily a spin eigenfunction in these cases, we classify the wave functions based on the expectation value of the spin projection operator, because M_S (defined above) is still a good quantum number while S is no longer a good quantum number.

LASSCF captures the near degeneracy of the septet and the quintet seen at the CASSCF

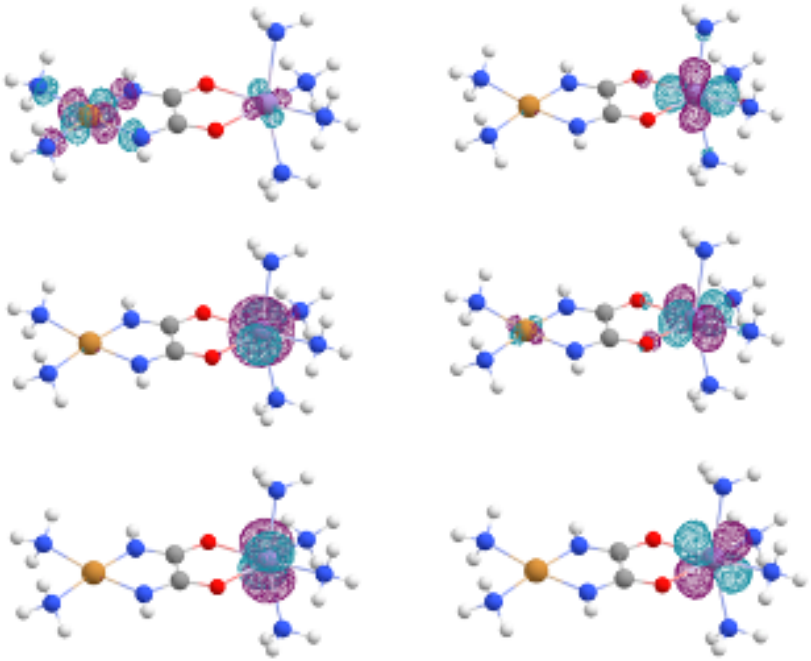

Figure 3.9: The active orbitals in the minimal active space of the bimetallic complex

level and also reproduces the relative energies of the higher-energy spin states, namely the triplet and the singlet. Consequently, LAS-PDFT reproduces the CAS-PDFT gaps with a difference much lower than one kcal/mol.

Table 3.1: Energy differences (kcal/mol) for different spin states and local spin orientations relative to the respective septet CASSCF or CAS-PDFT energies, calculated using different methods

Spin (M_S)	CASSCF	CAS-PDFT	Local Spin orientation	LASSCF	LAS-PDFT
Septet	0.0 (ref)	0.0 (ref)	ferromagnetic	0.0	0.0
Quintet	0.0	-0.1	anti-ferromagnetic	0.0	0.0
			ferromagnetic	71.5	43.1
Triplet	70.6	42.3	anti-ferromagnetic	71.5	43.1
			ferromagnetic	96.6	55.8
Singlet	96.6	55.8	anti-ferromagnetic	96.6	55.8

A key advantage of the LAS-PDFT method is that it allows us to compute electron correlation beyond the LASSCF needed for reliable energies of the spin states and also the relative energies of spin couplings that are not accessible (or separable) using CASSCF wave functions. The relative energetics of the ferro- and antiferromagnetic states demonstrate that the

true quintet and triplet ground states are almost certainly dominated by antiferromagnetic interactions between the two metal centers. The LAS form of the wave function exposes this information straightforwardly to the user, and the LAS-PDFT extension incorporates the effects of dynamic electron correlation into the analysis.

3.4 Conclusion

The LASSCF algorithm can be used to obtain a good reference wave function for post-MCSCF calculations, like PDFT, especially when the variational penalty of unentangling the subspace is not drastic. Not only does the LAS-PDFT method account for more correlation than the LASSCF itself, but it also reduces the disagreement between the CAS and LAS energies. In other words, MC-PDFT is in most cases more immune to the unentangling of the active space than is MCSCF. This expands the opportunity to use PDFT for systems for which the reference CASSCF calculation is not affordable. In addition to the favorable scaling, LASSCF also provides us with greater control on the local spin in different subspaces. While the current implementation does not guarantee that any arbitrary spin coupling will result in an overall spin eigenfunction, the different LAS wave functions provide a possible starting point for spin-adapting the wave function. Analysis of the spin density and the unpaired density in the various subspaces elucidates the effects of unentangling the active subspaces on the wave functions.

CHAPTER 4

CHEMICAL INSIGHTS FROM USING LOCALIZED ACTIVE SPACES BASIS FOR STATE INTERACTION

4.1 Introduction

Modeling chemically interesting phenomena like charge transfer, magnetic interactions, and excited states has long been an important objective for developments in electronic structure methods. Single-reference methods like density functional theory, popular for their ease of use, are poorly suited for systems with strong multireference character - i.e. significant non-dynamical correlation. Instead, multireference methods are required for such problems. A commonly used multireference method, the complete active space self-consistent field (CASSCF) model, provides a qualitatively correct description of the system that captures so-called static correlation.[18] This method requires the user to define the active space - a set of active orbitals and the number of electrons collectively occupying these orbitals. The CAS wave function is then expressed as a linear combination of all electronic configurations that can be obtained from all possible excitations of the active electrons in these active orbitals (within a given spatial and spin symmetry).

The exponentially growing cost of considering *all possible* configurations prevents CASSCF from being used for large systems with many strongly correlated electrons. Several cost-effective approximate methods have been developed based on the key insight that most of these configurations contribute very little to the wave function of the ground and low-lying excited states. Methods like the restricted (RAS)[60,61] or generalized active space (GAS)[62] models achieve this by limiting the number of electrons or holes in pre-defined subspaces. Alternatively, methods like density matrix renormalization group (DMRG)[67] iteratively optimize the matrix-product state representation of the wave function. Another popular approach, the selected configuration interaction (SCI)[150–155] model, usually starts with a

small number of configurations and dynamically and iteratively expands the configuration space, either perturbatively (CIPSI[156,157]), adaptively (ASCI),[158,159] or stochastically (heat-bath CI[160–162] or FCI-QMC[163,164]).

The framework of using a basis of localized or fragment wave functions to obtain the overall wave function has been explored previously through various different approaches. In 1979, Liu and McLean proposed the interacting correlated fragment (ICF)[165,166] method that can incrementally introduce levels of electronic correlation between fragments in weakly interacting multireference systems. The active space decomposition (ASD) introduced by Parker and Shiozaki[92–94,96] in 2013 uses a similar approach to efficiently compute the CASSCF wave function using direct products of localized, orthogonal fragment states. Another recent approach, rank-one basis states by Nishio and Kurashige, also uses similar ideas and has been shown to work for large π- stacked systems.[84,167]

The LAS approach is equivalent to the cluster-based mean-field (cMF)[91] approach by Jimenez-Hoyos and Scuseria that expresses wave functions as a tensor-product state (TPS). The exact wave functions can be expressed in the basis of these correlated states using ansatze like couple cluster[168,169], perturbation theory,[170] and many-body expansions[171]. The TPSCI algorithm by Abraham and Mayhall uses selected-CI methods to obtain the wave function in the basis of the TPS basis.[172]

While it is paramount that the cost of accurate multireference methods be lowered enough to be affordable for interesting systems, it is also important that we obtain substantial information *from* such calculations. For applications like computationally-guided materials design, or the study of site-site spin interactions in molecular magnets and environmentmental effects thereupon, calculations must not only give quantitatively accurate results, but to make progress they must also provide a better understanding of the system in terms of simpler chemical models used to interpret trends in properties and behavior. These models often use concepts that are easy to envision even if not accurate representations of under-

lying fundamental physics. For example, bonding in molecules is usually interpreted using concepts from valence bond theory (like bonding/anti-bonding orbitals, bond orders, etc.) even if the methods used for the calculations are not tied to such a representation. Similarly, reaction dynamics is often more easily interpreted by using diabatic surfaces. A noteworthy example is the J coupling parameter that is used to explain spin-spin coupling in magnets and the mechanisms by which that occurs: While a distinction between direct exchange and superexchange mechanisms may be useful for chemical interpretation, their effects are often difficult to quantify with electronic structure calculations. Instead, in many applications, the results from state-of-the-art electronic structure methods are fitted to these simple models to extract these parameters. In some simple cases, however, by comparing results from multiple cleverly selected active spaces one can directly obtain quantitative estimates for such parameters. There however is a need for a multireference method whose results are easy to interpret directly and is widely applicable to various problems.

As we continue to pursue multireference models that are widely applicable to various problems and whose results are easy to interpret, in this chapter we explore the new state interaction (SI)-LASSCF formalism that builds on the LAS approach. The LASSI wave function is defined as a linear combination of multiple LAS states that form eigenfunctions of the molecular Hamiltonian. The choice of the LAS wave functions as a basis specifically allows us to selectively introduce coupling between the various subspaces. This framework fits well with the conceptual descriptions of many phenomena that rely are described by such interactions, like charge transfer and spin-spin coupling. We show that many important parameters can be calculated directly in this framework rather than extracting them by fitting CASSCF results to model Hamiltonians. Section 4.2 establishes the theoretical foundation and technical aspects of LASSI. Section 4.3 discusses the application performance of LASSI to intra-molecular charge transfer in an organic cation, the spin-spin coupling in a di-chromium complex and the singlet-triplet gap in a growing series of conjugated polyenes.

4.2 Theory

4.2.1 LASSCF

The multireference LAS wave function decomposes the active space of the entire molecule into various subspaces. The wave function is then expressed as an antisymmetrized product of the full configuration interaction (FCI) wave functions of the individual subspaces and the single determinant wave function of the inactive space. The active subspaces are localized over the distinct user-defined fragments of the molecule while the inactive space is delocalized over the entire molecule. A general LAS wave function can be expressed as

$$|\mathrm{LAS}\rangle \;=\; \left(\bigwedge_K |\Psi_{A_K}\rangle\right) \wedge |\Phi_U\rangle\,, \tag{4.1}$$

where Ψ_{A_K} is the multi body (generally FCI) wave function of the K^{th} localized subspace and Φ_U is the single-determinantal wave function delocalized over the entire molecule. This is obtained by variationaly optimizing the energy (E_{LAS}) in equation 4.2

$$E_{\mathrm{LAS}} \;=\; \langle \mathrm{LAS}|\hat{H}|\mathrm{LAS}\rangle \tag{4.2}$$

where $\hat{H}$ is the molecular Hamiltonian.

In a typical LASSCF calculation, the user specifies the number of electrons (N), magnetization (M_S), spin (S), and spatial symmetry point group (Γ) for each subspace rather than for the entire molecule. A LAS state is uniquely defined by the set of these 'local quantum numbers' for all fragments $\{(N_K,\, M_{S_K}, S_K\,,\, \Gamma_K)\ \forall K\}$. Changing any one of these quantum numbers (within allowed values) creates different LAS states. In our previous work we have used this flexibility to change S and M_S for specific subspaces to model ground and excited spin states of the molecule.[46,173] For example the ferromagnetic and anti-ferromagnetic coupling of locally high-spin (quintet) $Fe^{[II]}$ centers were used to model the nonet and open-

shell singlet states of the bimetallic [[$Fe(H_2O)_4]_2$bipyrimidine] $^{+4}$ bimetallic molecule studied in references 46 and 2. In selected cases like the nonet, the LAS states can be accurate (if not exact) approximations. In other cases, however, a single LAS state can be only a crude approximation to the full molecular wave function. For instance, in the aforementioned case, the open-shell singlet is modeled using only one of many configurations that have an overall $M_S = 0$. As a consequence, these LAS wave functions are not eigenfunctions of the $\hat{S^2}$ operator in cases where multiple active subspaces have non-singlet spins that are not aligned to each other.[46] This requires the generation of symmetry adapted molecular wave functions as linear combinations of multiple LAS states.

Moreover, while the LAS approach has proven to be useful in studying localized excitations, it cannot be used directly to study delocalized excitations or strong inter-fragment coupling.[2,46,173] LASSCF accounts for the inter-fragment interaction only through a spin polarized mean-field. Further two-body interactions between the subspaces are often necessary for calculating quantities such as spin state ordering in strongly coupled multi-metallic compounds. In other words, the exact correlated wave functions for such systems cannot be expressed as a single tensor-product state, but instead need to be expanded as linear combinations of multiple states that couple to each other through such two-body interactions in the molecular Hamiltonian. In the limit of including all possible LAS states in the expansion, the resulting wave function accounts for the *exact* electron interaction. In many cases, however, even with a smaller number of LAS states, chosen based on chemical intuition, one can recover a significant part of this additional electron correlation.

4.2.2 Multiple LAS states

Similarly to state-average CASSCF, wave functions for multiple LAS states can be obtained in the same set of localized orbitals using the SA-LASSCF method by minimizing the energy

expression:

$$E_{\mathrm{SA-LAS}} = \sum_i w_i \langle \mathrm{LAS^{(i)}} | \hat{H} | \mathrm{LAS^{(i)}} \rangle , \tag{4.3}$$

where $|\mathrm{LAS}^{(i)}\rangle$ corresponds to the i^{th} LAS state with weight w_i The SA-LASSCF wave functions are orthogonal, i.e. they diagonalize the LASSCF effective Hamiltonian, but can have off-diagonal elements (coupling) in the full-molecule Hamiltonian. In other words, these SA-LAS states are not eigenfunctions of the full-molecule Hamiltonian and suffer form the same problem highlighted in the previous section - namely the spin contamination and lack of inter-fragment coupling. These wave functions, however, are an excellent basis for the molecular wave function. The LAS state interaction (LASSI) method proposed in this work diagonalizes the molecular Hamiltonian constructed in terms of the SA-LAS states, to obtain molecular wave functions as linear combinations of LAS states (rather than that of n-particle excited states) as shown in equation 4.4.

$$|\mathrm{LASSI_i}\rangle = \sum_j C_{ij} |\mathrm{LAS^{(j)}}\rangle , \tag{4.4}$$

The LASSI wave functions are eigenfunctions of the Hamiltonian in the given LAS state basis:

$$\hat{H} |\mathrm{LASSI_i}\rangle = E^{(i)}_{LASSI} |\mathrm{LASSI_i}\rangle \tag{4.5}$$

In general these can be solutions to any arbitrary Hamiltonian in the basis of SA-LAS states. In this study we use only the exact electronic Hamiltonian of the entire molecule, but in principle any other electronic structure method can be used to obtain this Hamiltonian (effective potentials, PDFT, etc.) and effects like spin-orbit coupling can also be included to couple the LAS states. The LASSI is a one shot diagonalization of the full-molecule

Hamiltonian in a basis much smaller than that of all configurations within the complete active space. Similar to methods like RAS/GAS-SCF, which approach the exact solution (CASSCF) as we increase the number of configuration state functions (CSF), the LASSI wave function also approaches the exact solution in the limit of including all possible LAS states in the LASSI. However, a LAS state typically includes more correlation than a CSF and thus the CI vector of the exact solution can be significantly more compact in this basis. This means that as we expand the basis of the wave function we can account for more correlation faster when expanding in the LAS basis than expanding in the CSF basis.

While the primary motivation of this method is the restoration of inter-fragment coupling, one can think at LASSI also in the context of diabatization. This perspective is particularly helpful when computing potential energy surfaces for chemical reactions. The LAS states do not change chemical character imposed on them along a reaction coordinates are analogous to diabatic states, while the LASSI wave functions are solutions of the Hamiltonian and are the adiabatic states. The LASSI procedure is simply a transformation of the LAS states (model diabatic states) - that are comparatively straight forward to compute- to obtain the LASSI states that correspond to the uniquely defined eigenfunctions of the molecular Hamiltonian that conserve symmetries across the potential energy surface.

4.2.3 Selecting the LAS states for state interaction

Form most chemical systems the choice of the LAS states is non trivial and a protocol that automates this choice is needed. We propose a scheme that incrementally includes different types of states to systematically improve the quality of the solution depending on the problem in hand.[117,174]

Each LAS calculation is initialized with a certain number of active electrons occupying the active orbitals in each subspace. Using these as a reference we can allow up to n excitation from one fragment to the other to obtain charge-transfer (CT) states. All possible states that

can be reached by having up n CT excitations are considered - including states with multiple concerted excitations - in order to achieve size consistency. For example for $n = 1$ (single charge transfer excitations) we also include states that have concerted single excitations in multiple different pairs of subspaces.

For any LAS state, the net difference in the active electrons belonging to a subspace in that state with respect to the reference LAS state is termed as the charge on the subspace. This charge defines only the total number of electrons in each active subspace. This can, in principle, allow a large number of spin states. Some of these spin states may be very high in energy and may not be of particular interest. Depending on the chemical characteristics of the subspace the user has an option to limit the spin (S) of each fragment to a certain range. For instance, in a subspace of 6 electrons in 6 orbitals localized on a phenyl ring, one might choose to only include singlet and triplet states and exclude the quintet and septet states that are technically possible but unlikely to contribute to the wave function. The spin projection quantum number (M_s) is the other quantum number that uniquely characterizes a LAS state. All M_s values ranging from -S to S for each spin for each subspace are included in the SI Hamiltonian. While it is possible to include only a subset of the M_s values in the state average manifold, we do not recommend this choice for it might result in the LASSI states not being proper spin eigenfunctions.

In general, the states included in the SI Hamiltonian are not necessarily low-lying states. In some cases, the inclusion of high-energy states (like a charge-separated state or an excited spin state) in the SI Hamiltonian may be necessary if they couple strongly with the ground or low-lying excited states. It can, however, be detrimental to include them in the state-average manifold while optimizing the orbitals. Since the orbitals in SA-LAS are optimized to minimize a collective energy, the description of the ground state (or the particular state of interest) is compromised by these states. To avoid this, we can exclude the high energy states from the orbital optimization procedure. This is similar to the strategy often used

in SA-CASSCF - where the orbitals optimized from a calculation with a fewer states are used to perform a CASCI calculation for a larger number of roots. Specific details of the state selection schemes used in each application are provided in the respective sections. It must be noted that in the limiting case of approaching CASSCF - i.e. considering all possible CT excitations and spins - the method also scales exponentially with respect to the size of the active space like CASSCF. Although reducing the size (and thus increasing the number of fragments) always reduces the cost of the computation for a single-state LASSCF calculation, that is not the case for LASSI since the number of states to be considered for SI increases with the number of fragments. Thus it is important to strike a balance in the fragmentation schemes used in LASSI such that the subspaces are not too large for the FCI solver in subspace but also not so numerous that the exponential scaling of the size of the SI Hamiltonian can be handled.

4.3 Applications and Discussion

We demonstrate the scope and performance of LASSI in three different applications.

4.3.1 Charge transfer

Charge transfer plays an important role in many chemical and biological processes.[175–180] The process of charge transfer is often modeled with two approaches: either by constructing the Hamiltonain in a basis of diabatic, charge-separated states and then diagonalizing it to get the adiabatic states or to obtain the adiabatic ground and excited states (with an electronic structure method of choice) to begin with and then assign charge-transfer character to them. While the later approach is more popular because of its generality, the former is often used to interpret results and understand mechanisms of charge transfer. A key challenge for the former approach, however, is to obtain this chemically intuitive diabatic basis in an efficient way. Approaches such as valence-bond theory and constrained density functional theory

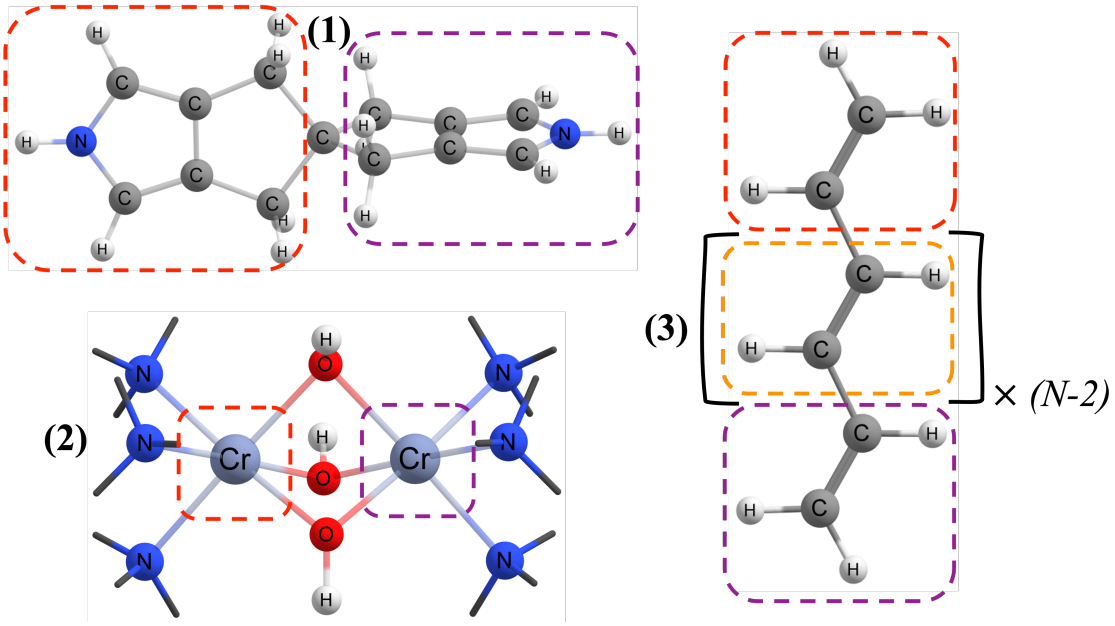

Figure 4.1: The systems studied: (1) is 2,2',6,6'-tetrahydro-4H,4'H-5,5'-spirobi[cyclopenta-[c]pyrrole] cation, (2) the $[Cr_2(OH)_3(NH_3)_6]^{+3}$and (3) represents a the *trans*-polyenes $C_{2N}H_{2N+2}$. The fragmentation scheme for their active space shown by dotted lines.

have been used previously for this purpose. In this section we highlight that LAS states can be an excellent choice for the diabatic basis, especially when the donor and acceptor species involved are multireference in nature. Moreover the adiabatic surfaces that can be easily obtained from these LAS states after state interaction, are just as good as the surfaces obtained from more expensive methods like CASSCF.

The 2,2',6,6'-tetrahydro-4H,4'H-5,5'-spirobi[cyclopenta- [c]pyrrole] cation, system **1**, is often used as a prototype to study the performance of electronic structure methods describing charge transfer. The compound consists of two cyclopenta[c]pyrrole rings that are perpendicular to each other. While the neutral compound is highly symmetric with a D_{2d} point group, the cation has most of the positive charge localized on one of the rings thus breaking the symmetry in its equilibrium structure. Since the two states of charge being localized on the two rings respectively are non-degenerate at the equilibrium geometry, there exists a finite barrier for this charge migration to happen. We study the potential energy surface

(fig 4.3) for this charge migration using CASSCF, LASSCF and LASSI with an active space containing the 11 π electrons in the 10 π orbitals. The LAS subspaces are composed of the 6 π orbitals localized on each ring with 5 electrons in one and 6 in the other. The other charge separated state is obtained when the number of electrons in each subspace is interchanged. The geometries along the potential energy surface were obtained from reference 181 that uses a unitless progress variable, ξ, to linearly parameterize the Cartesian coordinates along the reaction pathway. In this work, we consider ξ from -0.8 to +0.8 where -0.5 and 0.5 are the equilibrium structures corresponding to the charge being localized on the left and right side respectively. The potential energy curves for the two LASSCF states show a crossing

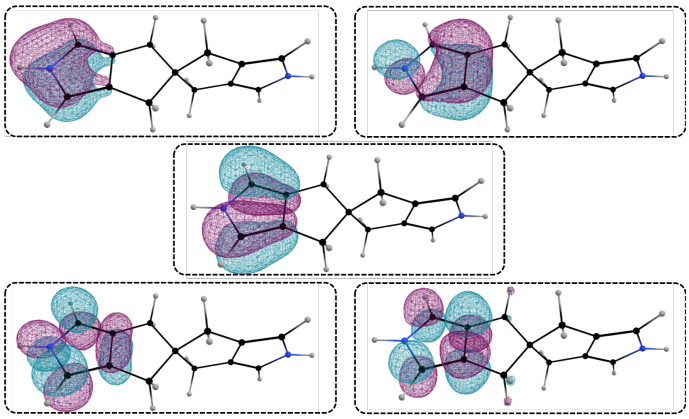

Figure 4.2: Active orbitals for the subspace localized on one of the cyclopenta-[c]pyrrole in system 1.

at $\xi = 0$. This is expected because the LAS states do not interact with each other. We consider only the LAS states corresponding to one subspace in a doublet spin-state (for the ring with the positive charge) and the other with a singlet spin in the LASSI calculation. Exited states with other spin-states or with more than one electron migrating between the subspaces are ignored.This only nominally adds to the computational cost of the problem but almost fully recovers the coupling between the states. The LASSI energies are identical to the larger CASSCF, showing that only these two states dominate the coupling term.

The Hamiltonain matrix element H_{ab} that couples the diabatic states is an important

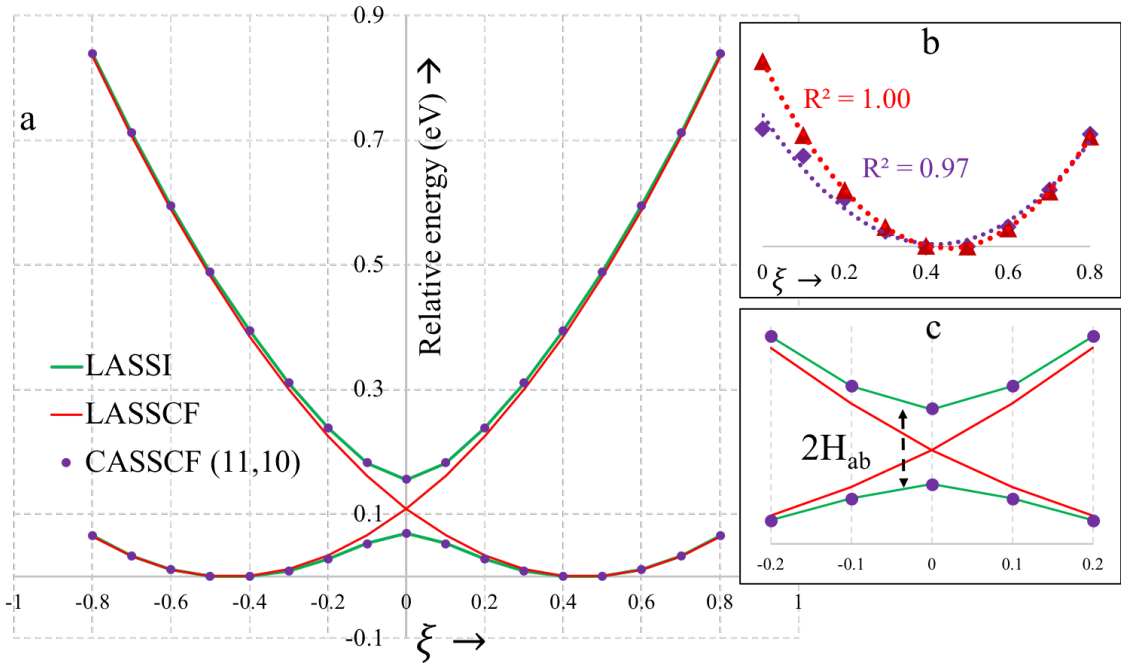

Figure 4.3: (a) Potential energy surface for the charge migration in **1** obtained from LASSCF, LASSI and CASSCF as a function of the dimensionless reaction coordinate (ξ). (b) The fitted quadratic curves (dotted lines) for the LASSCF and CASSCF energies along with their R^2 values. (c) a magnified plot of the PES on the left around the crossing point along with the gap indicating H_{ab}.

quantity that is used to classify and study charge transfer. This quantity is not explicitly computed using methods like CASSCF. The gap at the avoided crossing is often used to estimate H_{ab}. The gap with CASSCF is 0.16 eV. Since this is equal to $2 \times H_{ab}$ for a two-state model (fig. 4.3c) the coupling element (H_{ab}) is 0.8 eV. While LASSI reproduces this energy surfaces well and also gives a H_{ab} of 0.75 eV, LASSI arrives at this result in a different way. It explicitly calculates this coupling matrix in the basis of the LAS states and then mixes them to give the gap. This shows that the LAS states are good candidates for the diabatic states that provide interpretability as well as good accuracy. Another parameter that is needed for analyzing CT is λ, the stiffness of the parabola of the diabatic curve. The λ value along with the H_{ab} is used to calculate the rates for charge transfer. As seen in figure 4.3b, the LASSCF curves fit perfectly to a parabola and give a λ of 0.53 eV. If however, one

were to extract this number from the adiabatic CASSCF curves (or even LASSI) it would have some anharmonicity and give a λ of 0.42 eV. While this estimate for CASSCF can be made better by performing a finer scan in the region close to the equilibrium geometry, no such calculations are required for LASSCF. Any three points along the scan give similar value for λ.

The method of finding the CT state in CASSCF also involves significant trial-and-error in choosing sufficiently many excited states in the averaging manifold. Since we can selectively include only charge-states in the LASSI Hamiltonain, this approach does not suffer from the need to include all excited states lower than the CT states in the state-averaging manifold that might compromise the description of the CT states. This becomes helpful when studying systems like DNA base pairs and mixed-valency metal complexes that can have multiple excited states lower than the CT states.

4.3.2 Bimetallic compounds

Multi-metallic compounds are interesting for many applications.[182–184] The coupling between their spin centers is modeled using the effective Hamiltonian from the Heisenberg-Dirac-Van Vleck model.[185–187] This invokes a magnetic coupling parameter, J_{ab}, that couples the spins localized on the two centers a and b and characterizes the type and extent of coupling between them. By convention, a negative J indicates antiferromagnetic coupling and a positive J indicates a ferromagnetic one. The higher the magnitude of J, the stronger the coupling between the spin centers. Most computational methods calculate J using the Yamaguchi formula (4.6), that expresses it in terms of the energy difference between the high-spin and low-spin states:

$$J_{ab} = \frac{E_{HS} - E_{LS}}{\langle \hat{S^2} \rangle_{LS} - \langle \hat{S^2} \rangle_{HS}}, \tag{4.6}$$

To avoid the spin-symmetry breaking that occurs in DFT (and other single-determinant methods) to compute E_{LS}, multireference methods are needed. For quantitatively accurate spin gaps, however, large active spaces are required to model the interactions in such compounds. This becomes prohibitively costly in the presence of more that two metal centers. The coupling between the multiple metal centers is affected my many factors. Some of these are understood through different conceptual mechanisms like direct exchange/through space coupling or superexchange, etc. Most multireference methods, even with approximate solvers that allow us to go to larger systems, do not offer easily interpretable quantitative insights into the contributions of these mechanisms and in such situations, on the other hand, LASSI can be very useful.

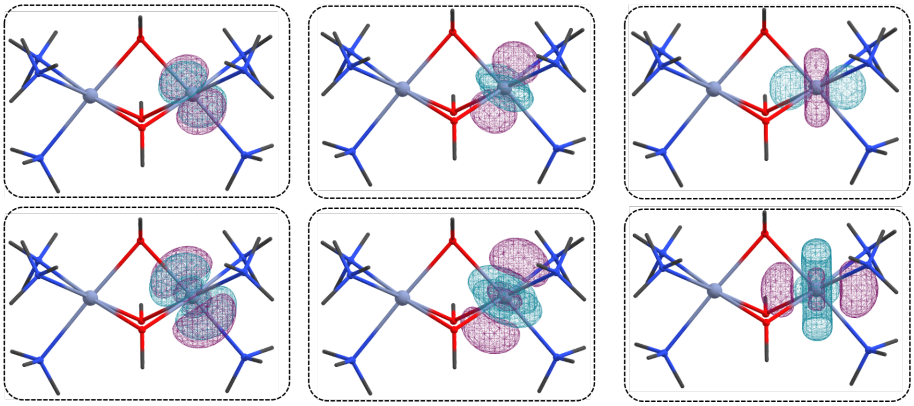

Figure 4.4: Active orbitals for the subspace localized on one Cr ion.

We consider the coupling between two high spin metal centers in compound **2**. This compound is a model for a tris-(μ-hydroxo)-bridged chromium compound studied experimentally and theoretically[188–192]. The ligands were truncated at coordinating nitrogen and were capped with hydrogen atoms. The two chromium [III] ions have three unpaired electrons each. The active space we consider is that of 6 electrons in 12 orbitals that corresponds to all the singly occupied 3d orbitals on the Cr centers and their corresponding 4d (correlation pair) orbitals (see Fig. 4.4). The CASSCF (6,12) calculations predicts a J_{ab} of -16.7 cm^{-1}. This indicates that the compound is anti-ferromagnetic. The spin ladder for

CASSCF in figure 4.5 shows that the singlet ($S = 0$) state is about 200 cm^{-1} lower than the septet ($S = 3$) state. The experimental value for the J-coupling constant is -66 cm^{-1}. Previous investigations have shown that a quantitative prediction of the constant will not only require a much larger active space but also needs to include post-MCSCF methods to include more dynamic correlation.[192,193] The purpose of this study is not to reproduce the experimental value, but to analyze how LASSI can approach the CASSCF limit.

The overall coupling captured in CASSCF is mainly affected by two conceptual mechanisms - the 'direct' exchange and the 'kinetic' exchange.[194,195] Note that superexchange mechanism is not captured here since we do not include the any linker orbitals in the active space. The 'direct' exchange contribution arises from the coupling elements emerging from direct exchange integrals between orbital pairs with one orbital localized on one spin center and the other on another spin center. Since these integrals are always positive they contribute to a positive value of J i.e. 'direct' exchange favours the high-spin state. The kinetic exchange, however, accounts for the coupling of the ground state with configurations involving excitations from one spin center to another (ionic configurations). It's magnitude depends on coupling between neutral and ionic configurations (hopping integral). This coupling favours an antiferromagnetic ground state and contributes to the lowering of the J. Thus the overall sign of J is determined by how large the kinetic exchange terms is. These concepts and relations are derived and explained for the case of two ($S = \frac{1}{2}$) doublets in two orbitals in references 195 and 194. The negative sign of the CASSCF J means that the compound is antiferromagnetic and thus that the kinetic exchange dominates the coupling. There, however, is no simple way to quantify this contibution the CASSCF wave function. This is where LASSI comes in - by selectively including the states corresponding to each of the mechanisms in the LASSI we can 'switch-on' or 'switch-off' different mechanisms of coupling between the fragments.

We perform LASSI calculations where we divide the (6,12) active space into two subspaces

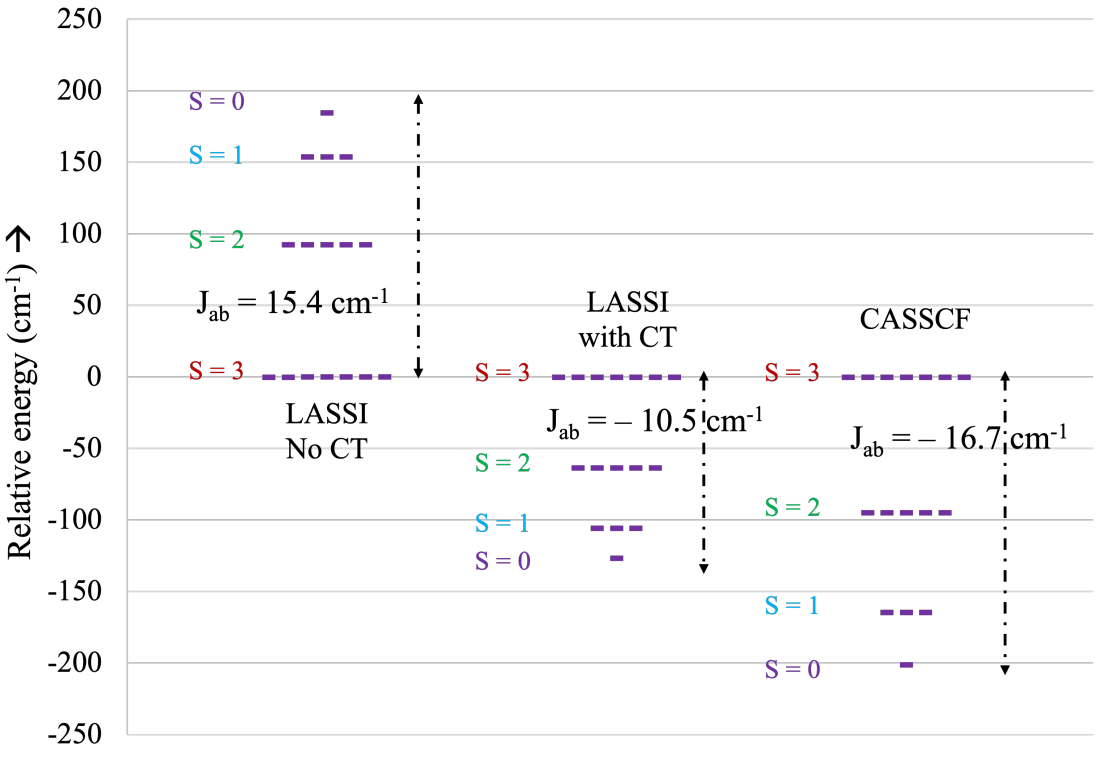

Figure 4.5: Spin ladder for the bimetallic compound calculated using various methods relative to the septet energies for the respective method. The number of purple dashes indicates the multiplicity of the state. The J value calculated using the singlet-septet gap is shown for each ladder.

of (3,6) localized on each Cr atom (see Fig. 4.4). If the SI Hamiltonian is constructed only in the space of the neutral states, the only off-diagonal terms are the direct exchange terms. This gives a wrong spin state ordering. The J value is positive as expected and significantly so at 15.4 cm^{-1}. As seen in figure 4.5, the singlet ($S = 0$) state is about 185 cm^{-1} higher than the septet ($S = 3$) state. This scheme of state interaction is not reliable since it accounts only for direct exchange and will always give a positive J.

When we include the states with inter-fragment electron hopping, however, the spin state ordering is correct and the J is lowered to -10.5 $^{-1}$. This means that the kinetic exchange terms, that are now introduced in the SI Hamiltonian, contribute about -25 cm^{-1}. In such a way we were able to quantify the two contributions separately. Figure 4.5 shows the qualitative similarity in the spin ladder predicted by CASSCF and LASSI with CT states.

By including the CT states in the SI Hamiltonian we have not only computed the correct spin state ordering but have reduced the disagreement with CASSCF in the J value from 30 cm^{-1} to 6 cm^{-1}. This calculation is, in principle, cheaper than CASSCF, but also provides more information and insight into the system. This J value however is still not the same as the CASSCF value because the LASSI even with all possible electron hopping and all possible spin states is approximate. This is because the CASSCF still included more terms - in particular the excitations within the same active subspace.

4.3.3 Delocalized spin states: Case study in polyenes

Methods to accurately predict singlet-triplet (S-T) gaps for long conjugated compounds are interest for a wide rage of applications.[136,196–200] A chemically intuitive fragmentation scheme, with a set of π and π^* orbitals localized on smaller units like C_2H_2 or C_4H_4, would in principle provide a significant advantage in terms of number of configurations needed with increasing size of the molecule. State-specific LASSCF with such a fragmentation describes reasonably well the ground-state singlet which is dominated by the closed shell configuration. However, it is not suited for calculating the S-T gaps as it is not able to capture the delocalized nature of the unpaired electrons of the triplet. Since only one of the active subspaces can have a triplet spin, the two unpaired electrons are localized only on that fragment. This is a nonphysical description since the true triplet has the two electrons delocalized over the entire molecule. This is a typical situation where LASSI is superior to LASSCF and more affordable than CASSCF.

Table 4.1 shows the singlet-triplet gaps computed with CASSCF, LASSCF and LASSI for four linear polyenes $C_{2n}H_{2n+2}$ with n = 2,3,4 and 8. The complete active space of size $(2n, 2n)$ composed of the π and $\pi*$ orbitals is divided into n subspaces of (2,2) for n=2,3,4 ($\bigwedge_n(2,2)$ fragmentation) and into $n/2$ subspaces of (4,4) for $n = 4$ and 8 ($\bigwedge_{n/2}(4,4)$ fragmentation). Two schemes have been used to construct the LASSI Hamiltonian: one

n	CASSCF	Subspace decomposition	LASSCF	LASSI		Experiment
				no CT	with CT	
2	3.42	$(4,4) \rightarrow \bigwedge_2(2,2)$	4.29	4.62	3.43	3.22 [201]
3	2.80	$(6,6) \rightarrow \bigwedge_3(2,2)$	4.10	4.79	2.86	2.61 [202]
4	2.39	$(8,8) \rightarrow \bigwedge_4(2,2)$	4.01	4.88	2.48	2.10
		$(8,8) \rightarrow \bigwedge_2(4,4)$	3.30	3.41	2.66	
8	–	$(16,16) \rightarrow \bigwedge_4(4,4)$	3.16	3.53	2.10	–
12	–	$(24,24) \rightarrow \bigwedge_4(6,6)$	2.62	2.37	1.98	–

Table 4.1: Singlet triplet gaps from CASSCF , LASSCF and the various schemes of LASSI

where only neutral configurations with singlets and triplet spins are used and the other where charge-transfer configurations with one electron hopping were also included. The orbitals for LASSI were obtained by state-averaging over the singlet ground state and states with up to two triplet fragments. This truncation of the space was used only for the orbital optimization for computational efficiency, while all possible states states were considered when constructing the LASSI Hamiltonian. The results for the gaps calculated using only the ground state singlet orbitals are reported in the SI and are compared to the CASCI gaps.

We observe that the CASSCF gap reduces with increasing length of the conjugated chain. The LASSCF with the triplet localised on one fragment not only gives the wrong quantitative gap but also shows minimal change with increasing chain size. The gap stays around the same as that of a single ethylene molecule for the $\bigwedge_n(2,2)$ fragmentation.

In the LASSI calculations, the cases without the charge transfer (hopping) states included in the SI Hamiltonian show poor performance. This accuracy of the singlet-triplet gaps is due to the treatment of the two spin states at equal footing and not because the LASSI states (and absolute energies) are necessarily individually close to their CASSCF equivalents. This is the reason we do not observe the gap for the octa-ene predicted by LASSI gets slightly worse w.r.t experiment and CASSCF when we have larger subspaces.

4.4 Conclusions

We presented an extension of the LASSCF methods, LASSI that overcomes some of the challenges associated with LASCSF by constructing eigenfunctions of the molecular Hamiltonian in the basis of LAS states. LASSI not only allows us to systematically improve the wave function - eventually approaching the CASSCF limit - but also provides a chemical interpretation of the results. We demonstrated how the control over the interactions between the fragments can be leveraged to study phenomena like charge transfer and spin-coupling in detail. In future work this method can be applied to larger systems with several locally correlated fragments to study phenomena like intravalent charge transfer in organometallic compounds and superexchange mediated J-coupling in multi-metallic compounds. Further improvements in scaling can be achieved by using other approaches to couple the subspaces like DMRG or (unitary) coupled cluster. Moreover, better quantitative predictions of the method can be achieved by including more electron correlation using methods like perturbation theory and pair-density functional theory.

CHAPTER 5

LOCALIZED QUANTUM CHEMISTRY ON QUANTUM COMPUTER

5.1 Introduction

Chemical systems with many close-lying electronic states or, more generally, strongly correlated electrons pose a significant challenge for modern electronic structure theories in computational quantum chemistry[56,203–206]. When transition metals or heavier elements are involved, degenerate and nearly degenerate electronic states are common, and single-reference electronic structure methods such as Kohn–Sham density functional theory often fail[195,207,208]. In these situations one has to use multireference methods to generate multiconfigurational wave functions and accurately describe these near degeneracies[126,127,209].

Scientists also want to compute properties of large chemical systems or solids with accurate quantum chemistry methods, in spite of steep computational requirements. One way to achieve such computations is to use fragmentation methods. Many variations of fragmentation methods exist[86,210–212], but the common feature is that a large molecular system is divided into fragments and quantum-mechanical calculations are performed on the fragments. An especially important case is the application of fragmentation methods to multireference wave functions because of the exponential explosion of the computational cost with respect to the size of the active space of electronic configurations.

In the complete active space self-consistent field (CASSCF) method[18], all the electronic configurations that can be formed for a given number of active electrons distributed in a given number of active orbitals are included in the wave function. Thus, the wave function scales exponentially with the number of active electrons and orbitals, and the method has only limited application to chemically relevant systems. If one wants to study systems containing, for example, several transition metals[76,194,213–215], the active site of a protein[159],

or extended organic chains in their ground and excited states[139,159], more affordable multireference methods have to be developed. This is one of the major challenges of modern electronic structure theory.

Reducing the computational cost of CASSCF or other multiconfiguration self-consistent field calculations is pursued both in the development of new well-motivated theoretical approximations and in the application of new developments in computational hardware[216,217]. On the theoretical side, one strategy is to identify subspaces of the CAS that can be treated on different footings[60,61] or interact with one another only weakly[62,63,84,93,218]. The localized active-space self-consistent field (LASSCF) method[1,2,46,173], also known as the cluster mean-field (cMF) method,[91] is an example of such a strategy. LASSCF is designed for applications in which electrons are strongly correlated in different weakly interacting physical regions of a molecule and approximates the strongly correlated part of the wave function as a single antisymmetrized product of subspace wave functions. The computational cost of LASSCF is a linear function of the number of such unentangled subspaces.

Some of the authors have recently shown that LASSCF accurately reproduces the CASSCF spin-state energy gaps of bimetallic compounds and the simultaneous dissociation of two double bonds in bisdiazene at a significantly reduced cost [2,46]. However, LASSCF fails to recover any electron correlation between fragments, for example in the *cis-trans* isomerization of stilbene and similar systems[173]. Moreover, methods to restore the missing correlation variationally[219], perturbatively[91,220], or *via* the coupled-cluster (CC) approach[221] on classical computers must usually enumerate a general many-body basis for each fragment. That is, they inherit the complications of multireference perturbation and CC theory[127,222] over traditional single-reference perturbative or truncated coupled-cluster (CC) corrections based on second quantization[223,224].

Recently, the development of quantum computers has led to an increased interest in novel quantum algorithms, especially for computational quantum chemistry, which is widely

seen as a potential "killer app" of quantum computers[225–227]. The quantum phase estimation (QPE) quantum algorithm [228] can potentially offer exponential speedups when large fault-tolerant quantum computers are available[229,230], under the assumption that an initial state with non-negligible overlap can be prepared[231,232]. Additionally, the variational unitary coupled cluster (UCC) requires only a polynomial number of gates to represent on a quantum computer, whereas representing the same ansatz classically has no known polynomial solution[233,234]. For the noisy, intermediate-scale quantum (NISQ)[235] devices that we have today, these algorithms are not tenable, since they require coherence times far beyond what is available. Variational algorithms, such as the variational quantum eigensolver (VQE)[234], have been used to perform calculations of the ground state energy of small molecules, with limited accuracy, on NISQ devices[236–238]. Quantum algorithms that have less stringent requirements compared with full QPE, and at the same time accuracy beyond that demonstrated by variational algorithms such as VQE, will be required to productively use the progressively larger and higher-quality quantum devices as they become available in the next few years.

In this chapter we describe a framework for such quantum algorithms, inspired by classical LASSCF. The wave function within a fragment is solved by using one method (e.g., QPE), and correlation between fragments is encoded variationally by using an ansatz that entangles the fragments. This approach goes beyond what can be achieved with classical fragment methods, such as LASSCF, by providing additional correlation between fragments, while significantly reducing the total computational time (estimated via the number of gates) compared with full QPE.

5.2 Theory

5.2.1 Multireference Methods with Exponential Scaling

We seek to find the ground state of the second-quantized molecular Hamiltonian for a given number of M electrons,

$$\hat{H} = \sum_{pq} h_q^p \hat{a}_p^\dagger \hat{a}_q + \frac{1}{4} \sum_{pqrs} h_{qs}^{pr} \hat{a}_p^\dagger \hat{a}_r^\dagger \hat{a}_s \hat{a}_q, \tag{5.1}$$

where $\hat{a}_p^\dagger$ ($\hat{a}_p$) creates (annihilates) an electron in spin orbital p; h_q^p and h_{qs}^{pr} are the one- and antisymmetrized two-electron Hamiltonian matrix elements, respectively; and repeated internal indices are summed. Generally, for N spin orbitals, $\hat{H}$ has a sparse-matrix representation in a space of size $O\binom{N}{M}$ and has $O(N^4)$ elements. Full-configuration interaction (FCI) determines the exact energy within a given one-electron basis set (the FCI energy) at exponential cost. Methods such as CASSCF (and its restricted[60,61] and generalized[62,239] active space approximations) or selected configuration interaction[240,241], can go beyond FCI in system size, maintaining comparable accuracy, but still scale exponentially. The density matrix renormalization group[242–245] and coupled cluster methods[224] can scale polynomially but introduce (sometimes uncontrollable) approximation errors. Here we briefly describe the LASSCF algorithm[1,46], which will serve as the basis for our fragment-based quantum algorithms.

5.2.2 LASSCF

In LASSCF, the wave function of a molecule is approximated as

$$|\mathrm{LAS}\rangle = \bigwedge_K |\Psi_K\rangle \wedge |\Phi\rangle, \tag{5.2}$$

where $|\Psi_K\rangle$ is a general many-body wave function describing M_K electrons occupying N_K active orbitals of the K^{th} "fragment" or "active subspace," $|\Phi\rangle$ is a single determinant spanning the complement of the complete active space, and the wedge operator ("$\wedge$") implies an antisymmetrized product.

In the variational[46] implementation of LASSCF, this wave function is obtained by minimizing the LAS energy,

$$E_{\text{LAS}} = \langle \text{LAS}|\hat{H}|\text{LAS}\rangle \,, \tag{5.3}$$

with respect to all orbital rotations and configuration interaction (CI) vectors defining $|\text{LAS}\rangle$. This is accomplished by introducing a unitary operator (see the Supporting Information of Ref. 46) that is parameterized in terms of all nonredundant transformations of the orbitals and CI vectors,

$$|\text{LAS}\rangle = \hat{U}_{\text{orb}} \prod_K \hat{U}_{\text{CI},K} \, |\text{HF}\rangle \,, \tag{5.4}$$

where $|\text{HF}\rangle$ is the Hartree-Fock wave function used as the initial guess and

$$\hat{U}_{\text{orb}} = \exp x_l^k \left(\hat{a}_k^\dagger \hat{a}_l - \hat{a}_l^\dagger \hat{a}_k \right), \tag{5.5}$$

$$\hat{U}_{\text{CI},K} = \exp x_{\vec{k}} \left(|\vec{k}\rangle \langle \Psi_K| - |\Psi_K\rangle \langle \vec{k}| \right), \tag{5.6}$$

where k, l index individual spin orbitals in two different subspaces (including the inactive and virtual subspaces outside of the CAS) and where $|\vec{k}\rangle$ is a determinant or configuration state function. First and second derivatives of Eq. (5.3) with respect to the generator amplitudes (x_l^k and $x_{\vec{k}}$) are obtained by using the Baker–Campbell–Hausdorff (BCH) expansion, and the energy is minimized by repeated applications of the preconditioned conjugate gradient (PCG) method[246,247].

The orbital unitary operator, $\hat{U}_{\text{orb}}$, corresponds to the UCC correlator truncated after

the first ("singles") term:

$$\hat{U}_{\mathrm{UCC}} \equiv \exp\left(\hat{T}_{\mathrm{UCC}}\right), \tag{5.7}$$

$$\hat{T}_{\mathrm{UCC}} \equiv x_l^k \left(\hat{a}_k^\dagger \hat{a}_l - \mathrm{h.c.}\right) + \frac{1}{4} x_{ln}^{km} \left(\hat{a}_k^\dagger \hat{a}_m^\dagger \hat{a}_n \hat{a}_l - \mathrm{h.c.}\right) + \ldots. \tag{5.8}$$

The use of the more general cluster operator, Eq. (5.8), in place of the orbital rotation unitary operator, Eq. (5.5), corresponds to a multireference unitary coupled cluster method[248] built on top of a $|\mathrm{LAS}\rangle$ reference wave function. Such a method is expected to more flexible than LASSCF itself, in that doubles and higher-order cluster amplitudes could encode electron correlation and entanglement between active subspaces. This would require the reference wave function, $|\mathrm{LAS}\rangle$, to be updated by explicit exponentiation of the general cluster operator, Eq. (5.8), after each execution of the PCG algorithm. On classical computer hardware, however, this is not an efficient way to extend LASSCF.

5.2.3 Quantum Algorithms

Here we describe two quantum algorithms that serve as the primary components for our fragment-based quantum algorithm.

Quantum Phase Estimation

The quantum phase estimation algorithm solves for the eigenvalue, λ_k, for an eigenvector $|v_k\rangle$ of some unitary matrix, U. In addition to its use in quantum chemistry, it forms the basis for many important quantum algorithms, such as Shor's prime number factoring algorithm[249] and the Hassidim–Harrow–Lloyd algorithm for inverting matrices[250]. For quantum chemistry problems, the unitary matrix U is generated by the Hamiltonian, H

(eq. (5.1)), over time steps τ:

$$U|v_k\rangle = e^{-i\hat{H}\tau}|v_k\rangle = e^{i2\pi\phi}|v_k\rangle, \tag{5.9}$$

and the desired energy is mapped to the phase acquired, $E = -2\pi\phi/\tau$, where units have been chosen such that $\hbar = 1$. By combining real-time evolution of the Hamiltonian, $\hat{H}$, with application of the quantum Fourier transform (QFT)[251], the value of the energy can be obtained in polynomial time using a quantum computer.

The computational complexity of the QPE is directly related to the complexity of implementing the unitary propagator $U = e^{-i\hat{H}\tau}$. Many strategies for implementing U exist, including Trotterization[252,253], Taylorization[254], and qubitization[255]. The Hamiltonian, Eq. (5.1), has $O(N^4)$ terms, where N is the number of spin orbitals. Each term in the Hamiltonian can be transformed into a Pauli string (that is, a product of Pauli operators X, Y, Z, or I) via one of the many fermion-to-spin transformations, such as the Jordan–Wigner[256], parity[257], and Bravyi–Kitaev[258] transformations. In this work we focus on QPE using Trotterization with the Jordan–Wigner transformation since they serve as standard reference points for the other variations. The complexity of QPE for the Hamiltonian, Eq. (5.1), using Trotterization with the Jordan–Wigner transformation is $O(N^5)$: N^4 arising from the number of terms in the Hamiltonian and an additional N from the Jordan–Wigner transform. Although QPE can obtain estimates of the ground state energy with only a polynomial number of quantum gates, the overheads are still too large for near-term quantum computers. The success of the QPE algorithm directly depends on the overlap of the initial state (which is often taken to be the Hartree-Fock state) and the true ground state. Realistic estimates, taking into account overheads such as quantum error correction, put the needed number of qubits to perform QPE on interesting molecules in the millions[259–261].

QPE is analogous to a Fourier analysis of a correlation function; and, for a given energy accuracy, ϵ, it requires propagation efforts (maximum times) on the order of $O(1/\epsilon)$[227,262].

Since the circuit depth for evaluating the propagator for individual fragments will naturally be lower than for the full system, the QPEs involved in our LAS approach will be significantly cheaper than full QPE.

Variational Quantum Eigensolver

The variational quantum eigensolver is a hybrid quantum-classical algorithm that relies on the variational principle to find an estimate of the ground state energy of a given molecule. A circuit with variable parameters, θ, serves as an ansatz, whose energy is evaluated on a quantum computer and whose parameters are iteratively optimized by a classical computer. For a circuit ansatz $|\psi(\theta)\rangle$, VQE estimates the energy as

$$E = \min_{\theta} \langle \psi(\theta)|\hat{H}|\psi(\theta)\rangle \,. \tag{5.10}$$

The Hamiltonian, $\hat{H}$, is transformed into a sum of Pauli strings via a fermion-to-spin transformation, and the expectation value of each term is measured from the quantum computer separately and summed on the classical computer. VQE has much less stringent quantum resource requirements than QPE has, since it offloads much of the work (such as optimization) to the classical computer. Hence, VQE has been used in proof-of-principle calculations for small molecules[263–265].

The accuracy of VQE is determined by the quality of the ansatz, $|\psi(\theta)\rangle$. The UCCSD ansatz is an interesting choice as wave function for VQE since there is no known way to efficiently implement UCCSD on classical computers[266–268], but it can be implemented with $O(N^5)$ gates on quantum computers[237,269,270]. The UCCSD ansatz is

$$|\psi_{\mathrm{UCCSD}}\rangle = \hat{U}_{\mathrm{UCCSD}}\,|\mathrm{HF}\rangle = \exp \hat{T}_{\mathrm{UCCSD}}\,|\mathrm{HF}\rangle \,, \tag{5.11}$$

where $\hat{T}_{\mathrm{UCCSD}}$ is defined by truncating the more general cluster operator of Eq. (5.8) at

the second term. While the UCCSD ansatz can be implemented on NISQ devices for small molecules[238,271], it is limited in its accuracy because of only including up to doubles excitations.

5.2.4 LAS Methods on Quantum Computers

Here we describe an algorithm for molecular calculations that goes beyond the limited accuracy of standard VQE[237,238], while having dramatically reduced computational complexity compared with QPE. The algorithm exploits the structure of the molecule by separating it into coupled fragments, as is done in the classical algorithm, LASSCF. The quantum algorithm, however, goes beyond classical LASSCF by providing some degree of entanglement between the fragments.

The algorithm begins by segmenting the orbital active space of a given molecule into distinct fragments defined by non-overlapping orbital subspaces, as in classical LASSCF. For instance, orthogonalized atomic orbitals generated by using the meta-Löwdin method[110] can be sorted into localized fragments and then projected onto a guess for the CAS of a given molecule to produce localized active orbitals. We construct an effective Hamiltonian that omits non-mean-field interfragment interactions, resulting in a sum of local fragment Hamiltonians,

$$\hat{H}_{\text{eff}} = \sum_{K}^{n_f} \left(\tilde{h}^{k_1}_{k_2} \hat{a}^\dagger_{k_1} \hat{a}_{k_2} + \frac{1}{4} h^{k_1 k_3}_{k_2 k_4} \hat{a}^\dagger_{k_1} \hat{a}^\dagger_{k_3} \hat{a}_{k_4} \hat{a}_{k_2} \right), \tag{5.12}$$

where $k_1, k_2, \ldots$ index distinct active orbitals of the Kth fragment and where

$$\tilde{h}^{k_1}_{k_2} \;=\; h^{k_1}_{k_2} + h^{k_1 i}_{k_2 i} + \sum_{L \neq K} h^{k_1 l_1}_{k_2 l_2} \gamma^{l_1}_{l_2}, \tag{5.13}$$

where i and l_n index respectively inactive orbitals [i.e., those defining $|\Phi\rangle$ in Eq. (5.2)] and active orbitals of the Lth fragment and where $\gamma^{l_1}_{l_2}$ is a one-electron reduced density matrix

element for spin orbitals l_1 and l_2,

$$\gamma_{l_2}^{l_1} \equiv \langle \mathrm{LAS}|\hat{a}_{l_1}^\dagger \hat{a}_{l_2}|\mathrm{LAS}\rangle = \langle \Psi_L|\hat{a}_{l_1}^\dagger \hat{a}_{l_2}|\Psi_L\rangle \,. \tag{5.14}$$

Given a set of localized active orbitals that minimize the LASSCF energy, if the density matrices in Eq. (5.13) are obtained from a classical LASSCF calculation on the same system, then the QPE algorithm applied to $\hat{H}_{\mathrm{eff}}$ generates the active-space part of the LASSCF wave function, $|\mathrm{QLAS}\rangle = \bigwedge_K |\Psi_K\rangle$, on the quantum computer. The same result is achieved if density matrices are obtained self-consistently from the QPE evaluation. If the density matrices are obtained in some other way, for instance from $|\mathrm{HF}\rangle$, then an approximation to the LASSCF wave function is obtained.

The QPE step provides the initial $|\mathrm{QLAS}\rangle$ for each fragment step by repeating the measurement of the phase until it is consistent with the phase representing the ground state energy, which collapses the system into the ground state wavefunction. This introduces some overhead, as each fragment will need to be in the ground state to continue to the next step. Furthermore, a full QPE solve, estimating the ground state energy, must be performed initially to provide a comparison value.

A sequence of UCC with singles and doubles (UCCSD) circuits, with variable parameters, is then applied across m fragments each (which we term m-local), leading to the LAS-UCC wave function,

$$|\mathrm{QLAS}(\boldsymbol{x})\rangle = \prod_\zeta \hat{U}_{\mathrm{UCCSD},\zeta}(\boldsymbol{x})\,|\mathrm{QLAS}\rangle \,, \tag{5.15}$$

where $\hat{U}_{\mathrm{UCCSD},\zeta}(\boldsymbol{x})$ is the UCCSD ansatz including only creation/annihilation operators within the m fragments that it spans, ζ is a list of fragment indices of size m, and $\boldsymbol{x}$ are the associated singles and doubles cluster amplitudes. The factorization of Eq. (5.8) implied by Eq. (5.15) is based on the intuition that physically adjacent active subspaces are likely

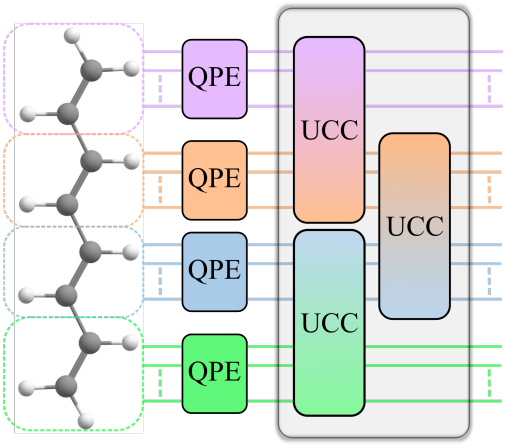

Figure 5.1: Diagram of example circuit using LAS-UCC. The system of interest is first separated into distinct fragments. QPE is used on each fragment to solve for the approximate unentangled ground state. Correlation between fragments is then added in, variationally, through a unitary coupled cluster ansatz.

to be more strongly entangled to one another than subspaces on opposite ends of a large molecule. The parameters of the UCCSD circuit are varied to minimize the total energy of the full system, as in VQE:

$$E = \min_{\boldsymbol{x}} \langle \mathrm{QLAS}(\boldsymbol{x}) | \hat{H} | \mathrm{QLAS}(\boldsymbol{x}) \rangle \,. \tag{5.16}$$

A schematic representation of the described circuit is shown in Fig. 5.1. This provides electron correlation between the fragments, in a way that scales exponentially on classical computers, but only polynomially on quantum computers. Moreover, this procedure provides a better estimate of the ground state energy than the product wave function or the UCCSD would provide alone. Note that, unlike LASSCF, this method is not strictly variational (despite the use of VQE) because the initial product-state wave function, $\bigwedge_K |\Psi_K\rangle$, is not variationally reoptimized in the presence of the UCCSD correlators. The QPE circuits could also be replaced with a local variational ansatz, leading to a fully variational algorithm, which we term LAS-VQE and describe in section 5.4.1.

To understand the large improvement in computational complexity of our approach, we

focus on a system of n_f fragments, with the number of orbitals per fragment, N_K, constant as the number of fragments grows. The total system size is defined by $N = N_K n_f$ orbitals. We also assume that each fragment interacts with only the m geometrically nearest fragments and that m does not grow with n_f. These are reasonable assumptions for many interesting molecules and mirror the assumptions made in classical LASSCF. Under these assumptions, the QPE solver for the unentangled fragments does not grow with N, since N_K is assumed to be fixed while n_f grows. The number of small QPE sections grows linearly with the number of fragments, of course. Typically, the Jordan–Wigner transformation would introduce an $O(N)$ term to enforce the anticommutation relations among the orbital creation and annhilation operators. However, in the case of linear chains, as we study here, ordering the orbitals such that all up and down occupied and virtual orbitals in a given fragment are close, the high-weight Z part of the Jordan–Wigner transformation effectively cancels out, causing no scaling with total number of orbitals.

Together, this leads to an overall $O(n_f N_K^4) \approx O(N)$ (linear) number of gates to solve for the n_f unentangled product wave functions. The UCCSD correlator, which is then applied, has $O\big(m^4 N_K^4\big)$ terms in the cluster operator for each correlator, because the UCCSD circuit spans only m fragments. Neither m nor N_K grows with the total size (number of spin orbitals) of the system, N. The number of m-local correlators grows as $O(n_f)$. Again, by careful ordering of the orbitals, the Jordan–Wigner transformation does not introduce any scaling overhead. The complexity of the m-local UCCSD correlator is then $O(n_f m^4 N_K^4) \approx O(N)$ (linear). This creates an overall linear scaling in the number of gates for linear chain geometries, with respect to only the total size of the system, N, and is polynomially ($O(N^4)$) better than performing QPE alone, while providing accuracy above VQE using the UCCSD ansatz and classical LASSCF. Many of the gates can be done in parallel, such as the local QPE circuits and the different m-local UCCSD correlators, leading to an expected overall sub-linear depth. If the fragments are coupled in a geometry more complicated than a

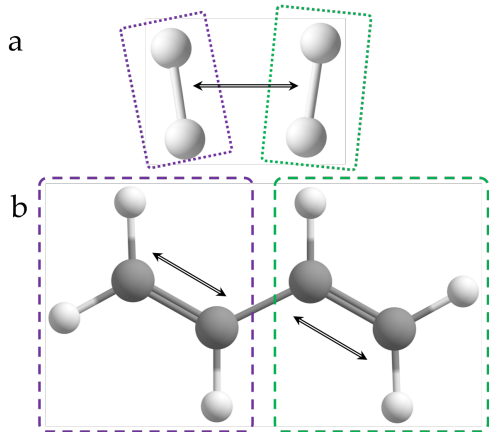

Figure 5.2: Two model systems used for testing. (a) The asymmetric hydrogen dimer, $(H_2)_2$. Each H_2 molecule is a fragment described by a 2-electron, 2-spatial orbital or (2,2) active subspace in the dimer's LAS wave function. The potential energy surface is scanned along the distance between the two H_2 bond midpoints, indicated by the black double line. (b) The *trans*-butadiene molecule at its CASSCF(8,8)/6-31G ground-state equilibrium geometry. Dashed boxes depict the two notional fragments containing the two (4,4) active subspaces in the LAS wave function. Black double lines indicate the internal coordinate along which the potential energy surface is scanned; the two terminal methylene units are simultaneously removed from the central acetylene unit.

linear chain, the UCCSD correlator will potentially incur the $O(N)$ Jordan-Wigner overhead, leading to an overall $O(N^2)$ scaling for arbitrary geometries with an expected $O(N)$ depth.

5.3 Computational Methods and Models

5.3.1 Illustrative Molecular Systems

In the calculations discussed below, we consider two systems, depicted in Fig. 5.2. The first, shown in Fig. 5.2(a), is a simplistic model of weakly interacting fragments, consisting of two H_2 molecules at various distances between their two midpoints using a minimal STO-3G atomic orbital (AO) basis set, and the two active subspaces in the LAS wave function correspond to the active spaces of the two H_2 molecules. We use this small basis set because of the size limitations of today's quantum computers and simulations. The bond lengths and internal angles of this system are set arbitrarily to remove point group symmetry so that

differences between various methods are not obscured by the simplicity of a symmetrized electronic wave function. The interaction between the two fragments in this model system are weak, and the LAS wave function is therefore expected to provide an excellent model of the FCI wave function except when the distance between the two molecules is very small. We additionally extend this system up to 20 H_2 in a linear chain, where we estimate only the total number of quantum resources necessary.

The second system, depicted in Fig. 5.2(b), is the *trans*-butadiene molecule. The potential energy surface of this molecule is scanned along the internal coordinate corresponding to the simultaneous stretching of both the C=C double bonds, leading to the removal of two methylene units from a central C_2H_2 (distorted acetylene-like) unit. In the LAS wave function, the molecule is divided into two fragments split across the central C–C bond, and each fragment is described by a (4,4) active subspace. Several molecular orbitals are therefore left inactive, described by an unfragmented single determinant. We employed the 6-31G AO basis set in this case.

The *trans*-butadiene system is a chemical model of the case of two strongly interacting units in a system, where the value of the stretching internal coordinate is a proxy for the strength of electron correlation. Near the equilibrium geometry, dividing the active space into two fragments is chemically reasonable: each fragment encloses one π-bond, and inasmuch as electron correlation affects the system at all, it is a reasonable approximation to consider it only locally. However, as the C=C double bonds are elongated, electrons from the two broken π bonds recouple across the central C_2H_2 unit, which spans the fissure between the two LAS fragments. The LAS wave function cannot model a π bond in this position, and the LASSCF method breaks down.

5.3.2 Computational Methods

To calculate the accuracy of the proposed method for small molecules, we use the following strategy. We first use a classical LASSCF solver, as implemented in the *mrh* package[117], to find the best product wave function. This effectively provides an equivalent solution to that of the QPE step of our proposed algorithm. We then represent this product wave function as a CI vector in the complete active Fock space and apply a UCCSD correlator, as well as its derivatives with respect to all amplitudes, to this reference CI vector. We employ the factorization reported by Chen et al.[272] to avoid the BCH expansion and its inevitable approximate truncation. The resulting $|\mathrm{QLAS}\rangle$ CI vector and its derivatives ($|\delta\mathrm{QLAS}\rangle$) with respect to the unitary coupled cluster amplitudes are used to compute the energy, $\langle\mathrm{QLAS}|\hat{H}|\mathrm{QLAS}\rangle$, and its derivatives, $\langle\delta\mathrm{QLAS}|\hat{H}|\mathrm{QLAS}\rangle$. We then minimize the former using the latter and the Broyden—Fletcher-–Goldfarb-–Shanno algorithm. We find that this approach is more efficient than directly simulating the quantum circuits. We note that this method scales exponentially on classical computers.

To provide gate count estimates, we use the Q# package[273], generally following the framework of Ref. 274. The full and reduced Hamiltonians are produced by using the *mrh* package[117], and both Hamiltonians are then passed to the Q# package to estimate the number of CNOT gates using the QPE algorithm with a single Trotter time step for each. Additionally, we estimate the number of CNOT gates necessary to calculate various UCCSD ansatzes, including a global UCCSD ansatz over the whole unfragmented molecule and multiple 2-local ansatzes that span only two fragments. We count only the number of logical quantum gates needed. Real quantum computers will require additional overheads, owing to limited connectivity and the need to use expensive quantum error correction protocols to deal with inevitable errors[260,261]. Furthermore, we provide gate counts only; no attempt was made to count gate depth, which is typically smaller, because many gates can be implemented in parallel.

5.4 Results and Discussion

5.4.1 LAS-VQE

Here we describe a more approximate approach than LAS-UCC wherein the QPE circuits for the fragments are replaced by UCC ansatzes, leading to a fully variational method. The chemical knowledge that guides us in defining subspaces of the LAS wave function can also be used to reduce the size of the unitary operator for the UCC ansatzes. It suggests that operators corresponding to the higher excitation from one fragment to another do not affect the wave function significantly. Thus, we introduce a modified ansatz for truncated UCC circuits where we consider the "locality" of the excitation. An excitation involving only orbitals localized on a particular fragment—that is defined by the user—is classified as a "local excitation." In this modified UCC ansatz the user not only can truncate the UCC excitation to a certain maximum number (doubles, triples, etc.) but also can impose a constraint of locality on the higher excitations. We develop here the theory and the algorithm of this method and name it LAS-VQE. In LAS-VQE, all the singles excitations are included while only the local ones are included for the higher excitations. This corresponds to having a mean-field interfragment interaction and allowing all possible orbital rotations. This does not reduce the number of qubits required to represent the system, but it does lower the complexity of the circuit as discussed below. In principle, one could use the locality argument to include only local excitations, allowing us to reduce the number of qubits required. This separate-fragments VQE approach, however, fails to account for any interaction between the fragments. We choose to always include the singles excitations (orbital rotations) across the entire system to account for some interfragment correlation and to make the method less sensitive to the localization schemes used.

We also choose to perform in the singles excitation among spin-restricted orbitals. We achieve this by using the same parameter to control the alpha and beta excitations corre-

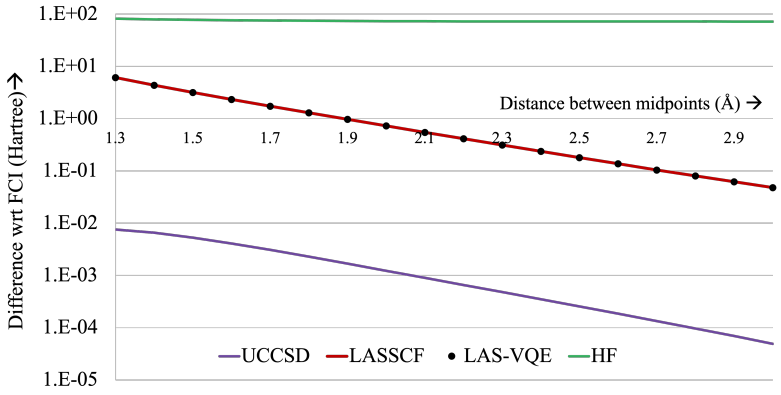

Figure 5.3: Energy difference (in Hartree) between FCI and the approximate methods as a function of the distance between the midpoints of the two H_2 molecules

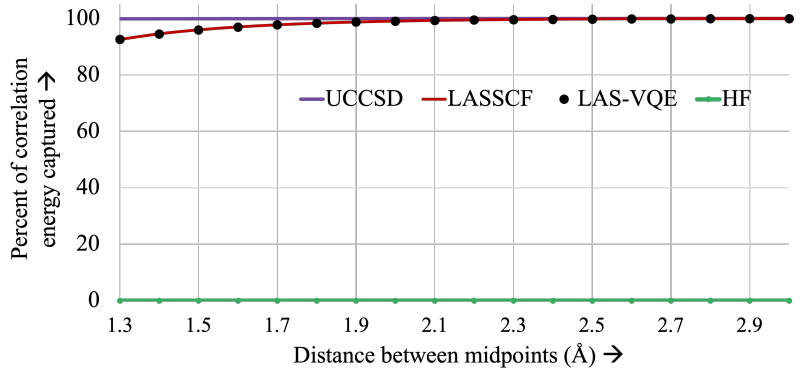

Figure 5.4: Percentage of correlation energy accounted for by the various methods for different intermolecular distances

sponding to a given pair of spatial orbitals. This is necessary to avoid artificial lowering of energies due to spontaneous symmetry breaking (the spin unrestricted solution). An example of the effect of this is seen for the hydrogen dimer shown in Figure 2 of the main text. The nonspin adapted UCCS energy is about 0.2 mHartree lower than the Hartree–Fock and has an spin contamination of 0.09, showing the symmetry breaking. Working with spin-restricted orbitals not only allows us to prepare symmetry preserving states for the subsequent excitations, but also lowers the number of parameters at the singles level by a factor of 2. This becomes a significant advantage for the classical optimizer in VQE as the size of the system gets larger. We study the ground state electronic structure of the hydrogen

dimer in various conformations with the STO-3G basis set. We use CASSCF with a (4,4) active space and LASSCF with a ((2,2),(2,2)) active space, UCCSD and LAS-VQE. Each H_2 molecule is considered as one fragment on which the molecular orbitals are localized. As one would expect, the performance of LASSCF with respect to CASSCF (which is also FCI in this case) worsens with decreasing distance between the two H_2 molecules. Figure 5.3 shows the energy difference between the various methods and the FCI/CAS(4,4) absolute energies. UCCSD in this case is not exactly FCI but does give accurate results. LAS-VQE is close to (but slightly lower than) the LASSCF energy. The LAS-VQE energy is not variationally bound by the LASSCF that it is based on. In contrast to the LAS-UCC method discussed in this chapter, this method uses a single determinant Hartree–Fock reference state. The UCCSD energy is a variational lower bound to the LAS-VQE method. There is, however, a significant advantage when it comes to the computational cost: gate count and the depth of the circuit. The number of doubles operators scales linearly with the number of fragments. The Table 5.1 shows the number of gates and parameters required for the various calculations for a system with increasing number of H_2 molecules with the same fragmentation scheme. LAS-VQE in considerably lower in both circuit depth and number of parameters, compared with full UCCSD.

Table 5.1: Circuit depth and number of parameters for the various methods for an increasing number of H_2 fragments

	Circuit Depth			Parameters		
	UCCS	LAS-VQE	UCCSD	UCCS	LAS-VQE	UCCSD
$1 \times H_2$	14	97	97	1	2	2
$2 \times H_2$	58	141	1791	4	6	22
$3 \times H_2$	147	230	11206	9	12	108
$4 \times H_2$	296	379	42789	16	20	344

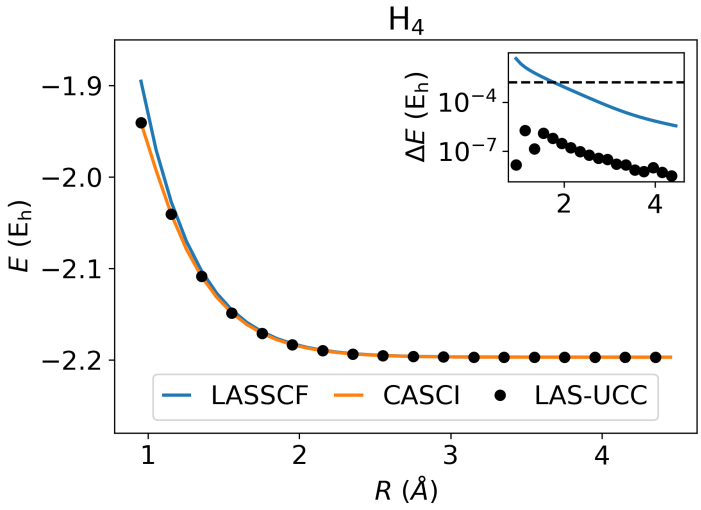

Figure 5.5: Energies for $(H_2)_2$ calculated by CASCI, LASSCF, and LAS-UCC. The inset shows the error, with respect to CASCI, of LASSCF and LAS-UCC. The black dashed line represents chemical accuracy. LAS-UCC is able to obtain chemical accuracy, with respect to CASCI, at all distances. LASSCF cannot obtain chemical accuracy at sufficiently short distances.

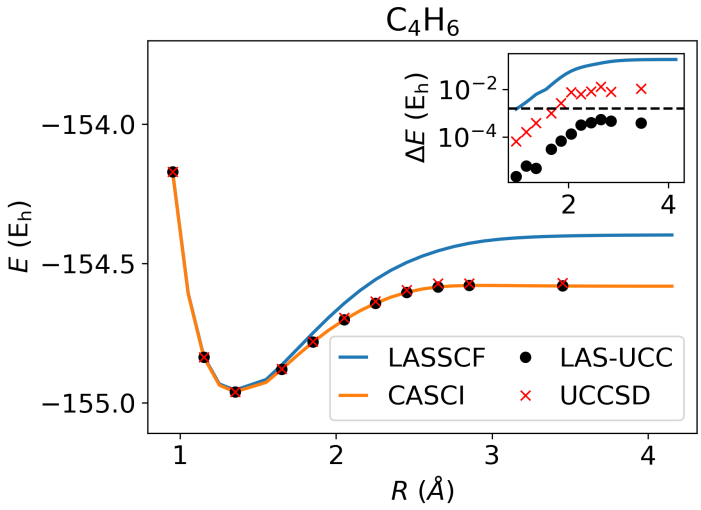

Figure 5.6: Energies for C_4H_6 calculated by CASCI, LASSCF, and LAS-UCC. The inset shows the error, with respect to CASCI, of LASSCF and LAS-UCC. The black dashed line represents chemical accuracy. LAS-UCC obtains chemical accuracy across the potential energy surface, whereas LASSCF, which cannot accurately represent the correlation between the fragments, fails to obtain chemical accuracy for most points.

5.4.2 LAS-UCC

We demonstrate the efficacy of our framework by simulating the two benchmark molecules, $(H_2)_2$ and *trans*-butadiene, described above. We compare three methods: LASSCF, CAS configuration interaction in the basis of LASSCF orbitals (CASCI), and our new algorithm, LAS-UCC. LASSCF represents the best unentangled set of wave functions and is equivalent to the solution after the QPE circuits but before the use of the UCCSD ansatz. Note that CASCI is slightly different from CASSCF since the orbitals are not variationally reoptimized. CASCI solves for the FCI wave function within the active space; in this case, it is equivalent to using QPE across the whole molecule and represents the reference result in these studies.

Figure 5.5 shows the results of applying the methods to the hydrogen dimer as the two H_2 molecules are pulled apart. We see that LASSCF, CASCI, and LAS-UCC agree except for very small distances where LASSCF no longer provides accurate energies.

Figure 5.6 shows the results for *trans*-butadiene, a model of strongly correlated fragments. Here, as the terminal methylene units are removed, the interfragment correlation grows as a double bond is formed between the fragments. The UCCSD ansatz can accurately represent this level of entanglement, allowing LAS-UCC to achieve nearly CASCI accuracy, whereas LASSCF fails to account for this entanglement. With a standard Hartree-Fock initial state, as is typically done in VQE, the UCCSD ansatz is unable to obtain chemical accuracy for the large distances. We also attempted to use the so-called 'hardware-efficient' ansatz[238], but were unable to obtain results significantly better than Hartree-Fock using depths up to 10 (which corresponds to a similar number of parameters as the UCCSD ansatz) at equilibrium.

5.4.3 Resource Estimates

To demonstrate the scaling advantage of our method, we perform resource estimation for the number of logical quantum gates necessary for several different quantum algorithms: the QPE algorithm over the full unfragmented molecule; the UCCSD ansatz over the full un-

fragmented molecule; and the two steps of our proposed LAS-UCC method, the fragmented QPE and the 2-local UCCSD (which corresponds to the circuit depicted in Fig. 5.1). We estimate the number of resources needed for the QPE algorithm if only a single Trotter time step were needed; $O(1000)$ time steps will be needed for typical systems to get to chemical accuracy[227,262]. Note that these estimates represent only the number of two-qubit CNOT gates, which we use as a primary gauge of the number of total resources. We also note here that we are only comparing the scaling number of gates; QPE, with a sufficiently good initial state and enough Trotter states, will of course be the most accurate of all compared algorithms.

We use a model system of an increasing number of H_2 molecules and look at how the number of CNOT gates increases as the number of molecules increases, as shown in Fig. 5.7. As the number of H_2 molecules increases, the number of gates needed for all methods also increases. As predicted in the complexity analysis of QPE [see Methods section], the total number of gates for a single Trotter step in the QPE algorithm grows as $O(N^5)$. Similarly, the number of gates needed for a global UCCSD ansatz also grows as $O(N^5)$, as expected[237]. This result is compared with the much smaller number of gates necessary to implement the two steps of our LAS-UCC algorithm. As expected, both the QPE and UCCSD parts of LAS-UCC provide dramatic scaling advantages, with the 2-local UCCSD ansatz and the QPE of the reduced Hamiltonian both scaling as only $O(N)$. We note that, in addition to evaluating the quantum circuits here, an additional optimization loop is needed when using the UCCSD ansatz, whether it is global or 2-local. Using a 2-local UCCSD ansatz also greatly reduces the number of parameters that need to be optimized compared with a global UCCSD ansatz.

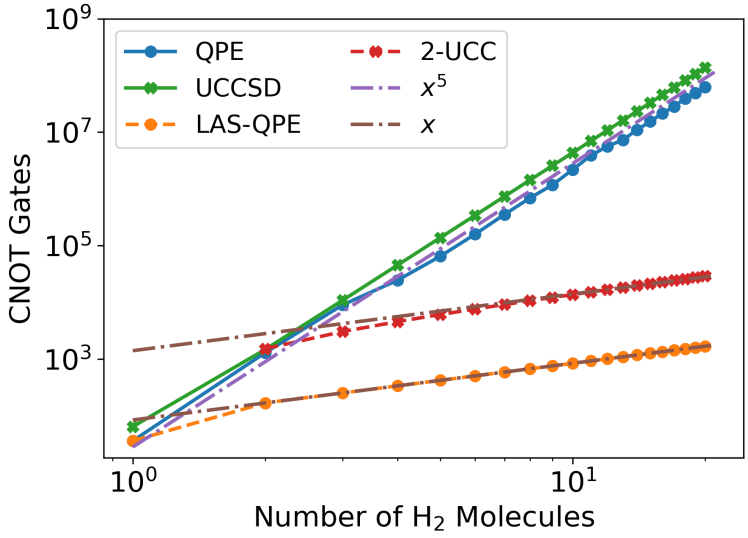

Figure 5.7: Estimated two-qubit gate counts using various algorithms. The QPE estimates assume only a single Trotter step; $O(1000)$ will need to be taken to obtain chemical accuracy. Polynomials of various orders have been plotted to demonstrate the scaling. Our algorithm, LAS-UCC, requires both the LAS-QPE and 2-UCC circuits and thus has an overall $O(N)$ scaling, compared with the $O(N^5)$ scaling of UCC and QPE.

5.4.4 Discussion

Here we compare LAS-UCC with the two quantum algorithms that it is composed of: QPE and variational UCCSD. Compared with global QPE, LAS-UCC reduces the total quantum resource cost by approximating the system with noninteracting fragments and adding in some interaction between fragments (those described by a UCCSD ansatz spanning the fragments). This in general reduces the accuracy; but as shown in the preceding sections, LAS-UCC provides accuracy comparable to CASCI (and therefore global QPE) for the systems considered here. The *trans*-butadiene molecule is a model for larger, more complicated systems of strongly interacting units. Many single molecular magnets have such pockets of strong correlation localized on the metal centers, which moderately interact with each other[275,276]. With LAS-UCC we not only can obtain the wave function efficiently but also can selectively couple the fragments with the UCC correlator, offering further insight into the

nature of these interactions. Affordable and accurate modeling of phenomena such as singlet fission[277,278] in molecular crystals of conjugated organic compounds can be performed with LAS-UCC, as fault-tolerant quantum computers become available. This approach will also be used to study chemical processes involving interfragment bond formation and breaking while still treating all points on a potential energy surface at comparable footing.

Compared with standard UCCSD, LAS-UCC can be seen as augmenting UCCSD with a multireference initial state. Instead of using single-determinant Hartree–Fock, as is standard in VQE demonstrations of UCCSD[238,263–265,271], LAS-UCC uses the unentangled product state of the ground state wave functions of each fragment (which is also the LASSCF wavefunction). This provides additional accuracy, above standard single-reference UCCSD, at a negligible increase in cost. When using a global UCCSD ansatz, the increase in the number of gates is negligible, even when taking into account the $O(1000)$ time steps that would be needed to implement the QPE step. Using the m-local ansatz provides further reduction. There have been other proposals for preparing interesting, multireference initial state in context of efficiently finding states with large overlap with the true ground state[279,280]. These algorithms could be used in-place of the QPE part of LAS-UCC to provide the initial state and potentially adapted to give similar LASSCF-like states with similar overhead reductions as shown for QPE.

Moreover, recent advances in VQE algorithms have developed various ways to reduce the cost associated with the UCC correlator[225,227,281–284]. As presented in the Theory section, LAS-UCC can also be seen as a post-LASSCF method that recouples select fragments at a level of theory beyond the mean field. The addition of the doubles or higher terms in the cluster operator provides a way to systematically improve the accuracy beyond the LASSCF reference. On classical computers, such an approach requires truncating[248] or approximating[285] the non-terminating BCH expansion in a more or less arbitrary way.

Not every system will be accurately described by LAS-UCC, of course, but one can

systematically increase the accuracy in several ways, while increasing the total resource cost. Increasing the size of each fragment (which in turn decreases the number of fragments) gradually increases the accuracy, until the limit of a single fragment, where the UCCSD ansatz becomes redundant and the algorithm becomes simply global QPE. On the UCC side, the order of the ansatz can be increased. Triples, quadruples, and so on can be included at increasing cost. If using an m-local ansatz, the scaling is unaffected, but the total number of gates increases. The locality of the ansatz, m, can also be increased, providing explicit correlation between more geometrically distant fragments.

5.5 Conclusions

We introduced LAS-UCC, a quantum algorithm that combines a fragmentation of the wave function of a chemical system with QPE and variational UCCSD to compute the ground state energy of such a system. LAS-UCC can describe compounds containing strongly interacting fragments, and it provides a polynomial scaling advantage in the number of quantum gates compared with other quantum algorithms such as QPE and UCCSD. Since the fragments' reduced Hamiltonians have fewer terms and by ensuring the locality of the Jordan-Wigner transform, the overall gate count will be $O(N)$ with respect to the total size of the system N for for linear geometries and $O(N^2)$ more generally, compared with $O(N^5)$ requirements for QPE. We also demonstrated the accuracy of LAS-UCC on $(H_2)_2$ and *trans*-butadiene molecules and performed resource estimations of larger systems to provide evidence for potential scaling advantages.

As larger fault-tolerant quantum computers are developed, we expect that our algorithm will be able to provide accurate calculations of large and useful chemical systems, such as molecular magnets and qubits, photovoltaic materials, and large biomolecules that are out of reach of classical computing algorithms but for which QPE would be too expensive.

CHAPTER 6
A NEW MIXING OF NONLOCAL EXCHANGE AND NONLOCAL CORRELATION WITH MULTICONFIGURATION PAIR-DENSITY FUNCTIONAL THEORY

6.1 Introduction

Multiconfiguration pair-density functional theory (MC-PDFT) theory[30,31] combines the explicit treatment of static correlation by multiconfiguration self-consistent field (MC-SCF) calculations with the efficiency of density functional theory for modeling dynamic electron correlation. In Kohn–Sham density functional theory (KS theory), the non-Coulomb (exchange and correlation) part of the electron-electron interaction energy is expressed as a functional of up-spin and down-spin densities, whereas MC-PDFT uses a functional (called an on-top functional) of both the total electron density and the on-top pair density.[30,286–288] Furthermore, practical KS theory uses a density optimized by employing an exchange–correlation functional that has self-interaction errors and involves modeling the density of open-shell systems with broken-symmetry Slater determinants, whereas MC-PDFT models the density using spin eigenfunctions that have the explicit multiconfigurational character required to reperesent static correlation (also called strong correlation) and that are determined by wave function theory without self-interaction error.

The on-top functionals used so far in MC-PDFT have been obtained by translating local exchange-correlation functionals from KS theory,[30,71] and they inherit some of the diffficulties of KS theory, for example, spin-changing atomic excitation energies are less accurate on average than those calculated by complete-active space 2nd-order perturbation theory (CASPT2) and only slightly better than those computed by complete-active-space

self-consistent-field (CASSCF) theory.[74] Reference 74 explored the possibility of improving the accuracy of MC-PDFT in this case by applying scaling factors to the exchange and correlation terms of the MC-PDFT on-top exchange-correlation energy functional (cf. the high local exchange [HLE] scaling in KS-DFT[289,290]), but the improvement was only modest.[74]

An alternative approach is to import the concept of "hybrid" functionals from KS theory, in which the nonlocal "exchange energy" term from the electron-electron interaction energy of the underlying wave function representation of the density is added to the local exchange-correlation energy expression of KS theory, and the terms in the combined expression are weighted. Progress in KS theory has involved both global weighting[291] and range-separated weighting[292–295] of the local and nonlocal components. Here we extend the "global hybrid" approach to MC-PDFT.

6.2 Theoretical background

The original hybrid KS (HKS) theory was obtained[291] by linearly combining the Hartree-Fock energy expression E_{HF} and the KS energy expression E_{KS} to obtain

$$E_{\mathrm{HKS}} = \lambda E_{\mathrm{HF}} + (1-\lambda)E_{\mathrm{KS}} \tag{6.1}$$

where λ is a parameter (originally taken as 0.5). By analogy, and with the same justification, we define our version of hybrid MC-PDFT (HMC-PDFT) by linearly combining a multiconfiguration wave function (MCWF) energy and the MC-PDFT energy expressions

$$E_{\mathrm{HMC-PDFT}} = \lambda E_{\mathrm{MCWF}} + (1-\lambda)E_{\mathrm{MC-PDFT}} \tag{6.2}$$

where λ is again a parameter.

For comparison to previous work it is useful to write Eq. (6.2) in another way. First we define the classical energy as[291] the sum of the kinetic energy and the nucleus-nucleus,

nucleus-electron, and electron-electron classical Coulomb energies. Then we write

$$E_{\mathrm{MCWF}} = E_{\mathrm{MC,class}} + E_{\mathrm{MC,XC}} \tag{6.3}$$

$$E_{\mathrm{MC-PDFT}} = E_{\mathrm{MC,class}} + E_{\mathrm{X}} + E_{\mathrm{C}} \tag{6.4}$$

where $E_{\mathrm{MC,class}}$ is the classical energy of the MC wave function, $E_{\mathrm{MC,XC}}$ is introduced in Eq. (6.3), E_{X} is the exchange portion of the on-top density functional energy, and E_{C} is the correlation portion of the on-top density functional energy. Then Eq. (6.2) becomes

$$E_{\mathrm{HMC-PDFT}} = E_{\mathrm{MC,class}} + \lambda E_{\mathrm{MC,XC}} + (1-\lambda)(E_{\mathrm{X}} + E_{\mathrm{C}}) \tag{6.5}$$

A hybrid MC-PDFT method already in the literature is the $\lambda-$MC-PDFT global hybrid method proposed by Mostafanejad et al.[296] That method was developed in the context of variational 2-RDM CASSCF[70,297,298] and was tested for ground-state reactions, but not for excited electronic states. The $\lambda-$MC-PDFT method was inspired by the multiconfiguration one-parameter hybrid (MC1H) method developed by Sharkas *et al.*,[299] which in turn is a generalization of their earlier one-parameter doubly hybrid (1DH) method[300] (see also Refs. 301–304). These methods, like Eq. (6.1), are all formally based on the adiabatic connection of density functional theory.[305] By manipulation of the Levy-Lieb universal functional,[306–309] Mostafanejad *et al.* obtained

$$E_{\lambda-\mathrm{MC-PDFT}} = E_{\mathrm{MC,class}} + \lambda E_{\mathrm{MC,XC}} + (1-\lambda)(E_{\mathrm{X}}) + (1-\lambda^2)(\tilde{E}_{\mathrm{C}}) \tag{6.6}$$

where $\tilde{E}_C$ is the correlation energy of a scaled density. Sharkas *et al.* omit the scaling of the density and the λ-MC-PDFT method by Mostafanejad *et al.* also makes this approxi-

mation,[296] yielding

$$E_{\lambda-\mathrm{MC-PDFT}} = E_{\mathrm{MC,class}} + \lambda E_{\mathrm{MC,XC}} + (1-\lambda)(E_{\mathrm{X}}) + (1-\lambda^2)(E_{\mathrm{C}}) \quad (6.7)$$

The omission of scaling is based on computational convenience and a small set of numerical tests which were carried out during the development of a doubly hybrid density functional approximation.[299,300] In the present work, we consider alternative approximations to the final term in Eqs. (6.5), (6.6), and (6.7). In their derivation of scaling relations for the unknown exact density functional, Levy and Perdew[310]established the inequalities

$$\tilde{E}_{\mathrm{c}} \leq \lambda^{-1} E_{\mathrm{c}}, \ \lambda \geq 1 \quad (6.8)$$

which, given that the correlation energy is negative, suggests a possible practical scheme with

$$\tilde{E}_{\mathrm{c}} \approx \lambda^{k-2} E_{\mathrm{c}}, \ k > 1 \quad (6.9)$$

where both λ and k are determined semiempirically. This motivates a method we will call two-parameter hybrid MC-PDFT (2HMC-PDFT) with the energy expression

$$E_{\mathrm{2HMC-PDFT}} = E_{\mathrm{MC,class}} + \lambda E_{\mathrm{MC,XC}} + (1-\lambda)(E_{\mathrm{X}}) + (1-\lambda^k)(E_{\mathrm{C}}) \quad (6.10)$$

where $\lambda = 0$ gives the original MC-PDFT energy expression, $k = 2$ corresponds to λ-MC-PDFT method of Mostafanejad *et al.* and $k = 1$ gives HMC-PDFT. Levy and Perdew show specifically[310] that $k = 1$ is not accurate in the context of an adiabatic connection between the exact functional and the exact wave-function solution to the Schrödinger equation. However we use it here as a practical approximation with non-exact energy functionals and an approximate multiconfiguration wave function.

6.3 Results and discussion

In order to explore the effect of different choices of hybridization parameter and exponent in Eq. (6.10), we perform 2HMC-PDFT calculations on four datasets: the lowest eight π,π^* singlet and triplet excitation energies in benzene, the SFAEE11 datasets of 11 spin-flip atomic excitation energies, the EE27 dataset of 27 first excitation energies of organic molecules, and the DBE6 dataset of 6 diatomic bond energies. These datasets have been studied previously using MC-PDFT with varying basis sets and active spaces.[31,74,77] In this study we use more recent theoretical reference values for the excitation energies.[311,312] The choices of basis sets and active spaces for the present tests are based on this previous work and are given in section 6.4.1. All MCWFs in the present chapter are complete active space self-consistent-field[313] (CASSCF) wave functions.

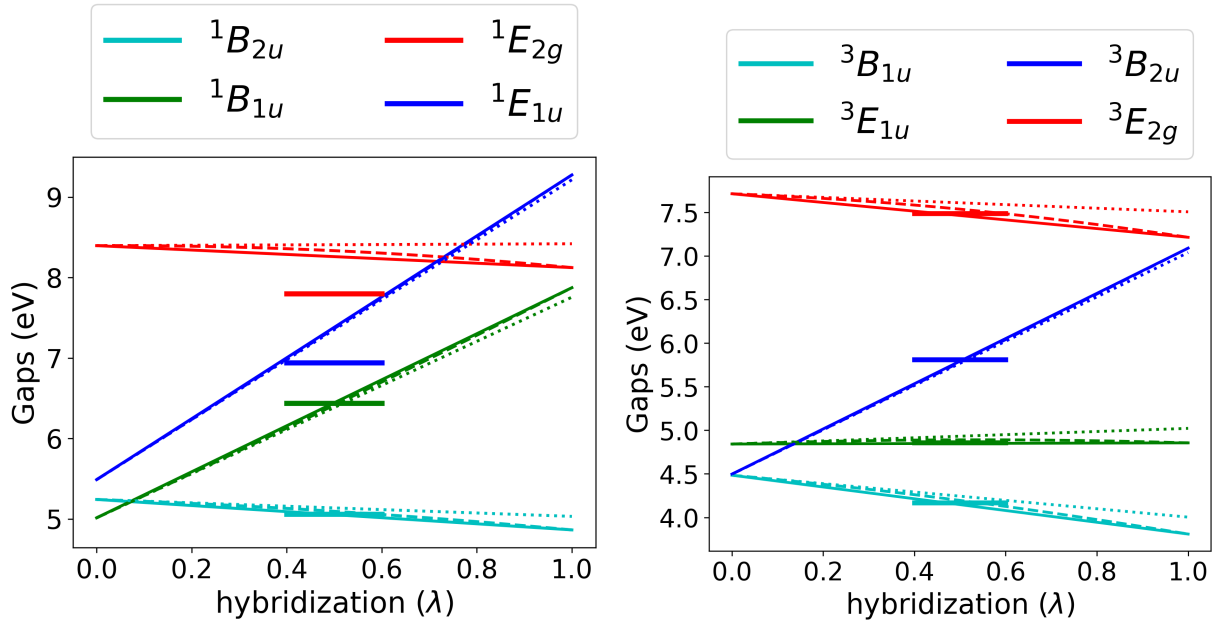

Figure 6.1: Singlet (left) and triplet (right) excitation energies in benzene calculated in the (6,6) active space with the tPBE functional for $k = 1$ (solid thin curve), $k = 2$ (dashed curve, and $k = \infty$ (dotted curve) along with the reference values (solid horizontal lines in the middle of the panels). Note that the solid curves obscure large portions of the dashed curves because the $k = 2$ and $k = \infty$ results are close to one another.

First we consider the excitation ladder of the π,π^* excitations of benzene as a follow-up

to the work in Ref. 77. In that work, MC-PDFT using the tPBE and ftPBE functionals were found to give only slightly better agreement with experiment overall than CASSCF, especially when compared to the performance of CASPT2; in order to rival the performance of the latter, MC-PDFT required a very large (6,24) active space in combination with the HLE scaling discussed above.

By contrast, 2-HMC-PDFT with a range of choices of λ and k decisively improves the quality of MC-PDFT results for all active spaces explored. Figure 6.1 shows the energies and the ordering of the singlet and triplet excited states in a (6,6) active space. Similar data for the (6,12) and (6,24) active spaces are presented in Figs. 6.2 and 6.3 respectively. In all cases, the excited states are in the correct energy order for most choices of λ; the closest agreement with experiment is obtained in the region of $\lambda = 0.5$.

Of special note is the profound effect of hybridization upon the excitation energies of the ionic states, $^1B_{1u}$, $^1E_{1u}$, and $^3B_{2u}$. Some caution is warranted in drawing too emphatic a conclusion about these states from Fig. 6.1 alone, because it is known that the CASSCF(6,6) model of these states is qualitatively incorrect due to the lack of Rydberg orbitals in the active space.[314,315] However, although tPBE without hybridization already reproduces the correct energy ordering in the larger (6,12) and (6,24) active spaces, hybridization still profoundly improves the quantitative accuracy of the ionic excitation energies in these cases, as shown in Figs. 6.2 and 6.3.

The value of (k) has almost no effect on the results for benzene excitations; $k = 1$, $k = 2$, and $k = \infty$ are all almost indistinguishable on the scales of Figs. 6.1, 6.2, and 6.3.

We next consider broader data sets as explored previously in Ref. 74, beginning with the spin-flip atomic excitation energies in SFAEE11. Figure 6.4 shows the heat map of mean unsigned errors (MUEs) of these excitation energies as a function of λ and k using the tPBE functional with minimal active spaces in the left panel and larger active spaces in the right panel. Notice that the minimal and larger active spaces are different from case to case in the

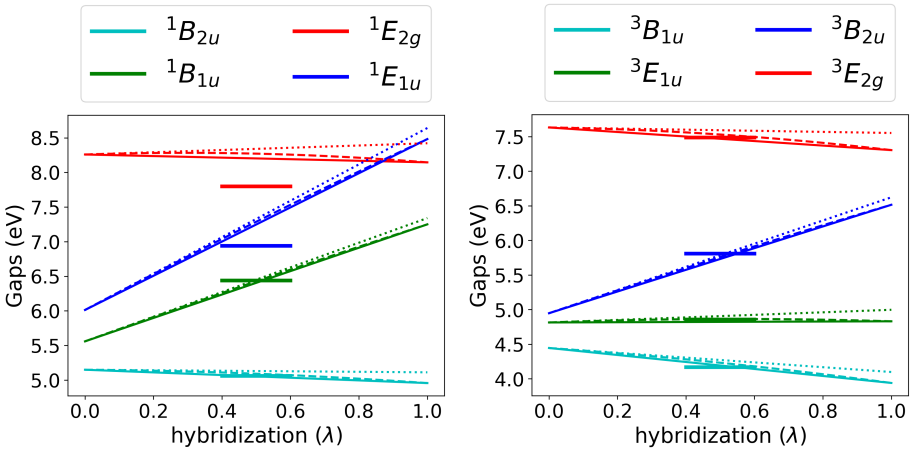

Figure 6.2: Singlet (left) and triplet (right) excitation energies in benzene calculated (with λ^{∞}) in the (6,12) active space with the tPBE functional.

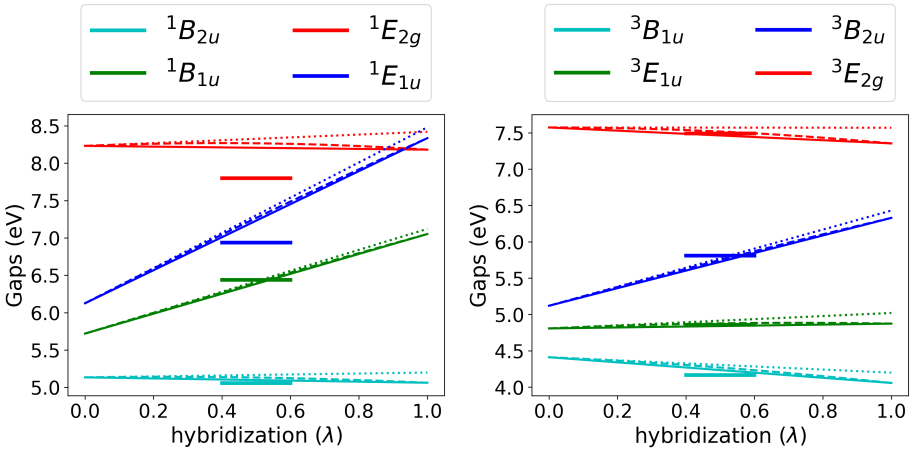

Figure 6.3: Singlet (left) and triplet (right) excitation energies in benzene calculated (with λ^{∞}) in the (6,24) active space with the tPBE functional.

data set, as described in section 6.4.2. (Similar data using the tBLYP functional is reported in the reference 316, and the analysis presented here of the tPBE data holds equally well for the tBLYP case.) We find that hybridization consistently reduces MUE of the excitation energies across a wide range of parameter choices and for both the minimal and larger active spaces. The optimal λ value has a weak positive correlation to the value of k; except in the case of very large k, the optimal λ falls in the range of 0.5-0.6. In particular, the difference between $k = 1$ (weighted averaging of CASSCF and MC-PDFT energies) and $k = 2$ (the

λ-MC-PDFT method) is negligible.

For the minimal active spaces, increasing k while optimizing λ *decreases* the MUE; for the larger active spaces, doing the same *increases* it. This observation can be rationalized in that larger active spaces include more of the dynamic correlation in the CASSCF energy, but dynamic correlation is already included in E_C, whereas larger k implies that more density functional correlation energy is included in the E_C term of Eq. (6.10). Therefore, a large active space runs a risk of double counting a portion of the correlation energy.

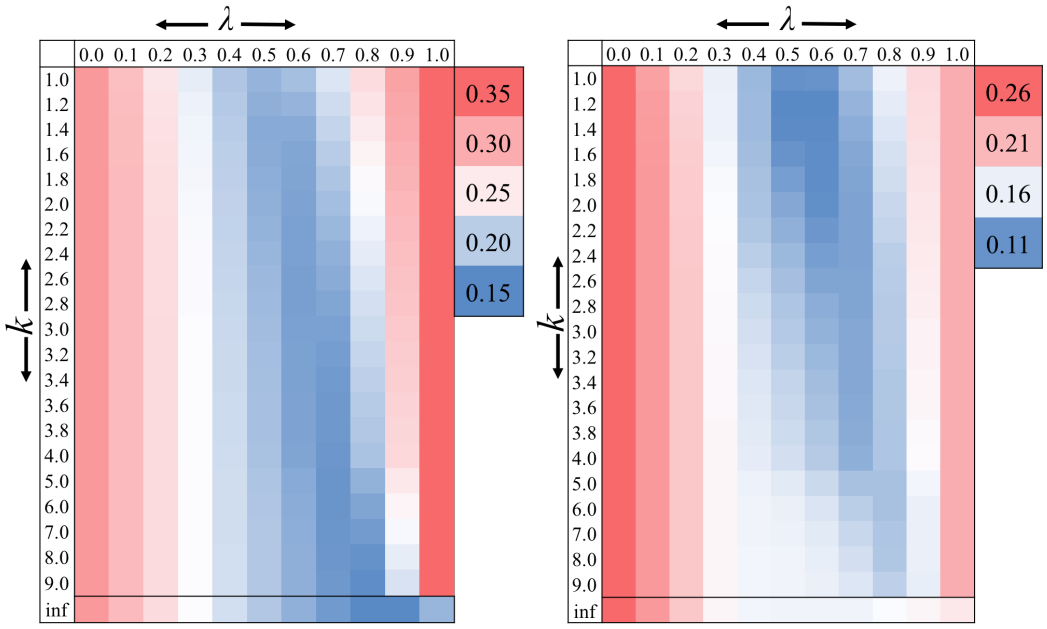

Figure 6.4: A heat map of mean unsigned errors (eV) for the SFAE11 data set for various values of λ and k for the small active space (left) and the larger active space (right)

Next consider the molecular excitation energies of the EE27 data set and the diatomic bond energies of the DBE6 data set; the MUEs for which are shown on the left and right, respectively, of Fig. 6.5 . In both of these cases, MC-PDFT itself already gives a dramatic improvement over CASSCF, much more than for the SFAEE11 case. Nevertheless, the accuracy of MC-PDFT is consistently improved by hybridization, although usually with a smaller optimal λ value than in previous examples.

The EE27 and DBE6 results differ in their dependence of the MUE upon k. The EE27

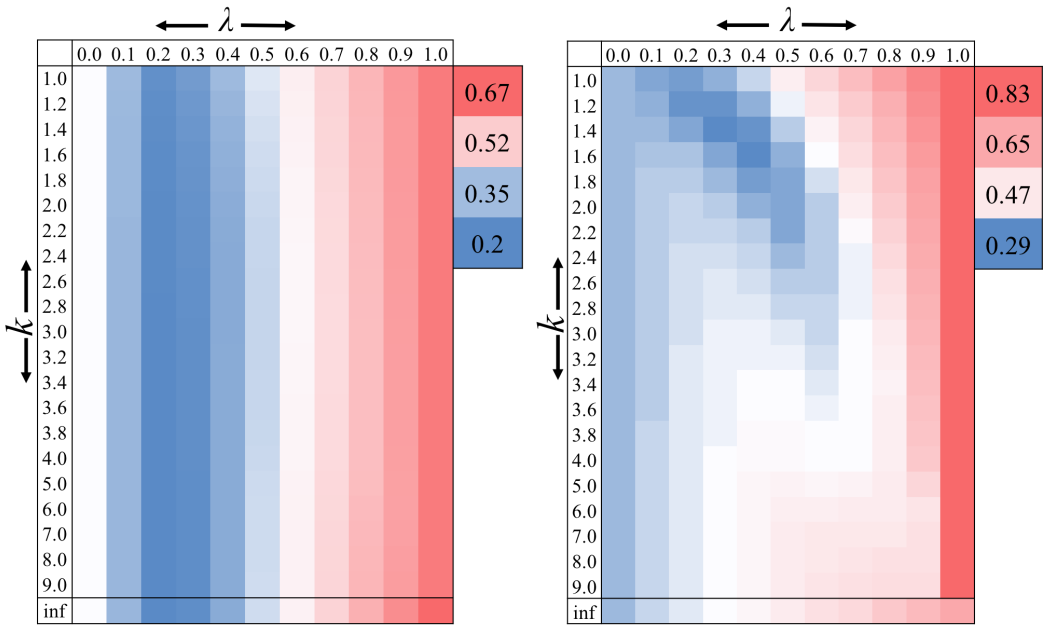

Figure 6.5: A heat map of mean unsigned errors for the EE27 data set (left) and the DBE6 data set (right) for various values of λ and k

results are very insensitive to this parameter. The DBE6 results, on the other hand, show a more intricate relationship between k, λ, and the MUE: for very small λ, results are insensitive to k; for larger λ, results resemble the SFAEE11 large active space case discussed above, except that the covariance of λ and k is more pronounced. The optimal parametrization for this case lies within the second "feature" of the heat map on the right-hand side of Fig. 6.5. DBE6 furnishes the only counterexample to the general observation in this work that the value of k (at least in the range [1,2]) has at most a minor impact upon success for any given fixed λ. For DBE6 and $k = 1$, the optimal λ lies near 0.3; while for $k = 2$, the optimal λ is closer to 0.5 and $\lambda \approx 0.3$ actually leads to larger MUE than unhybridized MC-PDFT. The optimal MUE in these two cases, however, is very similar.

Figures 6.1–6.5 collectively show that HMC-PDFT offers consistent and significant improvements of the accuracy as compared to either MC-PDFT or CASSCF for both same-spin and spin-changing excitations) as well as bond energies. They also show that no systematic improvement is possible by going to 2HMC-PDFT provided λ is chosen optimally for

a given k. Therefore, we propose to use simpler HMC-PDFT [Eq. (6.5)] for future studies with global hybrid MC-PDFT.

Table 6.1: The mean unsigned errors (eV) with respect to experimental measurements for each data set using CASSCF, MC-PDFT and the tPBE0 Hybrid PDFT – i.e. using $\lambda = 0.25$ and $k = 1$

Dataset	CASSCF	MC-PDFT/tPBE	HMC-PDFT/tPBE0[a]
Benzene Excitations (6,6)	0.78	0.69	0.34
SFAE11 [small active space]	0.35	0.32	0.24
SFAE11 [larger active space]	0.22	0.26	0.18
EE27[b]	0.63	0.31	0.21
DBE6	0.83	0.34	0.32

[a] The tPBE0 notation implies $\lambda = 0.25$, and the HMC prefix implies k = 1. [b] Some reference excitation energies in the EE27 data set are accurate theoretical estimates. See table S5 in reference 316, table 6 in reference 311 and table 11 in reference 312

As a final example of HMC-PDFT, we test the theory using the same value of λ (namely 0.25) as used n the PBE0 functional[317,318] of hybrid KS theory. We give the shorthand name tPBE0 to this choice. The MUEs of HMC-PDFT/tPBE0 for each of the datasets explored are presented and compared to CASSCF and MC-PDFT/tPBE in Table 6.1. The comparison provides a test of whether a single "standard" choice of λ can provide good results for diverse properties (spin-changing excitations, spin-conserving excitations, and bond energies). In all cases of Table 6.1, tPBE0 offers a lower MUE than both CASSCF and tPBE - this is true even in the one case where tPBE has a larger MUE than CASSCF. For the minimal-active-space benzene calculations, the error is decreased by about a factor of 2.0 with respect to tPBE and a factor of 2.3 with respect to CASSCF. Overall, our results indicate that a weighted average of CASSCF and MC-PDFT energies provides a promising way to extend the hybrid strategy of KS theory to MC-PDFT theory, and we find improved accuracy for both bond energies and excitation energies.

6.4 Appendix

6.4.1 Basis sets

The aug-cc-pVTZ[319] basis set was used for all the calculations in SFAEE11, the maug-cc-pVTZ[320] basis set was used for the 8π to π^* excitation energies in benzene and the jul-cc-pVTZ[321] basis set was used for most of the systems in EE27 with the following exceptions. The aug-cc-pVTZ basis set was employed for water, the 6-31+ G**[322,323] basis set was employed for para-nitroaniline (pNA) and 4-(dimethylamino)-benzonitrile (DMABN), and the aug-cc-pVDZ basis set was used for the benzene–tetracyanoethylene (B-TCNE) complex. The calculation of the dissociation energies of main group element diatomics and CaO were done using the cc-pVTZ basis set. The calculations for Cr_2 and NiCl were done using cc-pVTZ-DK[324] and ANO-RCC-VTZP[325] basis set respectively. The the second order Douglas–Kroll–Hess Hamiltonian[326,327] was used to account for relativistic effects in these two molecules.

6.4.2 Active space choice

For the small active space in SFAE11, the 2s and 2p orbitals were considered for the main group elements . The 3d and 4s orbitals were considered for the first row transition elements with the addition of the 4p orbitals for Mn. The 4d and 5s orbitals were included for the second row transition elements. The larger active space was considered by including the correlating orbitals - outer shell orbital - for each orbital in the minimal active space. The details about the active space for the systems in EE27 and DBE6 are given in table 6.2

Table 6.2: Details about the type of excitation and the active space used for the molecules in EE27 and DBE6 datasets

Compound	Excitation	Active space	Active orbitals
Be	${}^1S \rightarrow {}^1P(s \rightarrow p)$	(2,4)	$2s, 2p$
N_2	${}^1\Pi_g(\sigma_g \rightarrow \pi_g)$	(6,6)	$\pi, \pi^*, \sigma_{2p}, \sigma^*_{2p}$
N_2	${}^1\sigma_u^-(\pi_u \rightarrow \pi_g)$	(6,6)	$\pi, \pi^*, \sigma_{2p}, \sigma^*_{2p}$
Acetaldehyde	${}^1A''(n \rightarrow \pi^*)$	SA(2)-(12,12)	$\pi, \pi^*, 2(n, n^*), 3(\sigma, \sigma^*)$
Acetone	${}^1A_2(n \rightarrow \pi^*)$	SA(2)-(12,12)	$\pi, \pi^*, 2(n, n^*), 3(\sigma, \sigma^*)$
Formaldehyde	${}^1A_2(n \rightarrow \pi^*)$	SA(2)-(12,10)	Full valence
Pyrazine	${}^1B_{3u}(n \rightarrow \pi^*)$	SA(3)-(10,10)	$3(\pi, \pi^*), 2(n, n^*)$
Pyridazine	${}^1B_1(n \rightarrow \pi^*)$	SA(2)-(10,10)	$3(\pi, \pi^*), 2(n, n^*)$
Pyridine	${}^1B_1(n \rightarrow \pi^*)$	SA(3)-(8,8)	$3(\pi, \pi^*), n, n^*$
Pyrimidine	${}^1B_1(n \rightarrow \pi^*)$	SA(2)-(10,10)	$3(\pi, \pi^*), 2(n, n^*)$
s-tetrazine	${}^1B_{3u}(n \rightarrow \pi^*)$	SA(2)-(14,14)	$3(\pi, \pi^*), 4(n, n^*)$
Ethylene	${}^1B_{1u}(\pi \rightarrow \pi^*)$	SA(5)-(4,10)	$\pi, \pi^*, \sigma, \sigma*, 4\,\text{Ryd}$, 2 correlating π^*
Butadiene	${}^1B_u(\pi \rightarrow \pi^*)$	SA(4)-(10,15)	$2(\pi, \pi^*), 3(\sigma, \sigma^*)$, Ryd, 4correlating π^*
Cyclopentadiene	${}^1B_2(\pi \rightarrow \pi^*)$	(4,4)	$2(\pi, \pi^*)$
Benzene	${}^1B_{2u}(\pi \rightarrow \pi^*)$	SA(2)-(6,13)	$3(\pi, \pi^*), 7\pi^*$
Napthalene	${}^1B_{3u}(\pi \rightarrow \pi^*)$	SA(2)-(10,10)	$5(\pi, \pi^*)$
Furan	${}^1B_2(\pi \rightarrow \pi^*)$	SA(2)-(6,10)	$2(\pi, \pi^*), (n, n^*), 4\pi^*$
Hexatriene	${}^1B_u(\pi \rightarrow \pi^*)$	SA(2)-(6,12)	$3(\pi, \pi^*), 6\pi^*$
Water	$(2p_x \rightarrow 3s)$	SA(2)-(8,9)	$2(\sigma, \sigma^*), 2(n, n^*), 3s$
pNA	${}^1A_1(\pi \rightarrow \pi^*)$	SA(3)-(12,12)	$5(\pi, \pi^*), (n, n^*)$
DMABN	${}^1A_1(\pi \rightarrow \pi^*)$	SA(3)-(12,12)	$5(\pi, \pi^*), (n, n^*)$
B-TCNE	${}^1A_1(\pi \rightarrow \pi^*)$	SA(2)-(4,4)	$2(\pi, \pi^*)$
H_2	dissociation	(2,2)	valence orbitals
N_2	dissociation	(6,6)	valence orbitals
F_2	dissociation	(10,6)	valence orbitals
Cr_2	dissociation	(12,12)	3d and 4s orbitals
CaO	dissociation	(8,8)	hybridized orbital on Ca and 2s,2p,2p' on O.
NiCl	dissociation	(11,12)	3d,4s and 3d' on Ni and one 2p orbital for Cl

CHAPTER 7

CONCLUSION

This dissertation has primarily explored the localized active space method and its derivatives that leverage the chemical knowledge about the targeted system to simplify the costly wave function ansatzes like the complete active space methods. LASSCF is based on the observation that the strongly correlated electrons in many molecules are often localized in pockets of correlation that, although strongly correlated withing themselves, are only weakly correlated to each other. This enables us to fragments the active space of the molecule into multiple active sub-spaces that are localized on different parts of the molecule and express the wave function as an anti-symmetrized product of the many-body solutions of the individual subspaces.

We demonstrated that LASSCF is able to accurately reproduce the CASSCF results in cases where the fragments were well-separated from each other. The agreement shown between the two for computing localized spin-changing excitation energies in various bimetallic complexes opens up the opportunity to model larger systems at a much lower cost. It also shows good performance for systems like the bibenzyl molecule where the multireference fragments are connected to each other only through saturated bonds. The same performance is, however, not observed when the system has chemical bonds that conjugate across the fragments - as in the case of stilbene or polyenes. This motivated the methods that include more correlation across the fragments. The LAS-PDFT method uses the density and pair density obtained from the LAS wave function to recompute the total energy. The excitation energies and potential energy surfaces obtained using this method showed better agreement with there corresponding CAS counterparts. This method relies on the PDFT energy being less susceptible to approximations in the reference wave function rather than explicitly reconstructing correlation between the subspaces and thus cannot be systematically improved. This is addressed using the LASSI methods that constructs a compact Hamiltonian in the

basis of multiple LAS states. The LASSI solutions are linear combinations of the LAS states and can thus have entanglement across the fragments. This allows us to systematically and selectively reconstruct the bonds between fragments. The easily interpretible nature of the LAS states allows us to study phenomena like charge transfer in organic compounds and spin coupling in bimetallic compounds in greater detail than easily possible with methods like CASSCF. The cost scaling of LASSI in the limit of including all possible inter-fragment excitations approaches that the CASSCF. Thus a radically new algorithm is required to break the exponential wall in this limit. We proposed the LAS-UCC algorithm that leverages the power of quantum computers to overcome this exponential scaling. The unitary coupled cluster method is used to selectively correlate the fragments. This approach shows better performance compared to the conventional wave function ansatzs for quantum computers. The tests performed on simulators showed promising results and will help model complex systems on the fault-tolerent quantum computers of the future. Beyond the efforts to improve upon LASSCF to achieve results at par with CASSCF, we also explored ways to improve the post-MCSCF methods. The HMC-PDFT method improved the performance of the MC-PDFT in a wide range of testbeds. This helped us compute accurate excited states properties using PDFT, which has been a long-standing challenge and has found application in many ongoing investigations.

Altogether, the studies presented in this thesis open up many new directions for further explorations. The LASSCF method, though significantly cheaper than CASSCF, can be further improved upon. As a fragmentation-based method, it can benefit from the use of highly parallel computer architectures. The many-body wave functions of each subspace are obtained in independent processes within each iteration. While this is currently done serially, this task can be distributed over multiple processors to gain substantial reduction in computational time. Another aspect of this method that is yet unexplored is the standardization/automation of the fragmentation schemes. Many algorithms and protocols for

selecting active spaces have been developed based on various parameters.[58,107,328,329] Such techniques for further decomposing the active space into fragments that can be unentangled will take away the need for substantial effort and chemical intuition required from the user for each LAS calculation. This will facilitate the use of LAS methods in high-throughput screenings for materials. The LASSI method can be improved in future works by changing the Hamiltonian used for state interaction. The use of a PDFT Hamiltonian will allow quantitative predictions of molecular properties. Furthermore, the incorporation of spin-orbit coupling effects in future work will enable the study of magnetic properties of multi-metallic compounds.

Overall, the research highlighted in this dissertation has focused on the development and application of cost efficient multireference methods for computing properties of strongly correlated molecules. These methods use chemical intuition to overcome the crucial barrier of the scaling of the cost for modelling molecules on classical and quantum computers. Particular emphasis was given on the use of these methods for insights in practical applications like spin coupling in organometallic compounds and charge transfer in organic molecules. We hope that this research will not only benefit the greater community of computational chemists and scientists but also prove useful in the broader effort of chemical and material discovery.

REFERENCES

[1] Matthew R. Hermes and Laura Gagliardi. Multiconfigurational Self-Consistent Field Theory with Density Matrix Embedding: The Localized Active Space Self-Consistent Field Method. *J. Chem. Theory Comput.*, 15:972, 2019. doi: 10.1021/acs.jctc.8b01009.

[2] Riddhish Pandharkar, Matthew R. Hermes, Christopher J. Cramer, and Laura Gagliardi. Spin-State Ordering in Metal-Based Compounds Using the Localized Active Space Self-Consistent Field Method. *J. Phys. Chem. Lett.*, 10(18):5507–5513, 2019. ISSN 19487185. doi: 10.1021/acs.jpclett.9b02077.

[3] William L Jorgensen. The many roles of computation in drug discovery. *Science*, 303 (5665):1813–1818, 2004.

[4] Si-sheng Ou-Yang, Jun-yan Lu, Xiang-qian Kong, Zhong-jie Liang, Cheng Luo, and Hualiang Jiang. Computational drug discovery. *Acta Pharmacol. Sin.*, 33(9):1131–1140, 2012.

[5] Gregory Sliwoski, Sandeepkumar Kothiwale, Jens Meiler, and Edward W Lowe. Computational methods in drug discovery. *Pharmacol. Rev.*, 66(1):334–395, 2014.

[6] O Anatole von Lilienfeld and Kieron Burke. Retrospective on a decade of machine learning for chemical discovery. *Nat. Commun.*, 11(1):1–4, 2020.

[7] Daniel P Tabor, Loïc M Roch, Semion K Saikin, Christoph Kreisbeck, Dennis Sheberla, Joseph H Montoya, Shyam Dwaraknath, Muratahan Aykol, Carlos Ortiz, Hermann Tribukait, et al. Accelerating the discovery of materials for clean energy in the era of smart automation. *Nat. Rev. Mater.*, 3(5):5–20, 2018.

[8] Barbara Kirchner, Frank Wennmohs, Shengfa Ye, and Frank Neese. Theoretical bioinorganic chemistry: the electronic structure makes a difference. *Curr. Opin. Chem. Biol.*, 11(2):134–141, 2007.

[9] Per EM Siegbahn and Margareta RA Blomberg. Transition-metal systems in biochemistry studied by high-accuracy quantum chemical methods. *Chem. Rev.*, 100(2): 421–438, 2000.

[10] Per EM Siegbahn and Tomasz Borowski. Modeling enzymatic reactions involving transition metals. *Acc. Chem. Res.*, 39(10):729–738, 2006.

[11] Martin Karplus and J Andrew McCammon. Molecular dynamics simulations of biomolecules. *Nat. Struct. Biol.*, 9(9):646–652, 2002.

[12] Conrad AP Goodwin, Fabrizio Ortu, Daniel Reta, Nicholas F Chilton, and David P Mills. Molecular magnetic hysteresis at 60 kelvin in dysprosocenium. *Nature*, 548 (7668):439–442, 2017.

[13] You-Song Ding, Nicholas F Chilton, Richard EP Winpenny, and Yan-Zhen Zheng. On approaching the limit of molecular magnetic anisotropy: a near-perfect pentagonal bipyramidal dysprosium (iii) single-molecule magnet. *Angew. Chem. Int. Ed.*, 55(52): 16071–16074, 2016.

[14] Andrzej Rajca. Organic diradicals and polyradicals: from spin coupling to magnetism? *Chem. Rev.*, 94(4):871–893, 1994.

[15] John A Pople, J Stephen Binkley, and Rolf Seeger. Theoretical models incorporating electron correlation. *Int. J. Quantum Chem.*, 10(S10):1–19, 1976.

[16] Clifford E Dykstra. *Advanced theories and computational approaches to the electronic structure of molecules*, volume 133. Springer Science & Business Media, 2012.

[17] Stephen Wilson. *Electron correlation in molecules*. Courier Corporation, 2014.

[18] Björn O Roos, Peter R Taylor, Per EM Si, et al. A complete active space scf method (casscf) using a density matrix formulated super-ci approach. *Chem. Phys.*, 48(2): 157–173, 1980.

[19] George D Purvis III and Rodney J Bartlett. A full coupled-cluster singles and doubles model: The inclusion of disconnected triples. *J. Chem. Phys.*, 76(4):1910–1918, 1982.

[20] Rodney J Bartlett. Many-body perturbation theory and coupled cluster theory for electron correlation in molecules. *Annu. Rev. Phys. Chem.*, 32(1):359–401, 1981.

[21] Peter J Knowles, Claudia Hampel, and Hans-Joachim Werner. Coupled cluster theory for high spin, open shell reference wave functions. *J. Chem. Phys.*, 99(7):5219–5227, 1993.

[22] Kerstin Andersson, Per-Åke Malmqvist, and Björn O Roos. Second-order perturbation theory with a complete active space self-consistent field reference function. *J. Chem. Phys.*, 96(2):1218–1226, 1992.

[23] Pierre Hohenberg and Walter Kohn. Inhomogeneous electron gas. *Phys. Rev.*, 136 (3B):B864, 1964.

[24] Walter Kohn and Lu Jeu Sham. Self-consistent equations including exchange and correlation effects. *Phys. Rev.*, 140(4A):A1133, 1965.

[25] Axel D Becke. Density-functional thermochemistry. iii. the role of exact exchange. *J. Chem. Phys.*, 98(7):5648–5652, 1993.

[26] Chengteh Lee, Weitao Yang, and Robert G Parr. Development of the colle-salvetti correlation-energy formula into a functional of the electron density. *Phys. Rev. B*, 37 (2):785, 1988.

[27] John P Perdew, Kieron Burke, and Matthias Ernzerhof. Generalized gradient approximation made simple. *Phys. Rev. Lett.*, 77(18):3865, 1996.

[28] Yan Zhao and Donald G Truhlar. The m06 suite of density functionals for main group thermochemistry, thermochemical kinetics, noncovalent interactions, excited states, and transition elements: two new functionals and systematic testing of four m06-class functionals and 12 other functionals. *Theor. Chem. Acc.*, 120(1-3):215–241, 2008.

[29] Celestino Angeli, Renzo Cimiraglia, S Evangelisti, T Leininger, and J-P Malrieu. Introduction of n-electron valence states for multireference perturbation theory. *J. Chem. Phys.*, 114(23):10252–10264, 2001.

[30] Giovanni Li Manni, Rebecca K Carlson, Sijie Luo, Dongxia Ma, Jeppe Olsen, Donald G Truhlar, and Laura Gagliardi. Multiconfiguration pair-density functional theory. *J. Chem. Theory Comput.*, 10:3669–3680, 2014. doi: 10.1021/ct500483t.

[31] Laura Gagliardi, Donald G Truhlar, Giovanni Li Manni, Rebecca K Carlson, Chad E Hoyer, and Junwei Lucas Bao. Multiconfiguration Pair-Density Functional Theory: A New Way To Treat Strongly Correlated Systems. *Acc. Chem. Res.*, 50:66, 2017. doi: 10.1021/acs.accounts.6b00471.

[32] Soumen Ghosh, Andrew L Sonnenberger, Chad E Hoyer, Donald G Truhlar, and Laura Gagliardi. Multiconfiguration pair-density functional theory outperforms kohn–sham density functional theory and multireference perturbation theory for ground-state and excited-state charge transfer. *J. Chem. Theory Comput.*, 11(8):3643–3649, 2015.

[33] Fengyi Liu, Yajun Liu, Luca De Vico, and Roland Lindh. A casscf/caspt2 approach to the decomposition of thiazole-substituted dioxetanone: Substitution effects and charge-transfer induced electron excitation. *Chem. Phys. Lett.*, 484(1-3):69–75, 2009.

[34] Davide Presti, Donald G Truhlar, and Laura Gagliardi. Intramolecular charge transfer and local excitation in organic fluorescent photoredox catalysts explained by rasci-pdft. *J. Phys. Chem. C*, 122(22):12061–12070, 2018.

[35] Daniel Roca-Sanjuán, Francesco Aquilante, and Roland Lindh. Multiconfiguration second-order perturbation theory approach to strong electron correlation in chemistry and photochemistry. *Wiley Interdiscip. Rev. Comput. Mol. Sci.*, 2(4):585–603, 2012.

[36] Lluís Blancafort and Alexander A Voityuk. Exciton delocalization, charge transfer, and electronic coupling for singlet excitation energy transfer between stacked nucleobases in dna: An ms-caspt2 study. *J. Chem. Phys.*, 140(9):03B602_1, 2014.

[37] Antonio Francés-Monerris, Javier Segarra-Martí, Manuela Merchán, and Daniel Roca-Sanjuán. Complete-active-space second-order perturbation theory (caspt2//casscf) study of the dissociative electron attachment in canonical dna nucleobases caused by low-energy electrons (0-3 ev). *J. Chem. Phys.*, 143(21):12B614_1, 2015.

[38] Eduarda S Gil, Cláudia B da Silva, Pablo A Nogara, Carolina H da Silveira, João BT da Rocha, Bernardo A Iglesias, Diogo S Lüdtke, Paulo FB Gonçalves, and Fabiano S Rodembusch. Synthesis, photophysical characterization, casscf/caspt2 calculations and ct-dna interaction study of amino and azido benzazole analogues. *J. Mol. Liq.*, 297: 111938, 2020.

[39] Núria Queralt, David Taratiel, Coen de Graaf, Rosa Caballol, Renzo Cimiraglia, and Celestino Angeli. On the applicability of multireference second-order perturbation theory to study weak magnetic coupling in molecular complexes. *J. Comput. Chem.*, 29(6):994–1003, 2008.

[40] Daniel Aravena and Eliseo Ruiz. Spin dynamics in single-molecule magnets and molecular qubits. *Dalton. Trans.*, 49(29):9916–9928, 2020.

[41] Carmen J Calzado, Celestino Angeli, David Taratiel, Rosa Caballol, and Jean-Paul Malrieu. Analysis of the magnetic coupling in binuclear systems. iii. the role of the ligand to metal charge transfer excitations revisited. *J. Chem. Phys.*, 131(4):044327, 2009.

[42] Daniel Roca-Sanjuán, Mickael G Delcey, Isabelle Navizet, Nicolas Ferre, Ya-Jun Liu, and Roland Lindh. Chemiluminescence and fluorescence states of a small model for coelenteramide and cypridina oxyluciferin: a casscf/caspt2 study. *J. Chem. Theory Comput.*, 7(12):4060–4069, 2011.

[43] Maria del Carmen Marin, Luca De Vico, Sijia S Dong, Laura Gagliardi, Donald G Truhlar, and Massimo Olivucci. Assessment of mc-pdft excitation energies for a set of qm/mm models of rhodopsins. *J. Chem. Theory Comput.*, 15(3):1915–1923, 2019.

[44] Sijia S Dong, Laura Gagliardi, and Donald G Truhlar. Excitation spectra of retinal by multiconfiguration pair-density functional theory. *Phys. Chem. Chem. Phys.*, 20(10): 7265–7276, 2018.

[45] María Elena Martin, Fabrizia Negri, and Massimo Olivucci. Origin, nature, and fate of the fluorescent state of the green fluorescent protein chromophore at the caspt2//casscf resolution. *J. Am. Chem. Soc.*, 126(17):5452–5464, 2004.

[46] Matthew R Hermes, Riddhish Pandharkar, and Laura Gagliardi. Variational localized active space self-consistent field method. *J. Chem. Theory Comput.*, 16(8):4923–4937, 2020.

[47] Christopher J Cramer. *Essentials of computational chemistry: theories and models*. John Wiley & Sons, 2013.

[48] Trygve Helgaker, Poul Jorgensen, and Jeppe Olsen. *Molecular electronic-structure theory*. John Wiley & Sons, 2014.

[49] Erwin Schrödinger. An undulatory theory of the mechanics of atoms and molecules. *Phys. Rev.*, 28(6):1049, 1926.

[50] Douglas R Hartree. The wave mechanics of an atom with a non-coulomb central field. part i. theory and methods. In *Mathematical Proceedings of the Cambridge Philosophical Society*, volume 24, pages 89–110. Cambridge University Press, 1928.

[51] Paul Adrien Maurice Dirac. The quantum theory of the emission and absorption of radiation. *Proc. R. Soc. Lond. A*, 114(767):243–265, 1927.

[52] Vladimir Fock. Konfigurationsraum und zweite quantelung. *Zeitschrift für Physik*, 75 (9-10):622–647, 1932.

[53] Robert J Buenker and Sigrid D Peyerimhoff. Energy extrapolation in ci calculations. *Theor. Chim. Acta*, 39(3):217–228, 1975.

[54] Jeppe Olsen, Poul Jørgensen, and Jack Simons. Passing the one-billion limit in full configuration-interaction (fci) calculations. *Chem. Phys. Lett.*, 169(6):463–472, 1990.

[55] Joseph Ivanic and Klaus Ruedenberg. Identification of deadwood in configuration spaces through general direct configuration interaction. *Theor. Chem. Acc.*, 106(5): 339–351, 2001.

[56] Per-Olov Löwdin. Correlation problem in many-electron quantum mechanics i. review of different approaches and discussion of some current ideas. *Adv. Chem. Phys.*, pages 207–322, 1958. doi: 10.1002/9780470143483.ch7.

[57] Jie J Bao, Sijia S Dong, Laura Gagliardi, and Donald G Truhlar. Automatic selection of an active space for calculating electronic excitation spectra by ms-caspt2 or mc-pdft. *J. Chem. Theory Comput.*, 14(4):2017–2025, 2018.

[58] Christopher J Stein and Markus Reiher. Automated selection of active orbital spaces. *J. Chem. Theory Comput.*, 12(4):1760–1771, 2016.

[59] Achintya Kumar Dutta, Marcel Nooijen, Frank Neese, and Róbert Izsák. Automatic active space selection for the similarity transformed equations of motion coupled cluster method. *J. Chem. Phys.*, 146(7):074103, 2017.

[60] Per Åke Malmqvist, Alistair Rendell, and Björn O Roos. The restricted active space self-consistent-field method, implemented with a split graph unitary group approach. *J. Phys. Chem.*, 94(14):5477–5482, 1990. doi: 10.1021/j100377a011.

[61] Jeppe Olsen, Björn O Roos, Poul Jo/rgensen, and Hans Jo/rgen Aa Jensen. Determinant based configuration interaction algorithms for complete and restricted configuration interaction spaces. *J. Chem. Phys.*, 89(4):2185–2192, 1988. doi: 10.1063/1.455063.

[62] Dongxia Ma, Giovanni Li Manni, and Laura Gagliardi. The generalized active space concept in multiconfigurational self-consistent field methods. *J. Chem. Phys.*, 135(4): 044128, 2011. doi: 10.1063/1.3611401.

[63] Joseph Ivanic. Direct configuration interaction and multiconfigurational self-consistent-field method for multiple active spaces with variable occupations. I. Method. *J. Chem. Phys.*, 119:9364, 2003. doi: 10.1063/1.1615954. URL `http://aip.scitation.org/toc/jcp/119/18`.

[64] W_J Hunt, PJ Hay, and WA Goddard Iii. Self-consistent procedures for generalized valence bond wavefunctions. applications h3, bh, h2o, c2h6, and o2. *J. Chem. Phys.*, 57(2):738–748, 1972.

[65] Frank W. Bobrowicz and William A. Goddard. *The Self-Consistent Field Equations for Generalized Valence Bond and Open-Shell Hartree—Fock Wave Functions*, pages 79–127. Springer US, Boston, MA, 1977. ISBN 978-1-4757-0887-5. doi: 10.1007/978-1-4757-0887-5_4. URL `https://doi.org/10.1007/978-1-4757-0887-5_4`.

[66] Samuel O Odoh, Giovanni Li Manni, Rebecca K Carlson, Donald G Truhlar, and Laura Gagliardi. Separated-pair approximation and separated-pair pair-density functional theory. *Chem. Sci.*, 7(3):2399–2413, 2016.

[67] Garnet Kin-Lic Chan and Martin Head-Gordon. Highly correlated calculations with a polynomial cost algorithm: A study of the density matrix renormalization group. *J. Chem. Phys.*, 116(11):4462–4476, 2002.

[68] Mario Van Raemdonck, Diego R Alcoba, Ward Poelmans, Stijn De Baerdemacker, Alicia Torre, Luis Lain, Gustavo E Massaccesi, Dimitri Van Neck, and Patrick Bultinck. Polynomial scaling approximations and dynamic correlation corrections to doubly occupied configuration interaction wave functions. *J. Chem. Phys.*, 143(10):104106, 2015.

[69] Diego R Alcoba, Alicia Torre, Luis Lain, Ofelia B Oña, Elías Ríos, and Gustavo E Massaccesi. Incorporating dynamic correlation into the variational determination method of the second-order reduced density matrix in the doubly occupied configuration interaction space. *Int. J. Quantum Chem.*, 120(15):e26256, 2020.

[70] Gergely Gidofalvi and David A Mazziotti. Active-space two-electron reduced-density-matrix method: Complete active-space calculations without diagonalization of the-electron Hamiltonian. *J. Chem. Phys.*, 129:134108, 2008. doi: 10.1063/1.2983652. URL `https://doi.org/10.1063/1.2983652`.

[71] Rebecca K Carlson, Donald G Truhlar, and Laura Gagliardi. Multiconfiguration Pair-Density Functional Theory: A Fully Translated Gradient Approximation and Its Performance for Transition Metal Dimers and the Spectroscopy of Re2Cl82-. *J. Chem. Theory Comput.*, 11:4077–4085, 2015. doi: 10.1021/acs.jctc.5b00609.

[72] Rebecca K Carlson, Giovanni Li Manni, Andrew L Sonnenberger, Donald G Truhlar, and Laura Gagliardi. Multiconfiguration pair-density functional theory: Barrier heights and main group and transition metal energetics. *J. Chem. Theory Comput.*, 11(1):82–90, 2015.

[73] Chad E Hoyer, Laura Gagliardi, and Donald G Truhlar. Multiconfiguration pair-density functional theory spectral calculations are stable to adding diffuse basis functions. *J. Phys. Chem. Lett.*, 6(21):4184–4188, 2015.

[74] Davide Presti, Jan Kadlec, Donald G Truhlar, and Laura Gagliardi. Scaling exchange and correlation in the on-top density functional of multiconfiguration pair-density functional theory: effect on electronic excitation energies and bond energies. *Theor. Chem. Acc.*, 139(2):30, 2020.

[75] P P Hallmen, G Rauhut, H Stoll, A O Mitrushchenkov, and J Van Slageren. Crystal Field Splittings in Lanthanide Complexes: Inclusion of Correlation Effects beyond Second Order Perturbation Theory. *J. Chem. Theory Comput.*, 14:3998, 2018. doi: 10.1021/acs.jctc.8b00184. URL `https://pubs.acs.org/sharingguidelines`.

[76] Philipp P Hallmen, Hans-Joachim Werner, Daniel Kats, Samuel Lenz, Guntram Rauhut, Hermann Stoll, and Joris van Slageren. Toward fast and accurate ab initio calculation of magnetic exchange in polynuclear lanthanide complexes. *Phys. Chem. Chem. Phys.*, 21(19):9769–9778, 2019. doi: 10.1039/C9CP00785G.

[77] Prachi Sharma, Varinia Bernales, Donald G Truhlar, and Laura Gagliardi. Valence π π^* excitations in benzene studied by multiconfiguration pair-density functional theory. *J. Phys. Chem. Lett.*, 10(1):75–81, 2019.

[78] Satoshi Horike, Satoru Shimomura, and Susumu Kitagawa. Soft porous crystals. *Nat. Chem.*, 1(9):695–704, 2009. ISSN 17554330. doi: 10.1038/nchem.444.

[79] Jeongyong Lee, Omar K. Farha, John Roberts, Karl A. Scheidt, Sonbinh T. Nguyen, and Joseph T. Hupp. Metal-organic framework materials as catalysts. *Chem. Soc. Rev.*, 38(5):1450–1459, 2009. ISSN 03060012. doi: 10.1039/b807080f.

[80] Samuel O Odoh, Christopher J Cramer, Donald G Truhlar, and Laura Gagliardi. Quantum-Chemical Characterization of the Properties and Reactivities of Metal–Organic Frameworks. *Chem. Rev.*, 115:6051, 2015. doi: 10.1021/cr500551h. URL `https://pubs.acs.org/sharingguidelines`.

[81] François-Xavier Coudert and Alain H. Fuchs. Computational characterization and prediction of metal–organic framework properties. *Coord. Chem. Rev.*, 307:211, 2016. doi: 10.1016/j.ccr.2015.08.001. URL `https://ac.els-cdn.com/S0010854515002714/1-s2.0-S0010854515002714-main.pdf?{_}tid=7b1de078-fba4-402b-8006-965d7bea5f2d{&}acdnat=1537908614{_}3a797ae9b2557a35111c57bb811e7536`.

[82] Bing Yan. Lanthanide-Functionalized Metal–Organic Framework Hybrid Systems To Create Multiple Luminescent Centers for Chemical Sensing. *Acc. Chem. Res.*, 50:2789, 2017. doi: 10.1021/acs.accounts.7b00387. URL `https://pubs.acs.org/sharingguidelines`.

[83] Varinia Bernales, Manuel A Ortuño, Donald G Truhlar, Christopher J Cramer, and Laura Gagliardi. Computational Design of Functionalized Metal–Organic Framework Nodes for Catalysis. *ACS Cent. Sci.*, 4:5–19, 2018. doi: 10.1021/acscentsci.7b00500.

[84] Soichiro Nishio and Yuki Kurashige. Rank-one basis made from matrix-product states for a low-rank approximation of molecular aggregates. *J. Chem. Phys.*, 151:084111, 2019. doi: 10.1063/1.5093346. URL `https://doi.org/10.1063/1.5093346`.

[85] Yuqi Wang, Zhigang Ni, Wei Li, and Shuhua Li. Cluster-in-Molecule Local Correlation Approach for Periodic Systems. *J. Chem. Theory Comput.*, 15:2933, 2019. doi: 10.1021/acs.jctc.8b01200. URL `https://pubs.acs.org/doi/10.1021/acs.jctc.8b01200`.

[86] Mark S Gordon, Dmitri G Fedorov, Spencer R Pruitt, and Lyudmila V Slipchenko. Fragmentation methods: a route to accurate calculations on large systems. *Chem. Rev.*, 112(1):632–672, jan 2012. ISSN 1520-6890. doi: 10.1021/cr200093j. URL `http://www.ncbi.nlm.nih.gov/pubmed/21866983https://pubs.acs.org/sharingguidelines`.

[87] Gerald Knizia and Garnet Kin-lic Chan. Density Matrix Embedding : A Simple Alternative to Dynamical Mean-Field Theory. *Phys. Rev. Lett.*, 109:186404, 2012. doi: 10.1103/PhysRevLett.109.186404.

[88] Gerald Knizia and Garnet Kin-Lic Chan. Density matrix embedding: A strong-coupling quantum embedding theory. *J. Chem. Theory Comput.*, 9(3):1428–1432, 2013.

[89] Sebastian Wouters, Carlos A. Jiménez-Hoyos, Qiming Sun, and Garnet K L Chan. A Practical Guide to Density Matrix Embedding Theory in Quantum Chemistry. *J. Chem. Theory Comput.*, 12(6):2706–2719, 2016. doi: 10.1021/acs.jctc.6b00316.

[90] Sebastian Wouters, Carlos A Jiménez-Hoyos, and Garnet K L Chan. Five Years of Density Matrix Embedding Theory. In Mark S. Gordon, editor, *Fragmentation: Toward Accurate Calculations on Complex Molecular Systems*, chapter 8, page 227. Wiley, 2017. URL `https://onlinelibrary.wiley.com/doi/pdf/10.1002/9781119129271.ch8`.

[91] Carlos A. Jiménez-Hoyos and Gustavo E. Scuseria. Cluster-based mean-field and perturbative description of strongly correlated fermion systems. Application to the one- and two-dimensional Hubbard model. *Phys. Rev. B*, 92:085101, 2015. ISSN 1098-0121. doi: 10.1103/PhysRevB.92.085101.

[92] Shane M Parker, Tamar Seideman, Mark A Ratner, and Toru Shiozaki. Communication: Active-space decomposition for molecular dimers. *J. Chem. Phys.*, 139:021108, 2013. doi: 10.1063/1.4813827. URL `https://doi.org/10.1063/1.4794425`.

[93] Shane M Parker, Tamar Seideman, Mark A Ratner, and Toru Shiozaki. Model Hamiltonian analysis of singlet fission from first principles. *J. Phys. Chem. C*, 118:12700–12705, 2014. doi: 10.1021/jp505082a. URL `https://pubs.acs.org/sharingguidelines`.

[94] Shane M Parker and Toru Shiozaki. Quasi-diabatic states from active space decomposition. *J. Chem. Theory Comput.*, 10:3738, 2014. doi: 10.1021/ct5004753. URL https://pubs.acs.org/sharingguidelines.

[95] Inkoo Kim, Shane M Parker, and Toru Shiozaki. Orbital Optimization in the Active Space Decomposition Model. *J. Chem. Theory Comput.*, 11:3636, 2015. doi: 10.1021/acs.jctc.5b00429. URL https://pubs.acs.org/sharingguidelines.

[96] Shane M Parker and Toru Shiozaki. Communication: Active space decomposition with multiple sites: Density matrix renormalization group algorithm. *J. Chem. Phys.*, 141: 211102, 2014. doi: 10.1063/1.4902991. URL https://doi.org/10.1063/1.4902991.

[97] T. Helgaker, P. Jørgensen, and J. Olson. *Molecular Electronic-Structure Theory*. John Wiley & Sons, Ltd, Chichester, 2000.

[98] Hans-Joachim Werner and Wilfried Meyer. A quadratically convergent multiconfiguration-self-consistent field method with simultaneous optimization of orbitals and CI coefficients. *J. Chem. Phys.*, 73:2342, 1980. doi: 10.1063/1.440384. URL https://doi.org/10.1063/1.440384.

[99] Hans-Joachim Werner and Peter J Knowles. A second order multiconfiguration SCF procedure with optimum convergence. *J. Chem. Phys.*, 82:5053, 1985. doi: 10.1063/1.448627. URL https://doi.org/10.1063/1.448627.

[100] G. Chaban, M. W. Schmidt, and M. S. Gordon. Approximate second order method for orbital optimization of SCF and MCSCF wavefunctions. *Theor. Chem. Acc.*, 97:88, 1997. URL https://link.springer.com/content/pdf/10.1007{%}2Fs002140050241.pdf.

[101] Michael W Schmidt and Mark S Gordon. The Construction and Interpretation of MCSCF Wavefunctions. *Annu. Rev. Phys. Chem*, 49:233, 1998. doi: 10.1146/annurev.physchem.49.1.233. URL www.annualreviews.org.

[102] Debashree Ghosh, Johannes Hachmann, Takeshi Yanai, and Garnet Kin-Lic Chan. Orbital optimization in the density matrix renormalization group, with applications to polyenes and beta-carotene. *J. Chem. Phys.*, 128(14):144117, apr 2008. ISSN 0021-9606. doi: 10.1063/1.2883976. URL http://www.ncbi.nlm.nih.gov/pubmed/18412433.

[103] Takeshi Yanai, Yuki Kurashige, Debashree Ghosh, and Garnet Kin-Lic Chan. Accelerating Convergence in Iterative Solution for Large-Scale Complete Active Space Self-Consistent-Field Calculations. *Int. J. Quantum Chem.*, 109:2178, 2009. doi: 10.1002/qua.22099. URL https://onlinelibrary.wiley.com/doi/pdf/10.1002/qua.22099.

[104] David A Kreplin, Peter J Knowles, and Hans-Joachim Werner. Second-order MCSCF optimization revisited. I. Improved algorithms for fast and robust second-order

CASSCF convergence. *J. Chem. Phys.*, 150:194106, 2019. doi: 10.1063/1.5094644. URL https://aip.scitation.org/doi/pdf/10.1063/1.5094644?class=pdf.

[105] W. H. Press, S. A. Teukolsky, W. T. Vetterling, and B. P. Flannery. *Numerical Recipes in Fortran 77: The Art of Scientific Computing*. Cambridge University Press, Cambridge, U.K., 2nd edition, 1992.

[106] Valera Veryazov, Per Åke Malmqvist, and Björn O. Roos. How to select active space for multiconfigurational quantum chemistry? *Int. J. Quantum Chem.*, 111:3329, 2011. doi: 10.1002/qua.23068.

[107] Elvira R Sayfutyarova, Qiming Sun, Garnet Kin-Lic Chan, and Gerald Knizia. Automated Construction of Molecular Active Spaces from Atomic Valence Orbitals. *J. Chem. Theory Comput.*, 13:4063, 2017. doi: 10.1021/acs.jctc.7b00128. URL https://pubs.acs.org/sharingguidelines.

[108] Jie J Bao and Donald G Truhlar. Automatic Active Space Selection for Calculating Electronic Excitation Energies Based on High-Spin Unrestricted Hartree–Fock Orbitals. *J. Chem. Theory Comput.*, 15:5308, 2019. doi: 10.1021/acs.jctc.9b00535. URL https://pubs.acs.org/sharingguidelines.

[109] Abhishek Khedkar and Michael Roemelt. Active Space Selection Based on Natural Orbital Occupation Numbers from n-Electron Valence Perturbation Theory. *J. Chem. Theory Comput.*, 15:3522, 2019. doi: 10.1021/acs.jctc.8b01293. URL https://pubs.acs.org/doi/10.1021/acs.jctc.8b01293.

[110] Qiming Sun and Garnet Kin Lic Chan. Exact and optimal quantum mechanics/molecular mechanics boundaries. *J. Chem. Theory Comput.*, 10(9):3784–3790, 2014. ISSN 15499626. doi: 10.1021/ct500512f.

[111] Qiming Sun, Timothy C. Berkelbach, Nick S. Blunt, George H. Booth, Sheng Guo, Zhendong Li, Junzi Liu, James D. McClain, Elvira R. Sayfutyarova, Sandeep Sharma, Sebastian Wouters, and Garnet Kin Lic Chan. PySCF: the Python-based simulations of chemistry framework. *WIREs Comput. Mol. Sci.*, 8:e1340, 2018. doi: 10.1002/wcms.1340.

[112] E Schmidt. Zur Theorie der Linearen und Nichtlinearen Integralgleichungen. I Teil. Entwicklung Willkürlichen Funktionen nach System Vorgeschriebener. *Math. Annalen*, 63:433, 1907. doi: 10.1007/BF01449770. URL https://link.springer.com/content/pdf/10.1007{%}2FBF01449770.pdf.

[113] Ingo Peschel. Special Review: Entanglement in Solvable Many-Particle Models. *Braz J Phys.*, 42:267–291, 2012. doi: 10.1007/s13538-012-0074-1. URL https://link.springer.com/content/pdf/10.1007{%}2Fs13538-012-0074-1.pdf.

[114] P.O. Löwdin. Discussion on the Hartree-Fock approximation. *Rev. Mod. Phys.*, 35(3):496, 1963. ISSN 00346861. doi: 10.1103/RevModPhys.35.496.

[115] J. G. Valatin. Generalized Hartree-Fock method. *Phys. Rev.*, 122(4):1012–1020, 1961. ISSN 0031899X. doi: 10.1103/PhysRev.122.1012.

[116] Carlos A Jiménez-Hoyos, Thomas M Henderson, Takashi Tsuchimochi, and Gustavo E Scuseria. Projected Hartree-Fock theory. *J. Chem. Phys.*, 136(16):164109, apr 2012. ISSN 1089-7690. doi: 10.1063/1.4705280. URL `http://www.ncbi.nlm.nih.gov/pubmed/22559472`.

[117] Matthew R. Hermes. https://github.com/MatthewRHermes/mrh, 2018. URL `https://github.com/MatthewRHermes/mrh`.

[118] Juan E Peralta and Juan I Melo. Magnetic Exchange Couplings with Range-Separated Hybrid Density Functionals. *J. Chem. Theory Comput.*, 6:1894, 2010. doi: 10.1021/ct100104v. URL `https://pubs.acs.org/sharingguidelines`.

[119] Florian Weigend and Reinhart Ahlrichs. Balanced basis sets of split valence, triple zeta valence and quadruple zeta valence quality for h to rn: Design and assessment of accuracy. *Phys. Chem. Chem. Phys.*, 7(18):3297–3305, 2005.

[120] Florian Weigend. Accurate coulomb-fitting basis sets for h to rn. *Phys. Chem. Chem. Phys.*, 8(9):1057–1065, 2006.

[121] D Andrae, U Haeussermann, M Dolg, H Stoll, and H Preuss. Energy-adjustedab initio pseudopotentials for the second and third row transition elements. *Theor. Chim. Acta*, 77(2):123–141, 1990.

[122] Thom H. Dunning. Gaussian basis sets for use in correlated molecular calculations. i. the atoms boron through neon and hydrogen. *J. Chem. Phys.*, 90(2):1007–1023, 1989. doi: 10.1063/1.456153. URL `https://doi.org/10.1063/1.456153`.

[123] RHWJ Ditchfield, W J_ Hehre, and John A Pople. Self-consistent molecular-orbital methods. ix. an extended gaussian-type basis for molecular-orbital studies of organic molecules. *J. Chem. Phys.*, 54(2):724–728, 1971.

[124] Liam Wilbraham, Pragya Verma, Donald G Truhlar, Laura Gagliardi, and Ilaria Ciofini. Multiconfiguration pair-density functional theory predicts spin-state ordering in iron complexes with the same accuracy as complete active space second-order perturbation theory at a significantly reduced computational cost. *J. Phys. Chem. Lett.*, 8(9):2026–2030, 2017.

[125] Andrew M Sand, Chad E Hoyer, Kamal Sharkas, Katherine M Kidder, Roland Lindh, Donald G Truhlar, and Laura Gagliardi. Analytic Gradients for Complete Active Space Pair-Density Functional Theory. *J. Chem. Theory Comput.*, 14:126–138, 2018. doi: 10.1021/acs.jctc.7b00967.

[126] Peter G Szalay, Thomas Muller, Gergely Gidofalvi, Hans Lischka, and Ron Shepard. Multiconfiguration self-consistent field and multireference configuration interaction methods and applications. *Chem. Rev.*, 112(1):108–181, 2012. doi: 10.1021/cr200137a.

[127] Jae Woo Park, Rachael Al-Saadon, Matthew K MacLeod, Toru Shiozaki, and Bess Vlaisavljevich. Multireference electron correlation methods: Journeys along potential energy surfaces. *Chem. Rev.*, 120(13):5878–5909, 2020. doi: 10.1021/acs.chemrev.9b00496.

[128] Francesco A Evangelista. Perspective: Multireference coupled cluster theories of dynamical electron correlation. *J. Chem. Phys.*, 149(3):030901, 2018.

[129] Indrani Chakraborty, Kevin J Bodurtha, Nicholas J Heeder, Michael P Godfrin, Anubhav Tripathi, Robert H Hurt, Arun Shukla, and Arijit Bose. Massive electrical conductivity enhancement of multilayer graphene/polystyrene composites using a nonconductive filler. *ACS applied materials & interfaces*, 6(19):16472–16475, 2014.

[130] Nicholas C Handy and Aron J Cohen. Left-right correlation energy. *Mol. Phys.*, 99 (5):403–412, 2001.

[131] Katharina Boguslawski, Pawel Tecmer, Ors Legeza, and Markus Reiher. Entanglement measures for single-and multireference correlation effects. *J. Phys. Chem. Lett.*, 3(21): 3129–3135, 2012.

[132] Steven Vancoillie, Hailiang Zhao, Van Tan Tran, Marc FA Hendrickx, and Kristine Pierloot. Multiconfigurational second-order perturbation theory restricted active space (raspt2) studies on mononuclear first-row transition-metal systems. *J. Chem. Theory Comput.*, 7(12):3961–3977, 2011.

[133] Pierre-François Loos, Anthony Scemama, and Denis Jacquemin. The quest for highly accurate excitation energies: A computational perspective. *J. Phys. Chem. Lett.*, 11 (6):2374–2383, 2020.

[134] Andrew M Sand, Donald G Truhlar, and Laura Gagliardi. Efficient algorithm for multiconfiguration pair-density functional theory with application to the heterolytic dissociation energy of ferrocene. *J. Chem. Phys.*, 146(3):034101, 2017.

[135] Davide Presti, Samuel J Stoneburner, Donald G Truhlar, and Laura Gagliardi. Full correlation in a multiconfigurational study of bimetallic clusters: Restricted active space pair-density functional theory study of [2fe–2s] systems. *J. Phys. Chem. C*, 123 (18):11899–11907, 2019.

[136] Soumen Ghosh, Christopher J Cramer, Donald G Truhlar, and Laura Gagliardi. Generalized-active-space pair-density functional theory: an efficient method to study large, strongly correlated, conjugated systems. *Chem. Sci.*, 8(4):2741–2750, 2017.

[137] Junwei Lucas Bao, Samuel O Odoh, Laura Gagliardi, and Donald G Truhlar. Predicting bond dissociation energies of transition-metal compounds by multiconfiguration pair-density functional theory and second-order perturbation theory based on correlated participating orbitals and separated pairs. *J. Chem. Theory Comput.*, 13(2): 616–626, 2017.

[138] Shuhang J Li, Laura Gagliardi, and Donald G Truhlar. Extended separated-pair approximation for transition metal potential energy curves. *J. Chem. Phys.*, 152(12): 124118, 2020.

[139] Prachi Sharma, Varinia Bernales, Stefan Knecht, Donald G. Truhlar, and Laura Gagliardi. Density matrix renormalization group pair-density functional theory (DMRG-PDFT): Singlet-triplet gaps in polyacenes and polyacetylenes. *Chem. Sci.*, 10(6):1716–1723, 2019. ISSN 20416539. doi: 10.1039/c8sc03569e.

[140] Chen Zhou, Laura Gagliardi, and Donald G Truhlar. Multiconfiguration pair-density functional theory for iron porphyrin with cas, ras, and dmrg active spaces. *J. Phys. Chem. A*, 123(15):3389–3394, 2019.

[141] Roy McWeeny. The density matrix in many-electron quantum mechanics i. generalized product functions. factorization and physical interpretation of the density matrices. *Proc. R. Soc. A: Math. Phys. Eng. Sci.*, 253(1273):242–259, 1959.

[142] Rev McWeeny. Some recent advances in density matrix theory. *Rev. Mod. Phys.*, 32 (2):335, 1960.

[143] David A Mazziotti. Contracted schrödinger equation: Determining quantum energies and two-particle density matrices without wave functions. *Phys. Rev. A*, 57(6):4219, 1998.

[144] SY Chang, ER Davidson, and G Vincow. Theory of the hyperfine splittings of pi-electron free radicals. iii. methyl radical in a pyramidal configuration: Temperature dependence of the hyperfine splittings. *J. Chem. Phys.*, 52(11):5596–5606, 1970.

[145] Viktor N Staroverov and Ernest R Davidson. Distribution of effectively unpaired electrons. *Chem. Phys. Lett.*, 330(1-2):161–168, 2000.

[146] Viktor N Staroverov and Ernest R Davidson. Transition regions in the cope rearrangement of 1, 5-hexadiene and its cyano derivatives. *J. Am. Chem. Soc.*, 122(30): 7377–7385, 2000.

[147] Kazuo Takatsuka, Takayuki Fueno, and Kizashi Yamaguchi. Distribution of odd electrons in ground-state molecules. *Theor. Chim. Acta*, 48(3):175–183, 1978.

[148] M. J. Frisch, G. W. Trucks, H. B. Schlegel, G. E. Scuseria, M. A. Robb, J. R. Cheeseman, G. Scalmani, V. Barone, B. Mennucci, G. A. Petersson, H. Nakatsuji, M. Caricato, X. Li, H. P. Hratchian, A. F. Izmaylov, J. Bloino, G. Zheng, J. L. Sonnenberg, M. Hada, M. Ehara, K. Toyota, R. Fukuda, J. Hasegawa, M. Ishida, T. Nakajima, Y. Honda, O. Kitao, H. Nakai, T. Vreven, J. A. Montgomery, Jr., J. E. Peralta, F. Ogliaro, M. Bearpark, J. J. Heyd, E. Brothers, K. N. Kudin, V. N. Staroverov, R. Kobayashi, J. Normand, K. Raghavachari, A. Rendell, J. C. Burant, S. S. Iyengar, J. Tomasi, M. Cossi, N. Rega, J. M. Millam, M. Klene, J. E. Knox, J. B. Cross, V. Bakken, C. Adamo, J. Jaramillo, R. Gomperts, R. E. Stratmann, O. Yazyev, A. J.

Austin, R. Cammi, C. Pomelli, J. W. Ochterski, R. L. Martin, K. Morokuma, V. G. Zakrzewski, G. A. Voth, P. Salvador, J. J. Dannenberg, S. Dapprich, A. D. Daniels, Ö. Farkas, J. B. Foresman, J. V. Ortiz, J. Cioslowski, and D. J. Fox. Gaussian 09 Revision E.01, 2009. Gaussian Inc. Wallingford CT 2009.

[149] Laura Gagliardi, Giorgio Orlandi, Vicent Molina, Per-Åke Malmqvist, and Björn Roos. Theoretical study of the lowest 1bu states of trans-stilbene. *J. Phys. Chem. A*, 106 (32):7355–7361, 2002.

[150] C F Bender and E R Davidson. Studies in Configuration Interaction: The First-Row Diatomic Hydrides. *Phys. Rev.*, 183:23, 1969.

[151] J L Whitten and M Hackmeyer. Configuration Interaction Studies of Ground and Excited States of Polyatomic Molecules. I. The CI Formulation and Studies of Formaldehyde. *J. Chem. Phys.*, 51:5584, 1969.

[152] N M Tubman, J Lee, T Y Takeshita, M Head-Gordon, and K B Whaley. A deterministic alternative to the full configuration interaction quantum Monte Carlo method. *J. Chem. Phys.*, 145:44112, 2016.

[153] J B Schriber and F A Evangelista. Communication: An adaptive configuration interaction approach for strongly correlated electrons with tunable accuracy. *J. Chem. Phys.*, 144:161106, 2016.

[154] W Liu and M R Hoffmann. iCI: iterative CI toward full CI. *J. Chem. Theory Comput.*, 12:1169, 2016.

[155] Y Ohtsuka and J.-y. Hasegawa. Selected configuration interaction method using sampled first-order corrections to wave functions. *J. Chem. Phys.*, 147:34102, 2017.

[156] B Huron, J P Malrieu, and P Rancurel. Iterative perturbation calculations of ground and excited state energies from multiconfigurational zeroth-order wavefunctions. *J. Chem. Phys.*, 58:5745, 1973.

[157] S Evangelisti, J.-P. Daudey, and J.-P. Malrieu. Convergence of an improved CIPSI algorithm. *Chem. Phys.*, 75:91, 1983.

[158] N M Tubman, C D Freeman, D S Levine, D Hait, M Head-Gordon, and K B Whaley. Modern Approaches to Exact Diagonalization and Selected Configuration Interaction with the Adaptive Sampling CI Method. *J. Chem. Theory Comput.*, 16:2139, 2020.

[159] Daniel S Levine, Diptarka Hait, Norm M Tubman, Susi Lehtola, K Birgitta Whaley, and Martin Head-Gordon. CASSCF with extremely large active spaces using the adaptive sampling configuration interaction method. *J. Chem. Theory Comput.*, 16: 2340, 2020. doi: 10.1021/acs.jctc.9b01255. URL `https://dx.doi.org/10.1021/acs.jctc.9b01255`.

[160] A A Holmes, N M Tubman, and C J Umrigar. Heat-Bath Configuration Interaction: An Efficient Selected Configuration Interaction Algorithm Inspired by Heat-Bath Sampling. *J. Chem. Theory Comput.*, 12:3674, 2016.

[161] J Li, M Otten, A A Holmes, S Sharma, and C J Umrigar. Fast Semistochastic Heat-Bath Configuration Interaction. *J. Chem. Phys.*, 149:214110, 2018.

[162] J E T Smith, B Mussard, A A Holmes, and S Sharma. Cheap and Near Exact CASSCF with Large Active Spaces. *J. Chem. Theory Comput.*, 13:5468, 2017.

[163] G H Booth, A J W Thom, and A Alavi. Fermion Monte Carlo without fixed nodes: A game of life, death, and annihilation in Slater determinant space. *J. Chem. Phys.*, 131:54106, 2009.

[164] D Cleland, G H Booth, and A Alavi. Communications: Survival of the fittest: Accelerating convergence in full configuration-interaction quantum Monte Carlo. *J. Chem. Phys.*, 132:41103, 2010.

[165] B Liu and AD McLean. A binitio potential curve for be2 (1σ g+) from the interacting correlated fragments method. *J. Chem. Phys.*, 72(5):3418–3419, 1980.

[166] B Liu and AD McLean. The interacting correlated fragments model for weak interactions, basis set superposition error, and the helium dimer potential. *J. Chem. Phys.*, 91(4):2348–2359, 1989.

[167] Soichiro Nishio and Yuki Kurashige. Importance of dynamical electron correlation in diabatic couplings of electron-exchange processes. *J. Chem. Phys.*, 156(11):114107, 2022. doi: 10.1063/5.0075978. URL `https://doi.org/10.1063/5.0075978`.

[168] Tao Fang and Shuhua Li. Block correlated coupled cluster theory with a complete active-space self-consistent-field reference function: The formulation and test applications for single bond breaking. *J. Chem. Phys.*, 127(20):204108, 2007.

[169] Shuhua Li. Block-correlated coupled cluster theory: The general formulation and its application to the antiferromagnetic heisenberg model. *J. Chem. Phys.*, 120(11):5017–5026, 2004.

[170] Carlos A Jiménez-Hoyos and Gustavo E Scuseria. Cluster-based mean-field and perturbative description of strongly correlated fermion systems: Application to the one-and two-dimensional hubbard model. *Phys. Rev. B*, 92(8):085101, 2015.

[171] Vibin Abraham and Nicholas J Mayhall. Cluster many-body expansion: A many-body expansion of the electron correlation energy about a cluster mean field reference. *J. Chem. Phys.*, 155(5):054101, 2021.

[172] Vibin Abraham and Nicholas J Mayhall. Selected configuration interaction in a basis of cluster state tensor products. *J. Chem. Theory Comput.*, 16(10):6098–6113, 2020.

[173] Riddhish Pandharkar, Matthew R Hermes, Christopher J Cramer, Donald G Truhlar, and Laura Gagliardi. Localized active space pair-density functional theory. *J. Chem. Theory Comput.*, 17(5):2843–2851, 2021. doi: 10.1021/acs.jctc.1c00067.

[174] Riddhish Pandharkar. https://github.com/riddhish-P/mrh, 2022. URL `https://github.com/riddhish-P/mrh`.

[175] Melvin B Robin and Peter Day. Mixed valence chemistry-a survey and classification. In *Advances in inorganic chemistry and radiochemistry*, volume 10, pages 247–422. Elsevier, 1968.

[176] Alexander Heckmann and Christoph Lambert. Organic mixed-valence compounds: a playground for electrons and holes. *Angew. Chem. Int. Ed.*, 51(2):326–392, 2012.

[177] Deanna M D'Alessandro and F Richard Keene. Current trends and future challenges in the experimental, theoretical and computational analysis of intervalence charge transfer (ivct) transitions. *Chem. Soc. Rev.*, 35(5):424–440, 2006.

[178] Bruce S Brunschwig, Carol Creutz, and Norman Sutin. Optical transitions of symmetrical mixed-valence systems in the class ii–iii transition regime. *Chem. Soc. Rev.*, 31 (3):168–184, 2002.

[179] Christian Joachim, Jim K Gimzewski, and Arieh Aviram. Electronics using hybrid-molecular and mono-molecular devices. *Nature*, 408(6812):541–548, 2000.

[180] Paul F Barbara, Thomas J Meyer, and Mark A Ratner. Contemporary issues in electron transfer research. *J. Phys. Chem.*, 100(31):13148–13168, 1996.

[181] Jie J Bao, Chen Zhou, Zoltan Varga, Siriluk Kanchanakungwankul, Laura Gagliardi, and Donald G Truhlar. Multi-state pair-density functional theory. *Faraday Discuss.*, 224:348–372, 2020.

[182] Richard A Layfield. Organometallic single-molecule magnets. *Organometallics*, 33(5): 1084–1099, 2014.

[183] Michael N Leuenberger and Daniel Loss. Quantum computing in molecular magnets. *Nature*, 410(6830):789–793, 2001.

[184] Mark R Pederson and Tunna Baruah. Molecular magnets: Phenomenology and theory. *Handbook of Magnetism and Advanced Magnetic Materials*, 2007.

[185] Werner Heisenberg. Zur theorie des ferromagnetismus. In *Original Scientific Papers Wissenschaftliche Originalarbeiten*, pages 580–597. Springer, 1985.

[186] Paul Adrien Maurice Dirac. On the theory of quantum mechanics. *Proc. R. Soc. Lond. A*, 112(762):661–677, 1926.

[187] John Hasbrouck Van Vleck. *Electric and magnetic susceptibilities*. Clarendon Press, 1932.

[188] Thorbjørn J Morsing, Høgni Weihe, and Jesper Bendix. Probing effective hamiltonian operators by single-crystal epr: a case study using dinuclear cr (iii) complexes. *Inorg. Chem.*, 55(4):1453–1460, 2016.

[189] Stefan Kremer. Epr spectroscopic study of s= 1, 2, and 3 spin states of tris (. mu.-hydroxo)-bridged chromium (iii) dimers. *Inorg. Chem.*, 24(6):887–890, 1985.

[190] Andrea Niemann, Ursula Bossek, Karl Wieghardt, Christian Butzlaff, Alfred X Trautwein, and Bernhard Nuber. A new structure–magnetism relationship for face-sharing transition-metal complexes with d3–d3 electronic configuration. *Angew. Chem. Int. Ed.*, 31(3):311–313, 1992.

[191] Simon J Bennie, David Collison, and Joseph JW McDouall. Electronic and magnetic properties of kremer's tris-hydroxo bridged chromium dimer: A challenge for dft. *J. Chem. Theory Comput.*, 8(12):4915–4921, 2012.

[192] Dimitrios A Pantazis. Meeting the challenge of magnetic coupling in a triply-bridged chromium dimer: complementary broken-symmetry density functional theory and multireference density matrix renormalization group perspectives. *J. Chem. Theory Comput.*, 15(2):938–948, 2019.

[193] Prachi Sharma, Donald G Truhlar, and Laura Gagliardi. Magnetic coupling in a tris-hydroxo-bridged chromium dimer occurs through ligand mediated superexchange in conjunction with through-space coupling. *J. Am. Chem. Soc.*, 142(39):16644–16650, 2020.

[194] Jean Paul Malrieu, Rosa Caballol, Carmen J Calzado, Coen de Graaf, and Nathalie Guihery. Magnetic interactions in molecules and highly correlated materials: physical content, analytical derivation, and rigorous extraction of magnetic hamiltonians. *Chem. Rev.*, 114(1):429–492, 2014. doi: 10.1021/cr300500z.

[195] Frank Neese. Prediction of molecular properties and molecular spectroscopy with density functional theory: From fundamental theory to exchange-coupling. *Coord. Chem. Rev*, 253(5-6):526–563, 2009. doi: 10.1016/j.ccr.2008.05.014.

[196] Ting Chen, Lei Zheng, Jie Yuan, Zhongfu An, Runfeng Chen, Ye Tao, Huanhuan Li, Xiaoji Xie, and Wei Huang. Understanding the control of singlet-triplet splitting for organic exciton manipulating: a combined theoretical and experimental approach. *Sci. Rep.*, 5(1):1–11, 2015.

[197] Takuya Minami, Soichi Ito, and Masayoshi Nakano. Signature of singlet open-shell character on the optically allowed singlet excitation energy and singlet–triplet energy gap. *J. Phys. Chem. A*, 117(9):2000–2006, 2013.

[198] Prachi Sharma, Varinia Bernales, Stefan Knecht, Donald G Truhlar, and Laura Gagliardi. Density matrix renormalization group pair-density functional theory (dmrg-pdft): singlet–triplet gaps in polyacenes and polyacetylenes. *Chem. Sci.*, 10(6):1716–1723, 2019.

[199] Masayoshi Nakano. *Excitation energies and properties of open-shell singlet molecules: applications to a new class of molecules for nonlinear optics and singlet fission*. Springer, 2014.

[200] John E Anthony. Functionalized acenes and heteroacenes for organic electronics. *Chem. Rev.*, 106(12):5028–5048, 2006.

[201] Wayne M. Flicker, Oren A. Mosher, and Aron Kuppermann. Low energy, variable angle electron-impact excitation of 1,3,5-hexatriene. *Chem. Phys. Lett.*, 45(3):492–497, 1977. ISSN 0009-2614. doi: https://doi.org/10.1016/0009-2614(77)80073-0. URL `https://www.sciencedirect.com/science/article/pii/0009261477800730`.

[202] Allison G. Robinson, Paul R. Winter, and Timothy S. Zwier. The singlet–triplet spectroscopy of 1,3-butadiene using cavity ring-down spectroscopy. *J. Chem. Phys.*, 116(18):7918–7925, 2002. doi: 10.1063/1.1467903. URL `https://doi.org/10.1063/1.1467903`.

[203] C. David Sherrill, Antara Dutta, Micah L. Abrams, and John S. Sears. *Bond Breaking in Quantum Chemistry: A Comparison of Single- and Multi-Reference Methods*, chapter 5, pages 75–88. ACS Publications, 2007. doi: 10.1021/bk-2007-0958.ch005. URL `https://pubs.acs.org/doi/abs/10.1021/bk-2007-0958.ch005`.

[204] Anna I Krylov, Lyudmila V Slipchenko, and Sergey V Levchenko. Breaking the curse of the non-dynamical correlation problem: The spin-flip method. In *ACS Symposium Series*, volume 958, pages 89–102. Citeseer, 2007.

[205] Tamar Stein, Thomas M Henderson, and Gustavo E Scuseria. Seniority zero pair coupled cluster doubles theory. *J. Chem. Phys.*, 140(21):214113, 2014. doi: 10.1063/1.4880819.

[206] Carlo Alberto Gaggioli, Samuel J Stoneburner, Christopher J Cramer, and Laura Gagliardi. Beyond density functional theory: the multiconfigurational approach to model heterogeneous catalysis. *ACS Catal.*, 9(9):8481–8502, 2019. doi: 10.1021/acscatal.9b01775.

[207] Christoph R Jacob and Markus Reiher. Spin in density-functional theory. *Int. J. Quantum Chem.*, 112(23):3661–3684, 2012. doi: 10.1002/qua.24309.

[208] Haoyu S Yu, Shaohong L Li, and Donald G Truhlar. Perspective: Kohn–sham density functional theory descending a staircase. *J. Chem. Phys.*, 145(13):130901, 2016. doi: 10.1063/1.4963168.

[209] Christopher J Cramer, Marta Włoch, Piotr Piecuch, Cristina Puzzarini, and Laura Gagliardi. Theoretical models on the cu2o2 torture track: Mechanistic implications for oxytyrosinase and small-molecule analogues. *J. Phys. Chem. A*, 110(5):1991–2004, 2006. doi: 10.1021/jp056791e.

[210] Michael A Collins and Ryan PA Bettens. Energy-based molecular fragmentation methods. *Chem. Rev.*, 115(12):5607–5642, 2015. doi: 10.1021/cr500455b.

[211] Krishnan Raghavachari and Arjun Saha. Accurate composite and fragment-based quantum chemical models for large molecules. *Chem. Rev.*, 115(12):5643–5677, 2015. doi: 10.1021/cr500606e.

[212] Dmitri G Fedorov, Yuri Alexeev, and Kazuo Kitaura. Geometry optimization of the active site of a large system with the fragment molecular orbital method. *J. Phys. Chem. Lett.*, 2(4):282–288, 2011. doi: 10.1021/jz1016894.

[213] Giovanni Li Manni, Werner Dobrautz, Nikolay A. Bogdanov, Kai Guther, and Ali Alavi. Resolution of low-energy states in spin-exchange transition-metal clusters: Case study of singlet states in [Fe(III)4S4] cubanes. *J. Phys. Chem. A*, 125:4727, 2021. ISSN 1089-5639. doi: 10.1021/acs.jpca.1c00397.

[214] Prachi Sharma, Dale R Pahls, Bianca L Ramirez, Connie C Lu, and Laura Gagliardi. Multiple bonds in uranium–transition metal complexes. *Inorg. Chem.*, 58(15):10139–10147, 2019. doi: 10.1021/acs.inorgchem.9b01264.

[215] Ross W Hogue, Sandhya Singh, and Sally Brooker. Spin crossover in discrete polynuclear iron (II) complexes. *Chem. Soc. Rev.*, 47(19):7303–7338, 2018. doi: 10.1039/C7CS00835J.

[216] Edward G. Hohenstein, Nathan Luehr, Ivan S. Ufimtsev, and Todd J. Martínez. An atomic orbital-based formulation of the complete active space self-consistent field method on graphical processing units. *J. Chem. Phys.*, 142(22):224103, 2015. ISSN 00219606. doi: 10.1063/1.4921956. URL `http://dx.doi.org/10.1063/1.4921956`.

[217] James W. Snyder, Basile F.E. Curchod, and Todd J. Martínez. GPU-accelerated state-averaged complete active space self-consistent field interfaced with ab initio multiple spawning unravels the photodynamics of Provitamin D3. *J. Phys. Chem. Lett.*, 7(13): 2444–2449, 2016. ISSN 19487185. doi: 10.1021/acs.jpclett.6b00970.

[218] R K Kathir, Coen de Graaf, Ria Broer, and Remco W A Havenith. Reduced common molecular orbital basis for nonorthogonal configuration interaction. *J. Chem. Theory Comput.*, 2020. doi: 10.1021/acs.jctc.9b01144. URL `https://dx.doi.org/10.1021/acs.jctc.9b01144`.

[219] Vibin Abraham and Nicholas J. Mayhall. Selected Configuration Interaction in a Basis of Cluster State Tensor Products. *J. Chem. Theory Comput.*, 16(10):6098–6113, 2020. ISSN 15499626. doi: 10.1021/acs.jctc.0c00141.

[220] Athanasios Papastathopoulos-Katsaros, Carlos A Jiménez-Hoyos, Thomas M Henderson, and Gustavo E Scuseria. A cluster-based mean-field, perturbative and coupled-cluster theory description of strongly correlated systems. *arXiv preprint arXiv:2102.10043*, 2021. URL `http://arxiv.org/abs/2102.10043`.

[221] Qingchun Wang, Mingzhou Duan, Enhua Xu, Jingxiang Zou, and Shuhua Li. Describing Strong Correlation with Block-Correlated Coupled Cluster Theory. *J. Phys. Chem. Lett.*, 11(18):7536–7543, 2020. ISSN 19487185. doi: 10.1021/acs.jpclett.0c02117.

[222] Dmitry I. Lyakh, Monika Musiał, Victor F. Lotrich, and Rodney J. Bartlett. Multireference nature of chemistry: The coupled-cluster view. *Chem. Rev.*, 112(1):182–243, 2012. ISSN 00092665. doi: 10.1021/cr2001417.

[223] C. Møller and M. S. Plesset. Note on an Approximation Treatment for Many-Electron Systems. *Phys. Rev.*, 46:618, 1934. ISSN 1873734X.

[224] Isaiah Shavitt and Rodney J. Bartlett. *Many-Body Methods in Chemistry and Physics*. Cambridge University Press, Cambridge, U.K., 2009. ISBN 978-0-521-81832-2.

[225] Yudong Cao, Jonathan Romero, Jonathan P Olson, Matthias Degroote, Peter D Johnson, Mária Kieferová, Ian D Kivlichan, Tim Menke, Borja Peropadre, Nicolas PD Sawaya, et al. Quantum chemistry in the age of quantum computing. *Chem. Rev.*, 119 (19):10856–10915, 2019. doi: 10.1021/acs.chemrev.8b00803.

[226] Kade Head-Marsden, Johannes Flick, Christopher J Ciccarino, and Prineha Narang. Quantum information and algorithms for correlated quantum matter. *Chem. Rev.*, 121 (5):3061–3120, 2020. doi: 10.1021/acs.chemrev.0c00620.

[227] Sam McArdle, Suguru Endo, Alán Aspuru-Guzik, Simon C. Benjamin, and Xiao Yuan. Quantum computational chemistry. *Rev. Mod. Phys.*, 92:015003, Mar 2020. doi: 10.1103/RevModPhys.92.015003. URL `https://link.aps.org/doi/10.1103/RevModPhys.92.015003`.

[228] Seth Lloyd. Universal quantum simulators. *Science*, pages 1073–1078, 1996.

[229] A Yu Kitaev. Quantum measurements and the Abelian stabilizer problem. *arXiv preprint quant-ph/9511026*, 1995.

[230] Daniel S Abrams and Seth Lloyd. Quantum algorithm providing exponential speed increase for finding eigenvalues and eigenvectors. *Phys. Rev. Lett.*, 83(24):5162, 1999. doi: 10.1103/PhysRevLett.83.5162.

[231] Alexei Yu Kitaev, Alexander Shen, Mikhail N Vyalyi, and Mikhail N Vyalyi. *Classical and quantum computation*. Number 47 in 47. American Mathematical Soc., 2002.

[232] Bryan O'Gorman, Sandy Irani, James Whitfield, and Bill Fefferman. Electronic structure in a fixed basis is qma-complete. *arXiv preprint arXiv:2103.08215*, 2021.

[233] Jonathan Romero, Ryan Babbush, Jarrod R McClean, Cornelius Hempel, Peter J Love, and Alán Aspuru-Guzik. Strategies for quantum computing molecular energies using the unitary coupled cluster ansatz. *Quantum Sci. Technol.*, 4(1):014008, 2018. doi: 10.1088/2058-9565/aad3e4.

[234] Alberto Peruzzo, Jarrod McClean, Peter Shadbolt, Man-Hong Yung, Xiao-Qi Zhou, Peter J Love, Alán Aspuru-Guzik, and Jeremy L O'brien. A variational eigenvalue solver on a photonic quantum processor. *Nat. Commun.*, 5(1):1–7, 2014. doi: 10.1038/ncomms5213.

[235] John Preskill. Quantum computing in the nisq era and beyond. *Quantum*, 2:79, 2018. doi: 10.22331/q-2018-08-06-79.

[236] Dave Wecker, Matthew B Hastings, and Matthias Troyer. Progress towards practical quantum variational algorithms. *Phys. Rev. A*, 92(4):042303, 2015. doi: 10.1103/PhysRevA.92.042303.

[237] Jarrod R McClean, Mollie E Kimchi-Schwartz, Jonathan Carter, and Wibe A De Jong. Hybrid quantum-classical hierarchy for mitigation of decoherence and determination of excited states. *Phys. Rev. A*, 95(4):042308, 2017. doi: 10.1103/PhysRevA.95.042308.

[238] Abhinav Kandala, Antonio Mezzacapo, Kristan Temme, Maika Takita, Markus Brink, Jerry M Chow, and Jay M Gambetta. Hardware-efficient variational quantum eigensolver for small molecules and quantum magnets. *Nature*, 549(7671):242–246, 2017. doi: 10.1038/nature23879.

[239] Timo Fleig, Jeppe Olsen, and Christel M Marian. The generalized active space concept for the relativistic treatment of electron correlation, I. Kramers-restricted two-component configuration interaction. *J. Chem. Phys.*, 114(11):4775–4790, 2001. doi: 10.1063/1.1349076.

[240] Junhao Li, Yuan Yao, Adam A Holmes, Matthew Otten, Qiming Sun, Sandeep Sharma, and CJ Umrigar. Accurate many-body electronic structure near the basis set limit: Application to the chromium dimer. *Phys. Rev. Res.*, 2(1):012015, 2020.

[241] Junhao Li, Matthew Otten, Adam A Holmes, Sandeep Sharma, and Cyrus J Umrigar. Fast semistochastic heat-bath configuration interaction. *J. Chem. Phys.*, 149(21): 214110, 2018.

[242] Roberto Olivares-Amaya, Weifeng Hu, Naoki Nakatani, Sandeep Sharma, Jun Yang, and Garnet Kin-Lic Chan. The ab-initio density matrix renormalization group in practice. *J. Chem. Phys.*, 142(3):034102, 2015. doi: 10.1063/1.4905329.

[243] Stefan Knecht, Erik Donovan Hedegård, Sebastian Keller, Arseny Kovyrshin, Yingjin Ma, Andrea Muolo, Christopher J Stein, and Markus Reiher. New approaches for ab initio calculations of molecules with strong electron correlation. *arXiv preprint arXiv:1512.09267*, 2015. doi: 10.2533/chimia.2016.244.

[244] Yuki Kurashige and Takeshi Yanai. Second-order perturbation theory with a density matrix renormalization group self-consistent field reference function: Theory and application to the study of chromium dimer. *J. Chem. Phys.*, 135(9):094104, 2011. doi: 10.1063/1.3629454.

[245] Konrad Heinrich Marti and Markus Reiher. The density matrix renormalization group algorithm in quantum chemistry. In *Progress in Physical Chemistry Volume 3*, pages 293–309. Oldenbourg Wissenschaftsverlag, 2011. doi: 10.1524/9783486711639.293.

[246] Anders Bernhardsson, Roland Lindh, Jeppe Olsen, and Markus Fulscher. A direct implementation of the second-order derivatives of multiconfigurational SCF energies and an analysis of the preconditioning in the associated response equation. *Mol. Phys.*, 96(4):617–628, 1999. ISSN 1362-3028. doi: 10.1080/00268979909482998. URL `https://www.tandfonline.com/action/journalInformation?journalCode=tmph20`.

[247] Jonna Stålring, Anders Bernhardsson, Roland Lindh, Jonna Stalring, Anders Bernhardssont, and Roland Lindhf. Analytical gradients of a state average MCSCF state and a state average diagnostic. *Mol. Phys.*, 99(2):103, 2001. ISSN 1362-3028. doi: 10.1080/00268970010005642. URL `https://www.tandfonline.com/action/journalInformation?journalCode=tmph20`.

[248] Mark R. Hoffmann and Jack Simons. A unitary multiconfigurational coupled-cluster method: Theory and applications. *J. Chem. Phys.*, 88(2):993–1002, 1988. ISSN 00219606. doi: 10.1063/1.454125.

[249] Peter W Shor. Polynomial-time algorithms for prime factorization and discrete logarithms on a quantum computer. *SIAM Review*, 41(2):303–332, 1999. doi: 10.1137/S0036144598347011.

[250] Aram W. Harrow, Avinatan Hassidim, and Seth Lloyd. Quantum algorithm for linear systems of equations. *Phys. Rev. Lett.*, 103:150502, Oct 2009. doi: 10.1103/PhysRevLett.103.150502. URL `https://link.aps.org/doi/10.1103/PhysRevLett.103.150502`.

[251] P.W. Shor. Algorithms for quantum computation: discrete logarithms and factoring. In *Proceedings 35th Annual Symposium on Foundations of Computer Science*, pages 124–134, 1994. doi: 10.1109/SFCS.1994.365700.

[252] G. Ortiz, J. E. Gubernatis, E. Knill, and R. Laflamme. Quantum algorithms for fermionic simulations. *Phys. Rev. A*, 64:022319, Jul 2001. doi: 10.1103/PhysRevA.64.022319. URL `https://link.aps.org/doi/10.1103/PhysRevA.64.022319`.

[253] Ryan Babbush, Jarrod McClean, Dave Wecker, Alán Aspuru-Guzik, and Nathan Wiebe. Chemical basis of Trotter–Suzuki errors in quantum chemistry simulation. *Phys. Rev. A*, 91:022311, Feb 2015. doi: 10.1103/PhysRevA.91.022311. URL `https://link.aps.org/doi/10.1103/PhysRevA.91.022311`.

[254] Dominic W. Berry, Andrew M. Childs, Richard Cleve, Robin Kothari, and Rolando D. Somma. Simulating Hamiltonian dynamics with a truncated taylor series. *Phys. Rev. Lett.*, 114:090502, Mar 2015. doi: 10.1103/PhysRevLett.114.090502. URL https://link.aps.org/doi/10.1103/PhysRevLett.114.090502.

[255] Guang Hao Low and Isaac L. Chuang. Hamiltonian simulation by qubitization. *Quantum*, 3:163, July 2019. ISSN 2521-327X. doi: 10.22331/q-2019-07-12-163. URL https://doi.org/10.22331/q-2019-07-12-163.

[256] Pascual Jordan and Eugene Paul Wigner. über das paulische äquivalenzverbot. In *The Collected Works of Eugene Paul Wigner*, pages 109–129. Springer, 1993.

[257] Sergey Bravyi, Jay M Gambetta, Antonio Mezzacapo, and Kristan Temme. Tapering off qubits to simulate fermionic Hamiltonians. *arXiv preprint arXiv:1701.08213*, 2017.

[258] Sergey B. Bravyi and Alexei Yu. Kitaev. Fermionic quantum computation. *Ann. Phys.*, 298(1):210–226, 2002. ISSN 0003-4916. doi: https://doi.org/10.1006/aphy.2002.6254. URL https://www.sciencedirect.com/science/article/pii/S0003491602962548.

[259] Vincent E Elfving, Benno W Broer, Mark Webber, Jacob Gavartin, Mathew D Halls, K Patrick Lorton, and A Bochevarov. How will quantum computers provide an industrially relevant computational advantage in quantum chemistry? *arXiv preprint arXiv:2009.12472*, 2020.

[260] Hongbin Liu, Guang Hao Low, Damian S Steiger, Thomas Häner, Markus Reiher, and Matthias Troyer. Prospects of quantum computing for molecular sciences. *arXiv preprint arXiv:2102.10081*, 2021.

[261] Isaac H Kim, Eunseok Lee, Ye-Hua Liu, Sam Pallister, William Pol, and Sam Roberts. Fault-tolerant resource estimate for quantum chemical simulations: Case study on Li-ion battery electrolyte molecules. *arXiv preprint arXiv:2104.10653*, 2021.

[262] Bela Bauer, Sergey Bravyi, Mario Motta, and Garnet Kin-Lic Chan. Quantum algorithms for quantum chemistry and quantum materials science. *Chem. Rev.*, 120(22):12685–12717, 2020. doi: 10.1021/acs.chemrev.9b00829. URL https://doi.org/10.1021/acs.chemrev.9b00829.

[263] Francesco A. Evangelista, Garnet Kin-Lic Chan, and Gustavo E. Scuseria. Exact parameterization of fermionic wave functions via unitary coupled cluster theory. *J. Chem. Phys.*, 151(24):244112, 2019. doi: 10.1063/1.5133059. URL https://doi.org/10.1063/1.5133059.

[264] Alexander J McCaskey, Zachary P Parks, Jacek Jakowski, Shirley V Moore, Titus D Morris, Travis S Humble, and Raphael C Pooser. Quantum chemistry as a benchmark for near-term quantum computers. *npj Quantum Inf.*, 5(1):1–8, 2019. doi: 10.1038/s41534-019-0209-0.

[265] P. J. J. O'Malley, R. Babbush, I. D. Kivlichan, J. Romero, J. R. McClean, R. Barends, J. Kelly, P. Roushan, A. Tranter, N. Ding, B. Campbell, Y. Chen, Z. Chen, B. Chiaro, A. Dunsworth, A. G. Fowler, E. Jeffrey, E. Lucero, A. Megrant, J. Y. Mutus, M. Neeley, C. Neill, C. Quintana, D. Sank, A. Vainsencher, J. Wenner, T. C. White, P. V. Coveney, P. J. Love, H. Neven, A. Aspuru-Guzik, and J. M. Martinis. Scalable quantum simulation of molecular energies. *Phys. Rev. X*, 6:031007, Jul 2016. doi: 10.1103/PhysRevX.6.031007. URL `https://link.aps.org/doi/10.1103/PhysRevX.6.031007`.

[266] Rodney J. Bartlett, Stanislaw A. Kucharski, and Jozef Noga. Alternative coupled-cluster ansätze ii, the unitary coupled-cluster method. *Chem. Phys. Lett.*, 155(1):133–140, 1989. ISSN 0009-2614. doi: https://doi.org/10.1016/S0009-2614(89)87372-5. URL `https://www.sciencedirect.com/science/article/pii/S0009261489873725`.

[267] Andrew G Taube and Rodney J Bartlett. New perspectives on unitary coupled-cluster theory. *Int. J. Quantum Chem.*, 106(15):3393–3401, 2006.

[268] Werner Kutzelnigg. Error analysis and improvements of coupled-cluster theory. *Theor. Chim. Acta*, 80(4):349–386, 1991.

[269] Yangchao Shen, Xiang Zhang, Shuaining Zhang, Jing-Ning Zhang, Man-Hong Yung, and Kihwan Kim. Quantum implementation of the unitary coupled cluster for simulating molecular electronic structure. *Phys. Rev. A*, 95:020501, Feb 2017. doi: 10.1103/PhysRevA.95.020501. URL `https://link.aps.org/doi/10.1103/PhysRevA.95.020501`.

[270] Gaurav Harsha, Toru Shiozaki, and Gustavo E. Scuseria. On the difference between variational and unitary coupled cluster theories. *J. Chem. Phys.*, 148(4):044107, 2018. doi: 10.1063/1.5011033. URL `https://doi.org/10.1063/1.5011033`.

[271] Frank Arute, Kunal Arya, Ryan Babbush, Dave Bacon, Joseph C. Bardin, Rami Barends, Sergio Boixo, Michael Broughton, Bob B. Buckley, David A. Buell, Brian Burkett, Nicholas Bushnell, Yu Chen, Zijun Chen, Benjamin Chiaro, Roberto Collins, William Courtney, Sean Demura, Andrew Dunsworth, Edward Farhi, Austin Fowler, Brooks Foxen, Craig Gidney, Marissa Giustina, Rob Graff, Steve Habegger, Matthew P. Harrigan, Alan Ho, Sabrina Hong, Trent Huang, William J. Huggins, Lev Ioffe, Sergei V. Isakov, Evan Jeffrey, Zhang Jiang, Cody Jones, Dvir Kafri, Kostyantyn Kechedzhi, Julian Kelly, Seon Kim, Paul V. Klimov, Alexander Korotkov, Fedor Kostritsa, David Landhuis, Pavel Laptev, Mike Lindmark, Erik Lucero, Orion Martin, John M. Martinis, Jarrod R. McClean, Matt McEwen, Anthony Megrant, Xiao Mi, Masoud Mohseni, Wojciech Mruczkiewicz, Josh Mutus, Ofer Naaman, Matthew Neeley, Charles Neill, Hartmut Neven, Murphy Yuezhen Niu, Thomas E. O'Brien, Eric Ostby, Andre Petukhov, Harald Putterman, Chris Quintana, Pedram Roushan, Nicholas C. Rubin, Daniel Sank, Kevin J. Satzinger, Vadim Smelyanskiy, Doug Strain, Kevin J. Sung, Marco Szalay, Tyler Y. Takeshita, Amit Vainsencher, Theodore White,

Nathan Wiebe, Z. Jamie Yao, Ping Yeh, and Adam Zalcman. Hartree–Fock on a superconducting qubit quantum computer. *Science*, 369(6507):1084–1089, 2020. doi: 10.1126/science.abb9811. URL `https://www.science.org/doi/abs/10.1126/science.abb9811`.

[272] Jia Chen, Hai-Ping Cheng, and James Freericks. Quantum-Inspired Algorithm for the Factorized Form of Unitary Coupled Cluster Theory. *J. Chem. Theory Comput.*, 17: 841, 2021. ISSN 23318422. doi: 10.1021/acs.jctc.0c01052.

[273] Krysta Svore, Alan Geller, Matthias Troyer, John Azariah, Christopher Granade, Bettina Heim, Vadym Kliuchnikov, Mariia Mykhailova, Andres Paz, and Martin Roetteler. Q# enabling scalable quantum computing and development with a high-level DSL. In *Proceedings of the Real World Domain Specific Languages Workshop 2018*, pages 1–10, 2018.

[274] Guang Hao Low, Nicholas P Bauman, Christopher E Granade, Bo Peng, Nathan Wiebe, Eric J Bylaska, Dave Wecker, Sriram Krishnamoorthy, Martin Roetteler, Karol Kowalski, et al. Q# and NWChem: tools for scalable quantum chemistry on quantum computers. *arXiv preprint arXiv:1904.01131*, 2019.

[275] Muralee Murugesu, Malgorzata Habrych, Wolfgang Wernsdorfer, Khalil A. Abboud, and George Christou. Single-molecule magnets: A Mn25 complex with a record S = 51/2 spin for a molecular species. *J. Am. Chem. Soc.*, 126(15):4766–4767, 2004. doi: 10.1021/ja0316824. URL `https://doi.org/10.1021/ja0316824`. PMID: 15080666.

[276] Amer Baniodeh, Nicola Magnani, Yanhua Lan, Gernot Buth, Christopher E Anson, Johannes Richter, Marco Affronte, Jürgen Schnack, and Annie K Powell. High spin cycles: topping the spin record for a single molecule verging on quantum criticality. *npj Quantum Mater.*, 3(1):1–6, 2018. doi: 10.1038/s41535-018-0082-7.

[277] Millicent B Smith and Josef Michl. Recent advances in singlet fission. *Annu. Rev. Phys. Chem.*, 64:361–386, 2013. doi: 10.1146/annurev-physchem-040412-110130.

[278] David Casanova. Theoretical modeling of singlet fission. *Chem. Rev.*, 118(15):7164–7207, 2018. doi: 10.1021/acs.chemrev.7b00601.

[279] Norm M Tubman, Carlos Mejuto-Zaera, Jeffrey M Epstein, Diptarka Hait, Daniel S Levine, William Huggins, Zhang Jiang, Jarrod R McClean, Ryan Babbush, Martin Head-Gordon, et al. Postponing the orthogonality catastrophe: efficient state preparation for electronic structure simulations on quantum devices. *arXiv preprint arXiv:1809.05523*, 2018.

[280] Kenji Sugisaki, Shigeaki Nakazawa, Kazuo Toyota, Kazunobu Sato, Daisuke Shiomi, and Takeji Takui. Quantum chemistry on quantum computers: A method for preparation of multiconfigurational wave functions on quantum computers without performing post-hartree–fock calculations. *ACS Cent. Sci.*, 5(1):167–175, 2018.

[281] Harper R Grimsley, Sophia E Economou, Edwin Barnes, and Nicholas J Mayhall. An adaptive variational algorithm for exact molecular simulations on a quantum computer. *Nat. Commun.*, 10(1):1–9, 2019. doi: 10.1038/s41467-019-10988-2.

[282] Marco Cerezo, Andrew Arrasmith, Ryan Babbush, Simon C Benjamin, Suguru Endo, Keisuke Fujii, Jarrod R McClean, Kosuke Mitarai, Xiao Yuan, Lukasz Cincio, et al. Variational quantum algorithms. *Nat. Rev. Phys.*, pages 1–20, 2021. doi: 10.1038/s42254-021-00348-9.

[283] Kishor Bharti, Alba Cervera-Lierta, Thi Ha Kyaw, Tobias Haug, Sumner Alperin-Lea, Abhinav Anand, Matthias Degroote, Hermanni Heimonen, Jakob S Kottmann, Tim Menke, et al. Noisy intermediate-scale quantum (NISQ) algorithms. *arXiv preprint arXiv:2101.08448*, 2021.

[284] Dmitry A Fedorov, Yuri Alexeev, Stephen K Gray, and Matthew Otten. Unitary selective coupled-cluster method. *arXiv preprint arXiv:2109.12652*, 2021.

[285] Eric Neuscamman, Takeshi Yanai, and Garnet Kin-Lic Chan. A review of canonical transformation theory. *Int. Rev. Phys. Chem.*, 29(2):231–271, apr 2010. ISSN 0144-235X. doi: 10.1080/01442351003620540.

[286] Federico Moscardó and Emilio San-Fabián. Density-functional formalism and the two-body problem. *Phys. Rev. A*, 44(3):1549–1553, 1991.

[287] A. D. Becke, A. Savin, and H. Stoll. Extension of the local-spin-density exchange-correlation approximation to multiplet states. *Theor. Chim. Acta*, 91:147–156, 1995.

[288] John P Perdew, Andreas Savin, and Kieron Burke. Escaping the symmetry dilemma through a pair-density interpretation of spin-density functional theory. *Phys. Rev. A*, 51(6):4531–4541, 1995.

[289] Pragya Verma and Donald G Truhlar. HLE16: A local Kohn–Sham gradient approximation with good performance for semiconductor band gaps and molecular excitation energies. *J. Phys. Chem. Lett.*, 8:380–387, 2017. doi: 10.1021/acs.jpclett.6b02757. URL `https://pubs.acs.org/sharingguidelines`.

[290] Indrani Choudhuri and Donald G Truhlar. HLE17: An efficient way to predict band gaps of complex materials. *J. Phys. Chem. C*, 123:17416–17424, 2019. doi: 10.1021/acs.jpcc.9b04683. URL `https://pubs.acs.org/sharingguidelines`.

[291] A. D. Becke. A new mixing of Hartree–Fock and local density-functional theories. *J. Chem. Phys.*, 98:1372–1377, 1993.

[292] Andreas Savin. On degeneracy, near-degeneracy and density functional theory. In J. M. Seminario, editor, *Recent Developments and Applications of Modern Density Functional Theory*, pages 327–358. Elsevier, Amsterdam, 1996.

[293] Hisayoshi Iikura, Takao Tsuneda, Takeshi Yanai, and Kimihiko Hirao. A long-range correction scheme for generalized-gradient-approximation exchange functionals. *J. Chem. Phys.*, 115(8):3540—3544, 2001.

[294] Thomas Körzdörfer and Jean-Luc Brédas. Organic electronic materials: recent advances in the DFT description of the ground and excited states using tuned range-separated hybrid functionals. *Acc. Chem. Res.*, 47:3285–3291, 2014. doi: 10.1021/ar500021t.

[295] Soumen Ghosh, Pragya Verma, Christopher J Cramer, Laura Gagliardi, and Donald G Truhlar. Combining wave function methods with density functional theory for excited states. *Chem. Rev.*, 118:7249–7292, 2018. doi: 10.1021/acs.chemrev.8b00193.

[296] Mohammad Mostafanejad, Marcus Dante Liebenthal, and DePrince, A. E., III. Global hybrid multiconfiguration pair-density functional theory. *J. Chem. Theory Comput.*, 16:2274–2283, 2020. doi: 10.1021/acs.jctc.9b01178. URL `https://dx.doi.org/10.1021/acs.jctc.9b01178`.

[297] David A Mazziotti. Variational minimization of atomic and molecular ground-state energies via the two-particle reduced density matrix. *Phys. Rev. A*, 65:062511, 2002. doi: 10.1103/PhysRevA.65.062511.

[298] Jacob Fosso-Tande, Truong-Son Nguyen, Gergely Gidofalvi, and DePrince, A. E., III. Large-scale variational two-electron reduced-density-matrix-driven complete active space self-consistent field methods. *J. Chem. Theory Comput.*, 12:2260–2271, 2016. doi: 10.1021/acs.jctc.6b00190. URL `https://pubs.acs.org/sharingguidelines`.

[299] Kamal Sharkas, Andreas Savin, Hans Jørgen Aa. Jensen, and Julien Toulouse. A multiconfigurational hybrid density-functional theory. *J. Chem. Phys.*, 137:044104, 2012. doi: 10.1063/1.4733672. URL `https://doi.org/10.1063/1.4733672`.

[300] Kamal Sharkas, Julien Toulouse, and Andreas Savin. Double-hybrid density-functional theory made rigorous. *J. Chem. Phys.*, 134:064113, 2011. doi: 10.1063/1.3544215. URL `https://doi.org/10.1063/1.3544215`.

[301] Julien Toulouse, Kamal Sharkas, Éric Brémond, and Carlo Adamo. Communication: Rationale for a new class of double-hybrid approximations in density-functional theory. *J. Chem. Phys.*, 135:101102, 2011. doi: 10.1063/1.3640019. URL `https://doi.org/10.1063/1.3640019`.

[302] Emmanuel Fromager. Rigorous formulation of two-parameter double-hybrid density-functionals. *J. Chem. Phys.*, 135:244106, 2011. doi: 10.1063/1.3671384. URL `https://doi.org/10.1063/1.3671384`.

[303] Yann Cornaton and Emmanuel Fromager. Double hybrid density-functional theory using the Coulomb-attenuating method. *Int. J. Quantum Chem.*, 114(18):1199–1211, 2014. ISSN 1097461X. doi: 10.1002/qua.24682.

[304] Cairedine Kalai and Julien Toulouse. A general range-separated double-hybrid density-functional theory. *J. Chem. Phys.*, 148:164105, 2018. doi: 10.1063/1.5025561. URL `https://doi.org/10.1063/1.5025561`.

[305] John Harris. Adiabatic-connection approach to Kohn-Sham theory. *Phys. Rev. A*, 29 (4):1648–1659, 1984.

[306] Mel Levy. Universal variational functionals of electron densities, first-order density matrices, and natural spin-orbitals and solution of the v-representability problem. *Proc. Natl. Acad. Sci. USA*, 76(12):6062–6065, 1979.

[307] Elliott H. Lieb. Density functionals for Coulomb systems. *Int. J. Quantum Chem.*, 24: 243–277, 1983. ISSN 1097461X. doi: 10.1002/qua.560240302.

[308] Weitao Yang. Some Remarks on Scaling Relations in Density Functional Theory. In R Erdahl and V. H. Jr. Smith, editors, *Density matrices and density functionals*, pages 499–508. Riedel, Boston, 1987.

[309] Mel Levy and John P Perdew. Tight bound and convexity constraint on the exchange-correlation-energy functional in the low-density limit, and other formal tests of generalized-gradient approximations. *Phys. Rev. B*, 48:11638, 1993. doi: 10.1103/PhysRevB.48.11638.

[310] Mel Levy and John P Perdew. Hellmann-Feynman, virial, and scaling requisites for the exact universal density functionals. Shape of the correlation potential and diamagnetic susceptibility for atoms. *Phys. Rev. A*, 32:2010–2021, 1985. doi: 10.1103/PhysRevA.32.2010.

[311] Pierre-François Loos, Anthony Scemama, Aymeric Blondel, Yann Garniron, Michel Caffarel, and Denis Jacquemin. A mountaineering strategy to excited states: Highly accurate reference energies and benchmarks. *J. Chem. Theory Comput.*, 14(8):4360–4379, 2018.

[312] Pierre-François Loos, Filippo Lipparini, Martial Boggio-Pasqua, Anthony Scemama, and Denis Jacquemin. A mountaineering strategy to excited states: Highly accurate energies and benchmarks for medium sized molecules. *J. Chem. Theory Comput.*, 16 (3):1711–1741, 2020.

[313] Björn O. Roos. Multiconfigurational Quantum Chemistry. In Clifford E Dykstra, Gernot Frenking, Kwang S Kim, and Gustavo E Scuseria, editors, *Theory and applications of quantum chemistry: The first forty years*, pages 725–764. Elsevier, Amsterdam, 2005.

[314] Björn O Roos, Kerstin Andersson, and Markus P Fülscher. Towards an accurate molecular orbital theory for excited states: The benzene molecule. *Chem. Phys. Lett.*, 192:5, 1992.

[315] Johan Lorentzon, Per-Åke Malmqvist, Markus Fülscher, and Björn O Roos. A caspt2 study of the valence and lowest rydberg electronic states of benzene and phenol. *Theor. Chim. Acta*, 91(1-2):91–108, 1995.

[316] Riddhish Pandharkar, Matthew R Hermes, Donald G Truhlar, and Laura Gagliardi. A new mixing of nonlocal exchange and nonlocal correlation with multiconfiguration pair-density functional theory. *J. Phys. Chem. Lett.*, 11(23):10158–10163, 2020.

[317] John P Perdew, Matthias Ernzerhof, and Kieron Burke. Rationale for mixing exact exchange with density functional approximations. *J. Chem. Phys.*, 105:9982–9985, 1996. doi: 10.1063/1.472933. URL `https://doi.org/10.1063/1.472933`.

[318] Carlo Adamo and Vincenzo Barone. Toward reliable density functional methods without adjustable parameters: The PBE0 model. *J. Chem. Phys.*, 110:6158–6170, 1999. doi: 10.1063/1.478522. URL `https://doi.org/10.1063/1.478522`.

[319] Rick A Kendall, Thom H Dunning Jr, and Robert J Harrison. Electron affinities of the first-row atoms revisited. systematic basis sets and wave functions. *J. Chem. Phys.*, 96(9):6796–6806, 1992.

[320] Ewa Papajak, Hannah R Leverentz, Jingjing Zheng, and Donald G Truhlar. Efficient diffuse basis sets: cc-pvxz+ and maug-cc-pvxz. *J. Chem. Theory Comput.*, 5(5):1197–1202, 2009.

[321] Ewa Papajak and Donald G Truhlar. Convergent partially augmented basis sets for post-hartree- fock calculations of molecular properties and reaction barrier heights. *J. Chem. Theory Comput.*, 7(1):10–18, 2011.

[322] Warren J Hehre, Robert Ditchfield, and John A Pople. Self-consistent molecular orbital methods. xii. further extensions of gaussian-type basis sets for use in molecular orbital studies of organic molecules. *J. Chem. Phys.*, 56(5):2257–2261, 1972.

[323] Michelle M Francl, William J Pietro, Warren J Hehre, J Stephen Binkley, Mark S Gordon, Douglas J DeFrees, and John A Pople. Self-consistent molecular orbital methods. xxiii. a polarization-type basis set for second-row elements. *J. Chem. Phys.*, 77(7): 3654–3665, 1982.

[324] Nikolai B Balabanov and Kirk A Peterson. Systematically convergent basis sets for transition metals. i. all-electron correlation consistent basis sets for the 3 d elements sc–zn. *J. Chem. Phys.*, 123(6):064107, 2005.

[325] Björn O Roos, Roland Lindh, Per-Åke Malmqvist, Valera Veryazov, and Per-Olof Widmark. Main group atoms and dimers studied with a new relativistic ano basis set. *J. Phys. Chem. A*, 108(15):2851–2858, 2004.

[326] Marvin Douglas and Norman M Kroll. Quantum electrodynamical corrections to the fine structure of helium. *Ann. Phys.*, 82(1):89–155, 1974.

[327] Alexander Wolf, Markus Reiher, and Bernd Artur Hess. The generalized douglas–kroll transformation. *J. Chem. Phys.*, 117(20):9215–9226, 2002.

[328] Daniel S King and Laura Gagliardi. A ranked-orbital approach to select active spaces for high-throughput multireference computation. *J. Chem. Theory Comput.*, 17(5): 2817–2831, 2021.

[329] Christopher J Stein and Markus Reiher. Autocas: A program for fully automated multiconfigurational calculations. *J. Comput. Chem.*, 40(25):2216–2226, 2019.